ON THE MUTUAL INTERACTIONS BETWEEN CONVECTIVE STORMS AND THEIR ENVIRONMENTS DURING THE MIDLATITUDE CONTINENTAL CONVECTIVE CLOUDS EXPERIMENT (MC3E) FIELD CAMPAIGN IN OKLAHOMA

by

Sarah Doherty Bang

A thesis submitted to the faculty of
The University of Utah
in partial fulfillment of the requirements for the degree of

Master of Science

Department of Atmospheric Sciences

The University of Utah

December 2013

The University of Utah Graduate School

STATEMENT OF THESIS APPROVAL

The thesis of **Sarah Doherty Bang**

has been approved by the following supervisory committee members:

Edward J Zipser	, Chair	**8/26/2013** Date Approved
Chun Tao Liu	, Member	**8/26/2013** Date Approved
Steven K Krueger	, Member	**8/26/2013** Date Approved

and by **Kevin D Perry** , Chair/Dean of

the Department/College/School of **Atmospheric Sciences**

and by David B. Kieda, Dean of The Graduate School.

ABSTRACT

This work examines in detail the lifecycles of the convection on 20, 23, and 24 May 2011 during the Midlatitude Continental Convective Clouds Experiment (MC3E) field experiment in Oklahoma. Furthermore, specific attention is given to the environmental mechanisms that affect the propagation, maintenance, strength, and morphology of organized convection for the duration of the three cases.

This study was conducted using the MC3E field campaign observational database, with particular emphasis on ground and airborne radar, radiosonde, and Oklahoma Mesonet data. This work was motivated by the goals of the MC3E field campaign, including improved understanding of convective evolution, organized convection, microphysics, ultimately leading to improvement of parameterization of convection and mesoscale processes in weather and climate models, and improvement of retrievals of precipitation by remote sensing.

The three cases examined exhibited leading line/trailing stratiform mesoscale convective system, supercell, and back-building convective structures, each with a complex evolution. From the data analyzed for these cases, we suggest that given certain initial conditions, the vertical wind shear profile is the dominant factor in the determination of storm morphology. If the source of the buoyant updraft is renewed throughout a system's lifetime, then a convective system's propagation and longevity is tied strongly to the strength of the cold pool produced by convective downdrafts, and formation of new convection along the boundaries of the pool.

for Ramona, Ian, Jeff, and Ryan
without whom I wouldn't have made it this far

CONTENTS

CHAPTER 1

INTRODUCTION AND BACKGROUND

1.1 Motivation

Organized convection brings with it the possibility of severe weather, including flooding, damaging winds, lightning, hail, and tornadoes, all of which are threats to life and property.

Organized convection is the complex result of multiscale interactions between environmental shear and instability, synoptic forcing, pre-existing and developing mesoscale features, and the structures within a maturing storm that modify the cell and the surrounding environment. Supercells, MCSs, and back-building convection (the foci of this study) can develop in a variety of conditions, along a spectrum of instability (CAPES), shear, and they can be triggered and maintained by a myriad of boundaries (Schumacher and Johnson 2005; Coniglio et al. 2007; Schumacher and Johnson 2008). Weaver (1979) states that the relative strength of a specific mechanism is what controls the convective outcome.

An ever-present challenge presented to the modeling community is the resolution of organized convection from the cloud resolving to the global scales. Eventually, the coupling of interactions between processes on different scales will need to be incorporated into model frameworks (Bryan and Morrison 2012) if organized convection is to be modeled accurately. Several current modeling efforts focus on the shortcomings of microphysics parameterizations to resolve convection correctly (Moncrieff and Liu 2006; Morrison and Milbrandt 2011; Bryan and Morrison 2012) lament the difficulties associated with parameterization of "propagation, coherence, and upscale transport."

The dynamics of the propagation of organized convection determine its longevity (Rotunno et al. 1988), its strength (Naylor et al. 2012), and its motion (Corfidi 2003), all of which impact the populace. Bryan and Morrison (2012) note that operational forecasters are beginning to use cloud resolving system models, the improvement of which will continue to improve forecasting capabilities and our understanding of the nature of convective behavior throughout the spectrum of organized convection.

1.2 Objective

The aims of this study are twofold:

- To make a detailed reconstruction of the lifecycles of the convection on 20, 23, and 24 May 2011 in central Oklahoma
- To determine the dominant mechanisms in the determination of convective mode, severity, and longevity of the organized convection in each of these three cases.

Future modeling efforts of complex microphysical and dynamic processes require a firm understanding of the overarching physics of a convective history, and an accurate representation of a system's environment throughout its lifetime in order to model the systems genuinely.

Radar (ground and airborne), surface Mesonet, airborne radiometer, and radiosonde data taken during the MC3E field campaign are analyzed to determine the arrival and location of convergent boundaries, the lifecycle and behavior of the convective storms, and the surface characteristics of outflow and cold pools created by convective downdrafts.

1.3 Background

The Midlatitude Continental Convective Clouds Experiment (MC3E) campaign was held from April - June of 2011 at the Department of Energy Atmospheric Radiation Measurement Southern Great Plains site. The research facility is strategically situated in northern central Oklahoma, in the heart of the Great Plains region, which climatologically experiences frequent severe convection in Northern Hemisphere spring, as measured by hail frequency, severe wind gust frequency, or tornado frequency (Doswell 2001). Oklahoma is prone to supercells, both isolated and those that form in clusters, squall lines, derechos, isolated convective cells, and heavy stratiform rain (Bluestein and Parks 1983; Gallus et al. 2008; Hocker and Basara 2008).

1.4 The General Nature of Convection

As different convective morphologies behave differently and can be governed by different dynamics, we will discuss specific storm morphologies in detail in the pages to follow. There are, however, certain ingredients that are required of all convective storms. Preconditioning and slow destabilization throughout the column can support and maintain convective

development, once another more rapid or concentrated destabilizing "trigger" has initiated the convection (Weisman and Klemp 1986).

1.5 Preconditioning

The MC3E region is prone to convective events because it is situated in the lee of the Rocky Mountains and north of the Gulf of Mexico. Approaching extratropical cyclones or troughs serve to destabilize the air in the region and moisten the lower levels (Johnson and Mapes 2001). When a cyclone or trough approaches the region from the west, southerly low-level winds advect warm moist air from the Gulf of Mexico (often in the form of a low-level jet, or LLJ). At the same time, upper-level winds advect warm dry air from over the Rockies or from the plateau to the southwest.

1.5.1 The Dryline

The epitome of the strong juxtaposition of dry and moist air is evident in central/western Oklahoma in the presence of the dryline. The dryline is a sharp moisture gradient between the dry air flowing eastward from the semi-arid mountainous plateau to the west or southwest, and the moist air flowing northward from the Gulf of Mexico and its boundary is often convergent. Throughout its diurnal cycle, the dryline fluctuates over central and western Oklahoma.

The dryline is of importance for convection; as Schaefer (1986) noted, over 70% of dryline days studied coincided with a radar echo within 400 km. While convergence at the dryline can serve as an initiation mechanism, the dryline in collision with another mechanism for convective initiation (e.g. a frontal passage or outflow boundary) is particularly effective for initiation (Schaefer 1986).

1.5.2 Capping

As discovered first by Carlson and Ludlam (1968), a shallow (1-2 km) layer of moist air near the surface is extremely unstable, and this instability can build if the convection is restrained under a layer of dry air advection. This layer of stable air serves as a "cap," that, when removed or diminished can encourage convection. The removal of a cap after convective instability has increased underneath is often tied to severe and intense convective storms. There are different mechanisms, however, that can remove a cap: unstable air may "underrun" the cap, flowing out from underneath the cap to a region where there is no

overlaying stable air; or the passage of a concentrated lifting mechanism, such as a front or outflow boundary, may force ascent of the stable air enough to erode the cap sufficiently for convection to occur (Johnson and Mapes 2001).

1.6 The Role of Shear

The longevity of convection depends heavily on vertical wind shear (in both magnitude and direction). Wind shear provides a mechanism for displacing stable subsiding air in the convective downdraft away from the convective updraft, thus preventing the downdraft from cutting off the updraft from its supply of warm, moist inflow at the surface (Misumi et al. 1994). A simulated storm initiated in the absence of shear created a downdraft that surrounded the perimeter of the updraft, which then stood in the path of the warm moist inflow necessary to maintain convection (Weisman and Klemp 1982). Increasing the shear in numerical simulations, Weisman and Klemp (1982) found different convective modes were supported by differing intensities of shear. Moderately sheared environments supported secondary convective episodes, where simulated storms' downdrafts propagated ahead of the updrafts and forced new convection in a cyclical manner. Highly sheared environments supported strong, split cell development similar to the supercellular convection seen in observations.

Weisman and Klemp (1982) found that the spectrum of convective mode and intensity depends on the magnitude of the vertical wind shear and the magnitude of the buoyant forcing. To this end, they created an index known as the "Bulk Richardson Number," or **R**, that is the ratio of CAPE to the vertical wind shear.

$$R = \frac{CAPE}{\frac{1}{2}\bar{u}^2} \tag{1.1}$$

where R is the Bulk Richardson Number, CAPE is the Convective Available Potential Energy, and $\bar{u}$ is the difference between the density-weighted mean wind from 0-6 km and the windspeed in the lowest 500 m of the column. Weisman and Klemp (1982) found that convection lies along a spectrum of R-values, with linear multicellular storms lying in the range of $R \geq 50$, and supercells in the range $R \leq 50$.

In addition to magnitude, the curvature of the shear profile with height is a factor in determining a storm's morphology. Unidirectional shear is supportive of linear convective systems, one type of mesoscale convective system (MCS). A vertical wind shear profile that veers (turns clockwise) with height, however, is conducive to supercellular storm

development (Rotunno and Klemp 1981). For analysis purposes, we use the methods described by Bunkers (2002), in which hodographs must curve by at least 45° through the first 1 - 3 km in order to be classified as clockwise. Note also that with this criterion, turning that is confined to the lowest 0.5 km is classified as a straight hodograph.

Among other sources, an approaching trough that brings southerly low-level winds and westerly mid- to upper-level winds is particularly efficient at providing the veering vertical wind profile that is conducive to severe, rotating convective storm systems.

1.7 Initiation

Once conditions for instability and moisture have been met, a sufficient lifting mechanism is needed to initiate convection (Weisman and Klemp 1986; Johnson and Mapes 2001). The mechanisms and location of convective triggering have been the subjects of extensive study and are often separated from the process of preconditioning. Triggering mechanisms range from the convective to the synoptic scale, and more than one possible triggering mechanism may be present at the site of convective initiation. While preconditioning gradually destabilizes environment and modifies the wind shear, triggering processes involve rapid destabilization and lifting. Capping, as discussed above, is commonly seen in advance of severe convective events, and often requires a great deal of lifting or heating to remove the convective inhibition (CIN). This lifting can be provided by convergence at a frontal boundary, an outflow boundary from convection elsewhere, the convergent dryline boundary, or collision of any of these boundaries (e.g., a triple point made of a cold front intersecting a dryline) (Purdom 1982; Wilson and Schreiber 1986; Johnson and Mapes 2001).

1.8 The Role of Downdrafts

Once convection has been initiated and is progressing towards maturity, precipitation processes almost always lead to the development of convective downdrafts. Condensate loading alone is usually sufficient to initiate downdrafts (Markowski 2002), and once initiated, precipitation falling into subsaturated air will result in evaporative cooling, which strengthens the downdrafts. Frozen hydrometeors falling through the 0°C level will melt, serving as an additional cooling mechanism (Fovell and Ogura 1988). Precipitation rates exceeding 2 mm hr^{-1} can supply the necessary evaporative cooling to yield a downdraft (Barnes and Garstang 1982). Upon reaching the ground, the downdraft diverges horizontally at the surface (Weisman and Klemp 1986). The strength of the downdraft, and thereby

the downward vertical motion and the outward horizontal motion at the surface, is strongly affected by the humidity of the air into which the precipitation falls and the strength of the precipitation itself (Barnes and Garstang 1982; Wakimoto 2001). For this reason, the parameter "downdraft convective available potential energy" (DCAPE) was created (Emanuel 1994).

DCAPE between two pressure levels p_i to p_n is defined as:

$$\text{DCAPE}_i \equiv \int_{p_i}^{p_n} R_d(T_{\rho e} - T_{\rho p}) d \ln p \tag{1.2}$$

where p is the pressure at the desired levels, R_d is the gas constant of dry air, $T_\rho e$ is the environmental temperature, and $T_\rho p$ is the parcel temperature after the parcel has undergone a wet-bulbing process, bringing it to saturation. Approximations of the maximum downdraft vertical velocity can be made by taking the square root of twice the DCAPE value. The entirety of the DCAPE value is rarely realized in actuality, and precautions should be made because heavy precipitation can be sufficient to instigate a downdraft from drag forces if precipitation is falling into saturated air and does not evaporate (Knupp and Cotton 1985) and thus, the DCAPE calculation would not encompass this possibility.

Though convective downdrafts play different roles in the convective modes discussed herein, one unifying characteristic among different convective morphologies' downdraft behavior is the balance struck between convective lifecycle and downdraft speed and location relative to the updraft. The downdraft of a convective cell has the potential either to destroy or to maintain its convection. In the words of Chappell (1986), some convective cells carry with themselves "the seeds of their own destruction."

1.9 Characteristics of Specific Storm Morphologies

Some aspects of convection are more easily conveyed by detailing processes specific to each convective mode, as different convective morphologies exhibit different behaviors to a certain extent.

1.9.1 Supercell Behavior

Definitions of a "supercell" storm converge on the description of a quasi-steady deep convective system that has a persistent mesocyclone in the form of a rotating updraft (Browning 1964; Doswell and Burgess 1993). Supercells require sufficient buoyancy to create their trademark strong updrafts, as well as a great deal of vertical wind shear (Weisman and Klemp 1982).

Modeling studies (Klemp and Wilhelmson 1978; Rotunno and Klemp 1981; Weisman and Klemp 1982) describe how early in the storm's development, vertical shear creates vortices in the horizontal that are tilted in the vertical by a shear-induced pressure gradient, resulting in a large updraft with two cores of rotation, one cyclonic and one anticyclonic (Klemp 1987); the updraft as a whole does not rotate. Shortly after these cores are in place, a convectively generated downdraft "splits" the vortices producing an anticyclonic "left-mover" and a cyclonic "right-mover." In the presence of strong clockwise shear, the right-mover will strengthen and the left-mover will likely weaken (Klemp 1987). The updraft of the right-mover is then consistently fed with warm, moist air that enters the system perpendicular to the direction of shear and is drawn into the updraft (Browning 1964).

A supercell creates two characteristic downdrafts throughout its maturity: the forward flank and rear flank downdrafts. The forward flank downdraft descends and diverges predominantly forward of the edge of the supercell storm, the same edge as the mesocyclone. The rear flank downdraft, conversely, develops upshear of the main updraft. The apex of these downdrafts is a strong convergence point at which the updraft and mesocyclone are maintained, and is characterized by the hook echo (Johnson and Mapes 2001; Markowski 2002; Naylor et al. 2012). The outflow speed at the surface correlates to the downdraft strength, which in turn depends on the precipitation rate and the humidity of the midlevel air. Should the midlevels be too moist or the precipitation rate be too low, the downdraft will be weak and will not provide the convergence required to maintain the updraft. Should the midlevels be too dry, the low-level outflow will be too strong and if the propagation speed is faster than the speed of the mesocyclone, this will impede the mesocyclone's lifecycle. Moderately dry midlevel air in the presence of the veering vertical wind shear profile that supports supercell growth will delay the outflow propagation, and if the speed of the outflow is close to that of the mesocyclone, the updraft will be enhanced (Gilmore and Wicker 1998). Unlike the downdraft properties associated with squall line propagation, the downdrafts created by a supercell are not necessarily cold. A review of rear-flank downdraft simulations by Markowski (2002) finds that many simulations create uncharacteristically cold downdrafts, and attributes this to the exclusion of ice processes in the microphysical parameters. Frozen hydrometeors can be lofted over larger horizontal distances, thus lessening the concentration of melting hydrometeors in close proximity to the updraft. Several documented cases of severe (some tornadic) supercells cite instances of warm outflow, which Naylor et al. (2012) found was less inhibitive to the updraft and

more accurately represented supercell observations.

Supercells often exhibit certain characteristic structures that are detectable on radar imagery. Lemon and Doswell (1979) describe the initial hour of the right-mover's life cycle, during which it generally exhibits a weak echo region (WER) with a high reflectivity lofted above a lower reflectivity next to the core of the updraft. On a horizontal radar scan (or planned position indicator, PPI), there is a "vault": a weak reflectivity neighboring the strongest echo (Browning and Ludlam 1961; Browning 1964). Next, in the storm's "mature" phase, the storm exhibits an extreme weak echo region, a "bounded" weak echo region (or BWER), which has an exaggerated overhang around the weak echo region, signifying a persistent, strong updraft. The onset of the characteristic mesocyclone occurs near this time in the midlevels (Lemon and Doswell state 5-8 km above the ground). Midlevel rotation is the result of tilting of the horizontal vorticity created by environmental shear, whereas the lower level rotation of the mesocyclone forms at the boundary of the approaching outflow from the rear flank downdraft (Rotunno and Klemp 1985). The rotating updraft of a supercell creates a pressure gradient, which not only maintains the updraft, but also drives the propagation to the right of the shear vector (Rotunno and Klemp 1985; Davies-Jones 2002). Finally, as the storm collapses, the BWER weakens, as well as the updraft, while downdrafts strengthen (Lemon and Doswell 1979).

1.9.2 MCS Behavior

Zipser (1982) coined the term "Mesoscale Convective System" or MCS to describe the longer-lived more extensive thunderstorm systems, or specifically, all systems on a scale ranging from 2 km to 500 km that entail, at least for some of their lifetime, periods of deep convection. This term is derived from the earlier use of "Mesoscale Convective Complex" (MCC) that was used specifically for storm complexes that exhibited a specific structure on satellite imagery, had cold ($\leq$-32°C) IR brightness temperatures extending over 100,000 km^2 and an interior cold ($\leq$-52°C) region over 50,000 km^2, and both conditions were met for over 6 hours (Maddox 1980). This more general classification was proposed because the specific criteria for an MCC neglected the more common and more widely varied convective systems that resulted from similar processes. Prior to these terms, "squall line" was a term used to describe a narrow band of mature, active convection (Hane 1986).

There is a wealth of literature pertaining to the structure and behavior of MCSs. Broadly, an MCS is defined as a "cumulonimbus cloud system that produces a contiguous

precipitation area ~100 km or more in at least one direction" (Houze 2004). As described above, Weisman and Klemp (1986) found that linear multicell systems (MCS, squall line) form prevalently in strongly sheared environments with little curvature. MCSs take on many forms; however, the specific MCS structure discussed here ("leading-line/trailing-stratiform" or LL/TS) contains a leading convective line, characterized by a strong reflectivity echo (usually > 40dBZ) with a strong reflectivity gradient at its edges (Houze et al. 1990).

Characteristically, on satellite imagery, MCSs create significant, widespread cloud shields (Maddox 1980; Houze et al. 1990). On radar imagery, particularly for the MCS structure discussed above, on the leading edge of the system, a narrow (20 - 50 km) band of intense precipitation, usually over 40 dBZ, can be found. Edges are sharp, as the reflectivity gradient of this echo is very tight (Houze et al. 1990). Ahead of this line, visually, an anvil cloud may be present due to lofting of small ice particles at the top of the updraft (Zipser 1977), though this may not be visible in radar imagery.

Once the LL/TS MCS has matured, storm inflow at low-levels is strongly front-to-rear, which advects hydrometeors from the updraft towards the rear of the storm. Also, as aging cells decay, their cloud tops become progressively lower. This results in a broad swath of moderate reflectivities (the stratiform region) that trails behind the "leading line" of convective precipitation and extends through the midlevels. Houze (1989) categorizes a stratiform region as "any nonconvective echo on a scale of 40 km or more" and these regions can extend over 100,000 km^2 with reflectivities lower than the convective line (Houze et al. 1990). Hydrometeors advected from the mid- and upper-levels of the updraft are frequently frozen hydrometeors, and once advected to the stratiform region, where vertical perturbations are much lower than that of the updraft, snowflakes fall and aggregate. When the snowflakes reach the melting level, their melting can be seen as a "bright band" of reflectivity on radar imagery, as water-coated ice particles have a higher index of refraction and thus the radar reports high reflectivities in this region. This trait is used to characterize stratiform rain regions and is a frequent appearance during the lifetime of an MCS (Houze 1989). The stratiform region, while its reflectivities and precipitation rates are often lower than that of the convective line, in addition to covering a much larger expanse than the convective line, plays an important role in the thermodynamic structure and latent heating profile of the MCS. Significant cooling from melting and evaporation occurs beneath the stratiform cloud layer, and condensation and freezing aloft in the front-to-rear flow supplies

warming (Houze 1989). Though often considered an outgrowth of the convective line with weaker reflectivities and vertical motion than in the convective line, the stratiform region contains a mesoscale updraft and downdraft of its own (Houze 1989). The position of the stratiform with respect to the convective line depends on the advection of hydrometeors from the convective line by the mean mid- and upper-level winds (Parker and Johnson 2000) and can be classified as leading, trailing, or parallel.

Once initiation is triggered, what sets the MCS apart from other convective systems is the method of propagation. The strength of the vertical shear is a critical factor in the triggering and growth of new convective cells. In the presence of vertical wind shear, the new cells will be deeper and less inhibited (as simulated by Rotunno et al. (1988)) than those formed in the presence of weak or no vertical wind shear. The success of the gust front/leading edge of the cold pool is also the result of a balance between the strength of the cold pool and the strength of the low-level shear (Rotunno et al. 1988). The convergence of the outflow and the inflow air ingested into the storm cell above the outflow results in an upshear tilt of the new convective updraft due to a pressure gradient forced at the surface (LeMone et al. 1984; Fovell and Ogura 1988). Thus, new cells are forming ahead of mature cells at the forefront of the outflow boundary in the ambient air, while the mature cells decay because their supply of inflow air has been cut off. There is a quasi-continuous cyclical nature of growth and decay of convective cells, the periodicity of which was replicated in simulations by Fovell and Dailey (1995) and averages about 15 minutes.

In response to the formation of the upshear-tilted updraft, a "rear-inflow jet" forms when buoyancy gradients in the storm draw in air at the midlevels (Weisman 1992). The buoyant updraft located above the convergent gust front boundary expands over time as it strengthens, and the pressure within at the mid- and upper-levels is correspondingly low and draws the midlevel air into the system from the rear. Another balance must be struck here between the buoyancy gradient of the rising updraft and the surface cold pool. The strength of the rear-inflow jet also depends on the environmental CAPE and the vertical wind shear: if both are sufficiently strong, the rear-inflow jet will remain at the midlevels until just behind the gust front, which will maintain a sturdy and upright updraft (Weisman 1992), whereas if the CAPE and shear are weak, the rear inflow will reach the surface well behind the gust front and weaken the convection.

The "strength" of the cold pool is determined by its depth and by the amount of negative buoyancy created in the downdraft (Rotunno et al. 1988; Weisman 1992). MCS

propagation is not restricted to the cold pool boundary processes. There are observations of new convective cells developing well ahead of the existing convective line, displaced from the parent cell. This mechanism is known as "discrete propagation." MCSs are also capable of creating gravity wave disturbances in the more stable upper-levels of the troposphere. Both mechanisms will be discussed further in the section detailing the effects of MCSs on their environments.

1.9.3 Back-Building Storm Behavior

On occasion, storms develop in such a way that they do not propagate away from the source of initiation; rather, they appear to redevelop and mature over the same region throughout a portion of their lifetimes. This process, known as back-building or quasi-stationary convection, can lead to extensive damage if the storm is severe, and flooding regardless of storm severity, due to the prolonged exposure of one region to severe conditions (Chappell 1986). The system appears to "build backwards" because new cells form upstream of the parent cell, while mature cells propagate downstream. Thus, on radar imagery, the system remains in the same place (Schumacher and Johnson 2005).

Back-building convection is the result of the balance between downwind propagation and mean cell motion of a convective cell. If the new convective cells grow on the rear flank, the propagation vector can offset the mean cell motion due to the prevailing winds; the precipitating cloud can seemingly remain stationary (Chappell 1986; Schumacher and Johnson 2005). Discrete propagation at the intersection of a dryline and an approaching cold front generated the back-building convection during the 27 May 1997 Texas event studied by Houston and Wilhelmson (2007). Conversely, the same event featured a back-building storm resulting from continuous propagation, similar to the self-sustaining mechanism responsible for supercell development. This cell, also, was forced along a convergent boundary along a cold frontal segment. Thus, while the propagation mechanisms were different, the along boundary forcing remained the common factor between the two back-building storms.

The environment that supports back-building convection is shared with supercell development environments (Bluestein and Jain 1985). In order to maintain convection in a singular region for an extended period of time, there must first be an adequate source of fuel for the developing storm. For this reason, Scofield and Robinson (1990) designed a technique to forecast back-building development based on the location of the equivalent potential temperature maximum (θ_e ridge). Central Oklahoma convection benefits from its situation

in that southerly winds from the Gulf of Mexico in advance of an approaching trough can be a long lasting source of high θ_e air advection and maintain heavily precipitating systems (Schumacher and Johnson 2005).

The wind shear profile that supports back-building convection is not statistically significantly different from that which supports isolated supercell development (Bluestein and Jain 1985). Both storm morphologies are supported by strong veering wind shear profiles in the lower levels (surface to 850 mb) (Scofield and Robinson 1990), large instabilities (high CAPE), and low bulk Richardson numbers (Bluestein and Jain 1985). Upper-level winds, however, are supportive of stationary convective development if they are weaker (Chappell 1986; Scofield and Robinson 1990; Schumacher and Johnson 2005).

There are conflicting schools of thought about the necessity of a surface boundary to initiate and maintain back-building convection. While the forcing mechanism need not be externally imposed (i.e. the boundary is self-imposed by the storm in the form of an outflow boundary and not from a front) Schumacher and Johnson (2005) state, "there must be some trigger" to initiate this convection and back-building often occurs at a meso- or storm-scale boundary.

Schumacher and Johnson (2005) surmised that while back-building systems may initiate along external meso- or storm-scale boundaries, they can be self-maintained by their own outflow boundaries, similar to MCS propagation. Houston and Wilhelmson (2007) found that supercells transitioned into a severe back-building system as a cold front interacted with a dryline and "pinched" the region, which provides further evidence that back-building can also result at the juxtaposition of two external boundaries.

1.10 Storm-Environment Interactions

1.10.1 Larger Scale Interactions

Convection serves to drive the local troposphere towards equilibrium by increasing static stability of the troposphere. Vertical perturbations decrease the vertical wind shear (Doswell 2001). On shorter timescales, still, organized convection can have an even more pronounced effect on its surroundings and any other convection in its environs.

1.10.2 Supercell Competition

When multiple convective systems grow in close proximity, they can possibly compete for access to inflow, or possibly merge, and later strengthen (Westcott and Kennedy 1989;

Rigo and Llasat 2005). Supercell storms, by way of their continual convergence at the apex of the front flank downdraft and the rear flank downdraft, are able to propagate if they are aligned in such a way that the updraft can ingest warm moist air (Markowski 2002). Often, supercells fire along a boundary (e.g. a dryline or frontal boundary) and as they grow and mature, they can interact with each other (Bluestein and Parker 1993). If the boundary is aligned directly north-south, for example, in an environment of southerly low-level winds, all supercells but the southernmost cell will be impeded by the cells to the south, as those cells will intercept the southerly flow that supplies the supercells with warm, moist air, that is the necessary fuel for thunderstorm maintenance.

As the storms propagate, especially when right- and left-movers are in the process of splitting, the collision of storms can be either constructive or destructive as postulated by Lilly (1979). Bluestein and Weisman (2000) simulated supercell interactions along a line and studied in particular the angle between the line of forcing and the midlevel shear (1.7 - 6 km in their analysis). 45° forcing to shear angle was found to be the best for supercell growth. The supercell at the end of the line has the most favorable conditions for growth and behaves as if it was isolated and is slightly different from the inner-line supercells. In a 45° shear environment, the left-moving cells were in competition with the right-moving storms they encountered and weakened significantly. The right-movers, on the other hand, still had access to warm, moist air, and could grow without much interference with their neighbors.

The closer the angle between the vertical shear and the boundary came to 0°, however, the downshear supercell is the only system that propagated as if isolated, and the other cells forced along the boundary develop a multicellular character. If the shear was oriented normal to the line of forcing, a squall line developed in the simulations. Finally, if the angle approached 135°, the left-movers were maintained, except if the low-level hodograph veered, in which case the supercells also became multicellular in character (Bluestein and Weisman 2000).

1.10.3 Cold Pools

As discussed above, mature storm cells will create a downdraft via precipitation drag forces and evaporative cooling as hydrometeors fall through subsaturated air. The downdraft will diverge at the surface and the cool, subsiding air will propagate outwards. This cold pool, in addition to the mechanism of MCS propagation, can initiate and interact with

convection beyond the frame of the cell itself. The effects of the gust front on convection are multifaceted and range from the convective to the mesoscale.

Weaver and Nelson (1982) present a history of the discovery of outflow boundaries beginning in 1841 when early meteorologists described the outward flow of cool air from a heavy rain shower. In the late 1970s, with the dawn of satellite meteorology, convective outflow boundaries were first noticeable on visible satellite imagery. Purdom (1976) observed convectively created "arc clouds" that, when intersecting other convective, synoptic, or terrain boundaries, will instigate convection at the intersection, provided there is sufficient moisture and instability to support and maintain the convection past infancy.

However strong an impetus a surface boundary may present to convective initiation, it is not always the responsible party. There is competition amongst boundary layer convergence, mean cloud-layer forcing, and convectively forced boundaries, and whichever is the strongest will dominate (Weaver 1979).

1.10.4 Discrete Propagation

Separate from the cyclical quasi-continuous gust front induced MCS propagation mechanism is the notion of discrete propagation, wherein convective cells are triggered by one of the propagation mechanisms discussed above and in the section on MCS behavior; however, they are displaced from the main updraft (Crook and Moncrieff 1988). Weaver and Nelson (1982) discovered supercells that propagated discretely along outflow boundaries, while Houze (2004) argues that in MCSs, discrete propagation often occurs well ahead of the gust front.

In an analysis by Crook and Moncrieff (1988), the environment was already one of large-scale lifting, and a smaller perturbation was sufficient to instigate convection. Like many convective triggering mechanisms that are the combination of multiple boundaries, discrete propagation may occur when smaller, convectively driven boundaries interact with large-scale lifting or potential temperature ridges that exist on scales larger than the MCS itself (Houze 2004).

Discrete propagation is also possibly the result of gravity wave dynamics (Houze 2004). The localized diabatic heating from precipitation processes drives a secondary circulation that propagates upward and away from the heating source. As gravity waves propagate outward, they induce vertical displacements in the lower level tropospheric air (displaced from the convection) and this may then destabilize the atmosphere enough to instigate other

convection ("gregariously" as described by Mapes (1993)). The wavelength and spacing of the gravity wave propagation depends on the parent convection, and will be stronger in high CAPE, high shear environments (Schmidt and Cotton 1990).

CHAPTER 2

THE MC3E EXPERIMENT AND DATASET

The data analyzed for this study were collected during the Midlatitude Continental Convective Clouds Experiment (MC3E) in northern Oklahoma from 22 April - 6 June 2011. This study focuses on the events of 20, 23, and 24 May 2011. The experiment was centered in Lamont, Oklahoma in the northern central part of the state. This experiment was a collaborative effort between the Department of Energy (DOE) Southern Great Plains (SGP) branch of the Atmospheric Radiation Measurement (ARM) program and NASA's Global Precipitation Measurement Mission (GPM) Ground Validation Program for the upcoming precipitation satellite launch. Both organizations set out to make detailed, three-dimensional observations of precipitation, for which each organization had different goals. DOE wished to improve convective inititation, updraft and downdraft resolution, and microphysics parameterizations for modeling purposes, while NASA wished to develop algorithms for precipitation and land-surface processes for the upcoming launch of the GPM satellite in the spring of 2014.

The area of study and locations of ground-based radars and instruments is shown in Figure 2.1. The DOE SGP research facility provided 7 ground-based radars: 4 precipitation radars (3 X-band (X-SAPR, 1 C-band (C-SAPR)), 1 cloud radar (Scanning ARM cloud radar: SACR), 1 vertically pointing Ka-band radar (KAZR), and a vertically pointing S-band profiler. NASA provided 1 polarimetric S-band radar (NPOL) and 1 Ku/Ka-band radar (D3R). The X-SAPR, C-SAPR, NPOL, and D3R radars were operated in both PPI (plan position indicator) and RHI (range height indicator) modes, with customized sectors and radar swaths taken as directed by the mission scientists.

The DOE SGP facility also provided an extensive suite of ground instruments that contained: 18 autonomous Parsivel disdrometers (APU), 16 rain gauge pairs, 7 video disdrometers (2DVD), and 6 radiosonde launch sites throughout Oklahoma and Kansas that would launch soundings every 3 hours during observation periods.

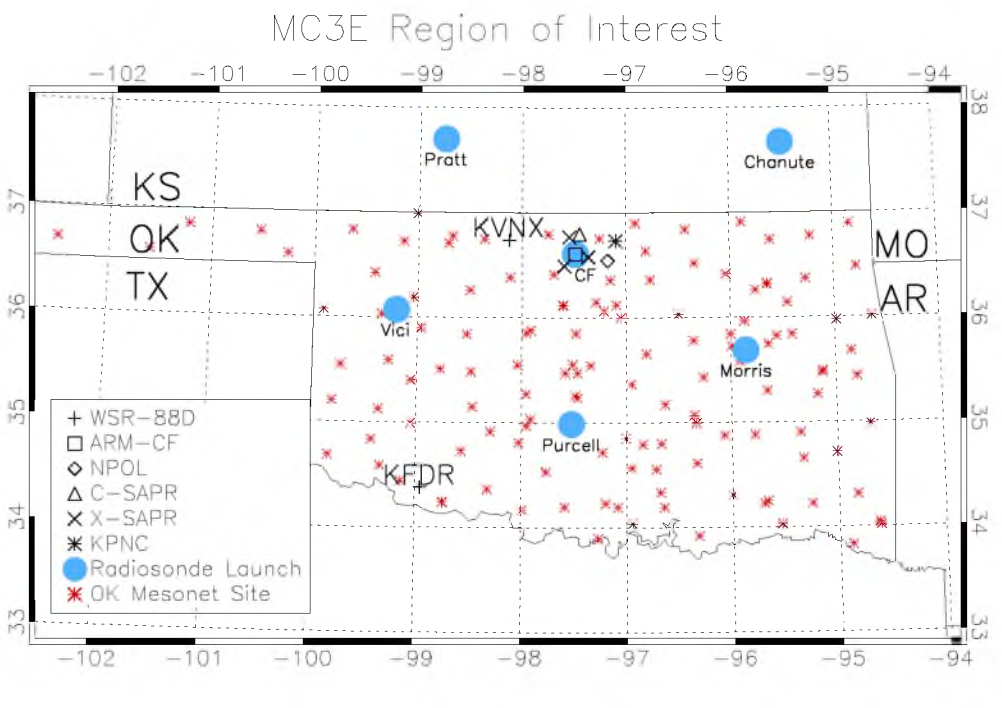

Figure 2.1. The MC3E region of study in northern central Oklahoma

Critical to this campaign's data are two aircraft: the NASA ER-2 and the University of North Dakota Citation. The NASA ER-2 flew at high altitudes (~20 km) above the clouds and was outfitted with onboard dual-frequency Ka/Ku-band radar (High-Altitude Imaging Wind and Rain Airborne Profiler or HIWRAP), the Advanced Microwave Precipitation Radiometer (AMPR: 10.7, 19.35, 37.1, and 85.5 GHz) and the Conical Scanning Millimeter-wave Imaging Radiometer (CoSMIR: 50.3, 52.6, 89 (H & V), 165.5 (H & V), 183.3±1, 183.3±3, and 183.3±7 GHz).

The University of North Dakota Citation flew *in situ* and was instrumented with 2 hot wire liquid water probes (King and Nevzorov), 1 cloud droplet probe (PMS FSSP-100), 2 cloud and precipitation probes (2D-C and 2D-P), 1 large hydrometer probe (SPEC HVPS), 1 particle imager (SPEC CPI), 1 cloud droplet profiler (DM CDP), 1 icing probe (Rosemount), and 1 laser diode hygrometer (Jensen 2010). The aircraft flew in parallel to measure cloud systems concurrently from high altitude and *in situ*. The instrumentation described above and measurement strategies are summarized nicely in Petersen and Jensen (2012).

The MC3E experiment database includes 5- and 15-minute measurements by 134 Oklahoma Mesonet stations that record temperature, pressure, dewpoint, wind speed and direction, potential and equivalent potential temperatures, and (tipping bucket) precipitation estimates. The Mesonet dataset also includes a host of radiative and soil characteristics not analyzed here.

This analysis focuses on convective dynamics and the interactions with the surrounding environment; thus, we focused on data collected by the NASA polarimetric radar (NPOL), the MC3E radiosonde network, the Oklahoma Mesonet (Mesonet 2012), the Vance and Frederick, OK WSR-88D dual-polarization radar imagery (Saxion and Ice 2012), the NASA ER-2 HIWRAP and CoSMIR measurements, and environmental data found in the University Corporation for Atmospheric Science satellite, surface, and radar image archive (UCAR Archive 2012). A detailed summary of the campaign objectives and instrumentation can be found in Petersen and Jensen (2012).

CHAPTER 3

EVOLUTION OF THE CONVECTION ON 19 AND 20 MAY 2011

3.1 Overview

Over the course of 19 and 20 May, a large trough pushed through Oklahoma, Kansas, and Texas, forcing many waves of convection in a 12-hour period. This analysis focuses on three such waves: a band of supercells (system 1), and small line of intense convective cells (system 2), and a long-lived leading line/trailing stratiform MCS (system 3). An overview of the pertinent boundaries and positions of convection are shown in Figure 3.1. Before the event, MC3E forecasters struggled with accurately predicting the onset of convection, as model guidance wavered on the arrival of the trough. Convection fired overnight (local) and the MC3E scientists awoke to a mature MCS (system 3) pushing into central Oklahoma. Though mission operations rapidly commenced, the ER-2 aircraft did not arrive in Oklahoma until 1345 UTC, and the NPOL radar was not in operation.

3.2 Prestorm Environment

Throughout the course of 19 May, an upper-level trough deepened over the Western US, as the corresponding low-pressure center at lower levels pushed eastwards from Nevada and Utah and deepened. Ahead of the trough, southerly flow was dominant, advecting warm moist air from the Gulf of Mexico into the Great Plains region of the US. The exit region lower level jet associated with the approaching trough was situated along the western borders of Kansas, Oklahoma, and Texas, providing strong divergence aloft. By 0000 UTC 20 May, the divergence maximum was situated over northern Texas, close to the southwestern corner of Oklahoma. By 1200 UTC, there was strong divergence aloft over the western edge of Oklahoma (east of the panhandle) (Figure 3.2).

The lower level trough pushed eastwards over the course of 19 May, its central axis reaching the Oklahoma panhandle at 1200 UTC 19 May. The trough continued to push over Oklahoma throughout the day.

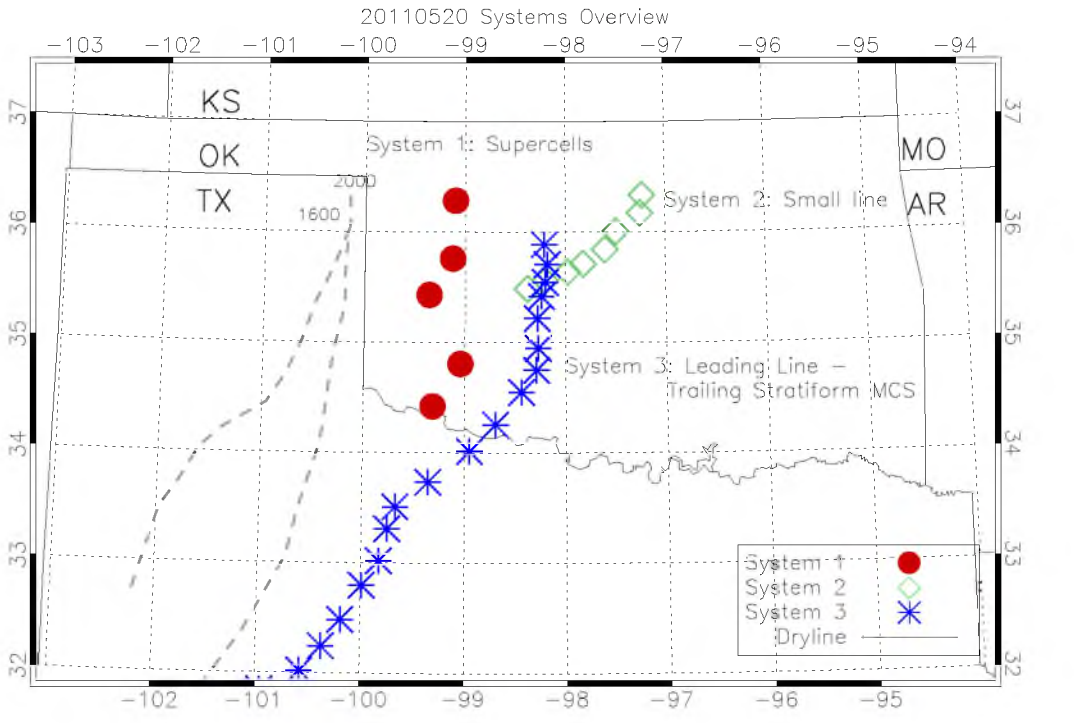

Figure 3.1. Overview of the prominent boundaries and convective systems that occurred on 19 and 20 May, 2011 in Southern Central Oklahoma

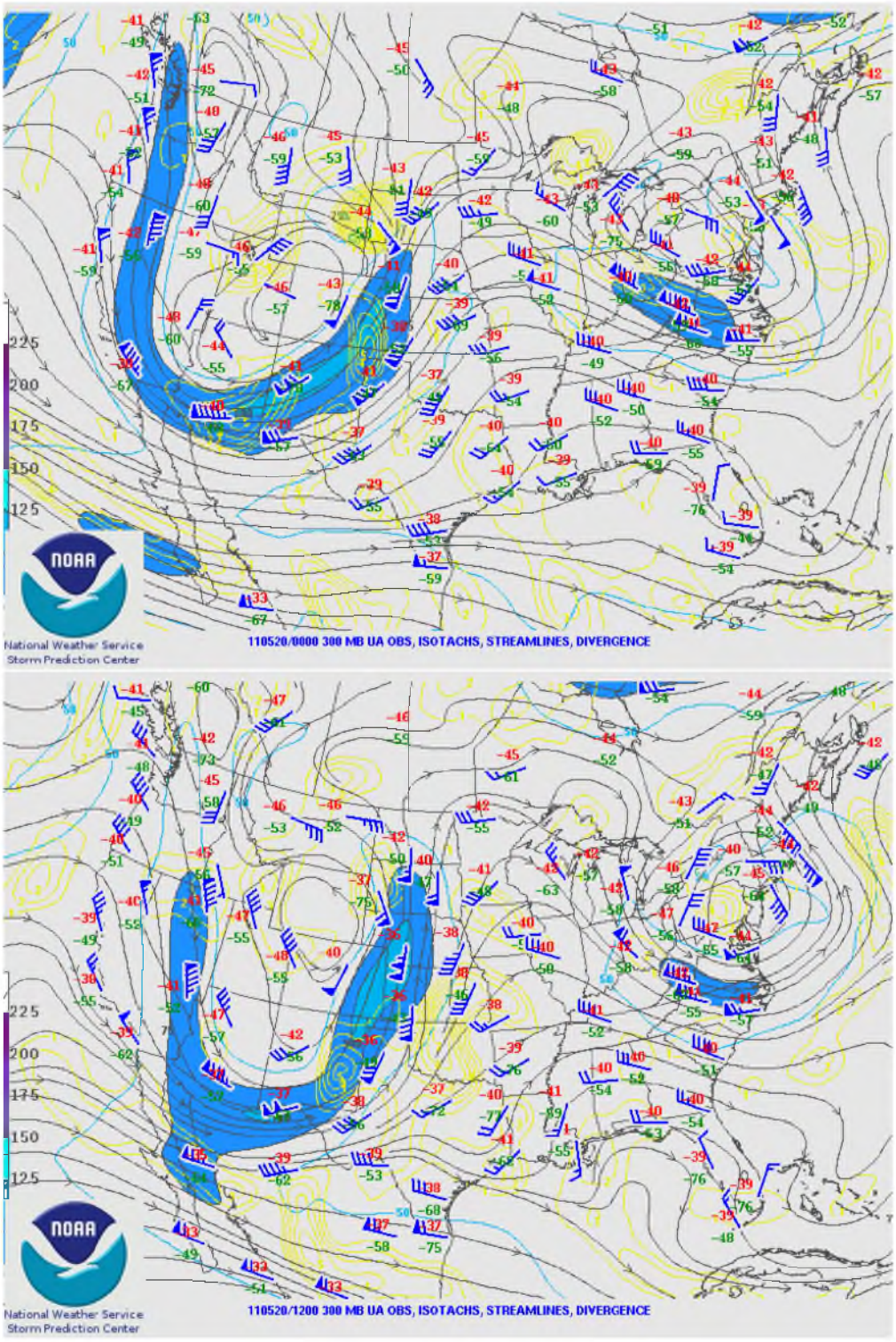

Figure 3.2. 300 mb analysis at 00 and 12 UTC 20 May 2011. Rawinsonde retrieved temperature, dew point, and wind observations (wind barbs coincident with numbers) and RUC Analysis streamlines, isotachs (fill), and divergence (contours). Courtesy of the National Weather Service.

Looking at the entire atmospheric column, there is a great deal of atmospheric instability throughout the state of Oklahoma beginning 19 May. Throughout the course of 19 May, the vertical atmosphere at Vici, OK (closest radiosonde launch location to the convective initiation) shows an increasing instability (CAPE progressed through the day from 1307 J kg^{-1} to 2409 J kg^{-1} to 3209 J kg^{-1} to 3696 J kg^{-1}) (Figure 3.3).

Vici, during May, was often west of the dryline, and therefore its boundary layer air was often dry (see Hoch and Markowski (2005) for statistics). On 19 May 2011, however, the lower atmosphere was uncharacteristically moist over the entire day, with 13 g kg^{-1} at 0530 UTC and over 14 g kg^{-1} at the surface at 1430 UTC.

There are two large capping inversions present at the beginning of the day, one at 900 hPa - 750 hPa and one at 600 hPa - 550 hPa. As the trough approached during the afternoon of 19 May, lifting rendered the higher inversion obsolete. The lower inversion, being deeper and stronger, took longer to erode. Lifting helps to erode the cap, as does daytime heating, pushing the surface temperature closer to the convective temperature, and by 1730 UTC 19 May, both mechanisms had removed the cap (Figure 3.3).

The soundings, in addition to significant lifting, show drastic changes in the vertical wind shear as 19 May progresses. At Vici, the 1130 and 1430 UTC hodographs show significant clockwise curvature, particularly in the lowest 2 km.

Shear throughout the column at Vici changes dramatically throughout the day. Strong shear is present as of 1130 UTC, as is clockwise veering directional shear (according to the criteria of Bunkers (2002)). The orientation of the winds is rotated slightly counterclockwise by 1430 UTC, and the directional wind shear is supportive of "supercell" formation by 1430 UTC (Figure 3.4).

By 2030 UTC, the Vici and Pratt, KS (southwestern Kansas) soundings have changed drastically from clockwise curved shear to linear shear in the lowest 2 km of the troposphere (Figure 3.5).

The position of the dryline fluctuates over western Oklahoma over the course of 19 May. Close to initiation, however, the dryline is aligned almost directly over the western edge of Oklahoma and extends into northern Texas (Figure 3.6). It is clearly demarcated in the surface observations by an abrupt drop in dewpoint temperatures and a shift from southeasterly winds (east of the dryline) to southwesterly winds (west of the dryline). By 0407 UTC May 20, the winds behind the dryline and the winds east of the dryline are nearly entirely oriented opposite from each other, providing extreme surface convergence.

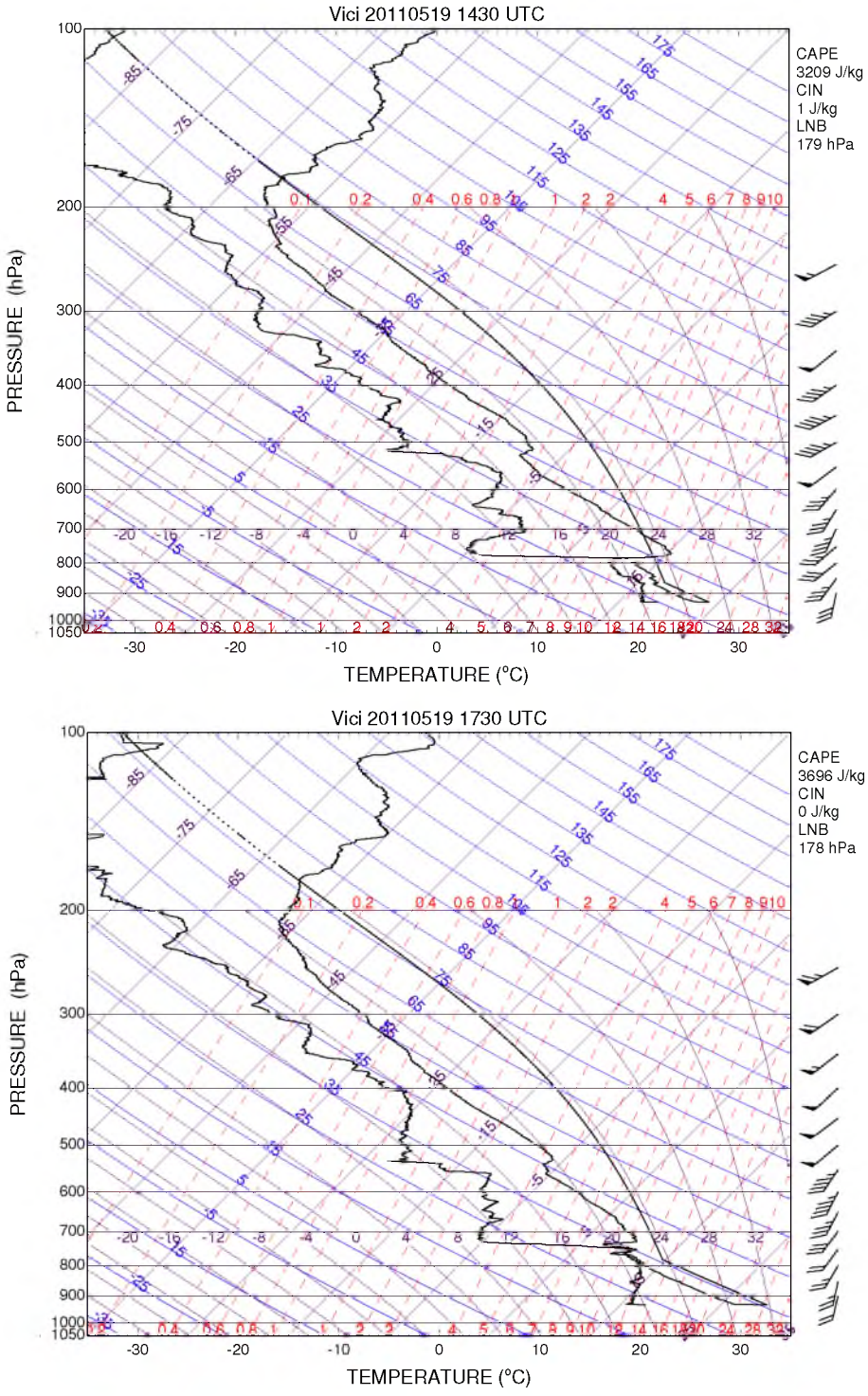

Figure 3.3. Skew-T/Log-P representations of the 1430 UTC (left) and 1729 UTC (right) soundings launched at Vici, OK (36.15°N/99.3°W). Radiosonde launch locations are shown in Chapter 2.

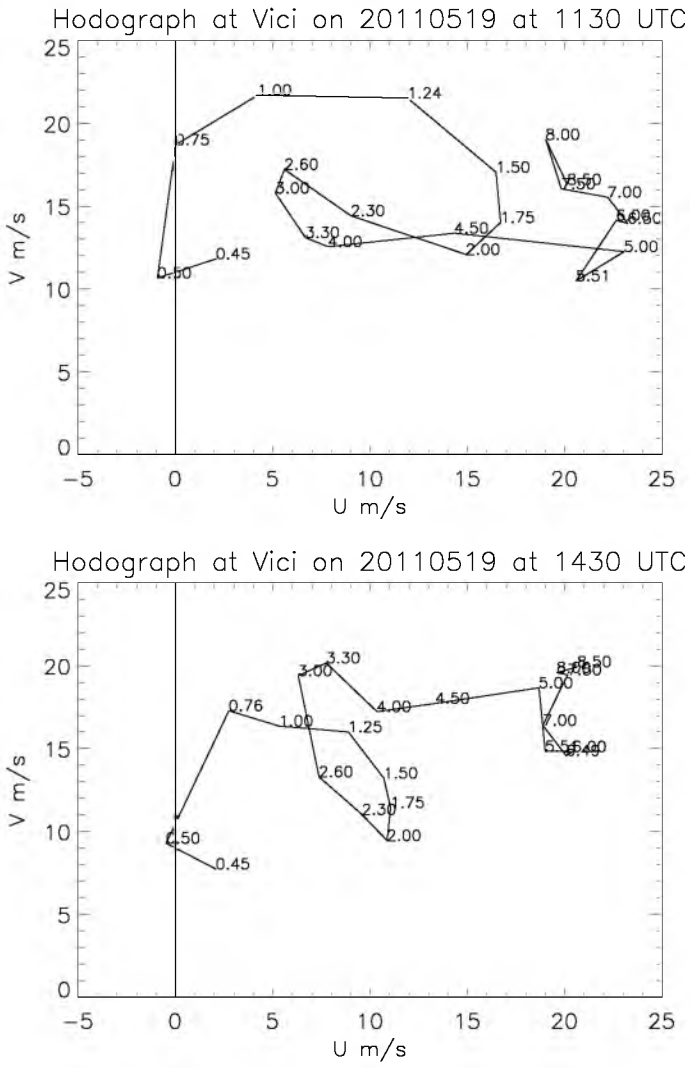

Figure 3.4. Hodographs created from the 1130 UTC (top) and 1430 UTC (bottom) 19 May 2011 Vici (36.15°N/99.3°W) radiosonde data.

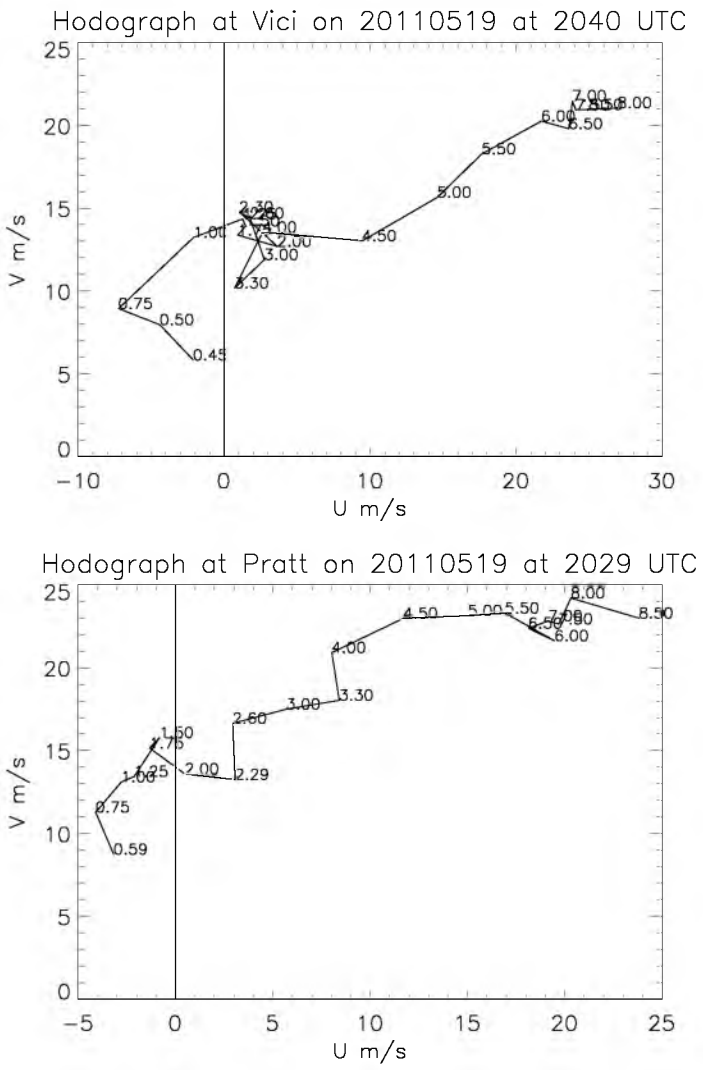

Figure 3.5. Hodographs created from the 2040 UTC Vici,OK (top) and 2030 UTC Pratt, KS (bottom) 19 May 2011 radiosonde data.

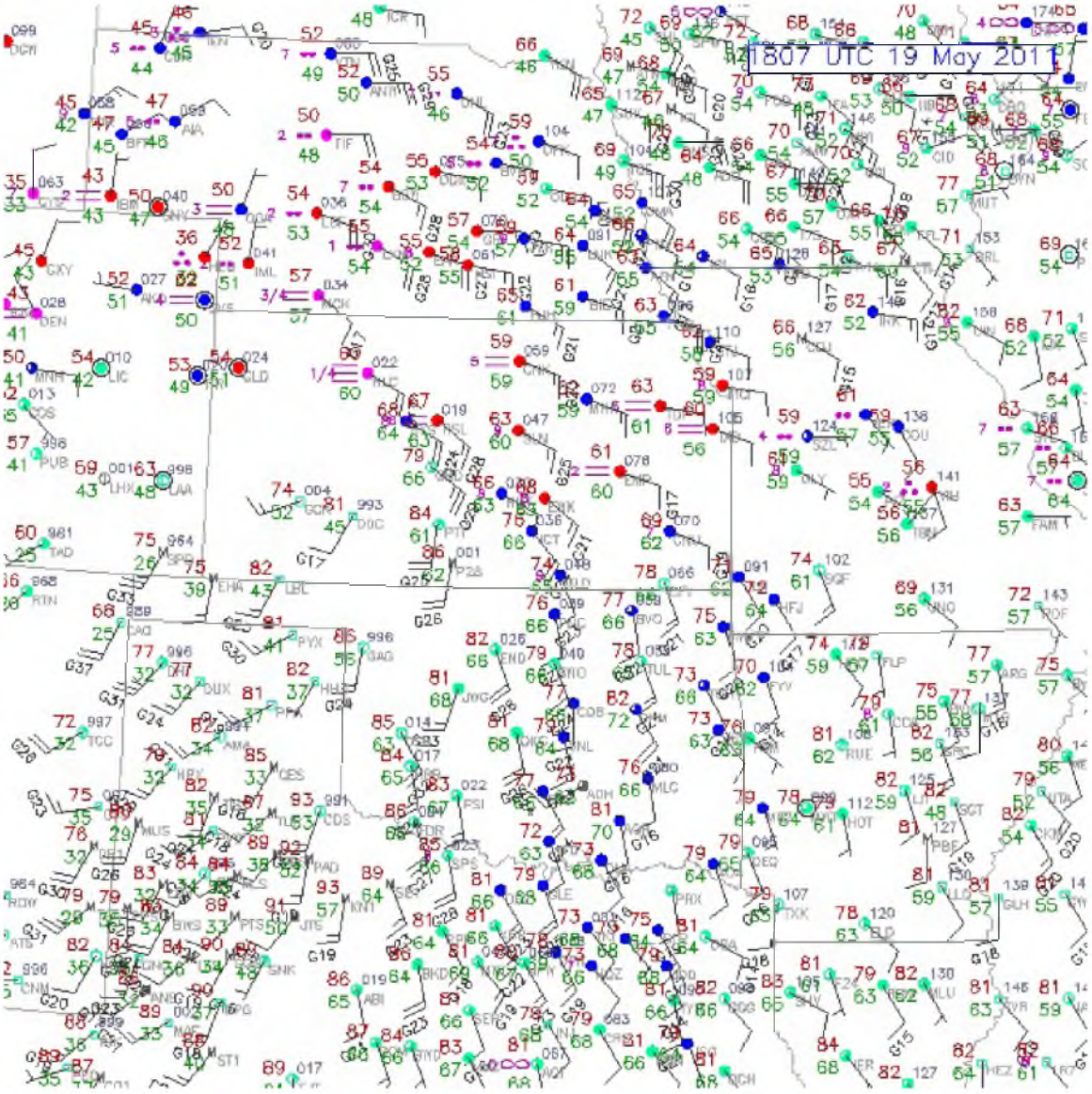

Figure 3.6. Surface observations at 1800 UTC 19 May 2011. Temperatures in Fahrenheit (red), dew point temperatures (green), wind speed and direction (barbs), and observed weather (pink) are shown. Courtesy of the National Weather Service.

3.3 System 1: 19 May Supercells

System 1 is constituted of cells that fire on the dryline just south of the Oklahoma/Texas border and rapidly evolve into left- and right-moving supercell storms. As the storms mature, they lose their rotation, bow out their alignment, and propagate across central southern Oklahoma. An overview of the position of the dryline and the positions of the line of cells at various times is shown in Figure 3.7.

At 1705 UTC 19 May, cells fired on the dryline in northern Texas in the region of strong convergence near the southern Oklahoma border at (34.2°N/100°W). The cells moved northeastward as they developed into supercells. The cells are aligned by 1800 UTC roughly along the 99.75 W meridian (Figure 3.8). Cells that develop in close proximity and propagate along a north-south line suggest the growth of both left- and right-movers during this time. The first hook echo is visible on the Frederick, OK radar at 34.5°N/99.7°W (Figure 3.9) at 1823 UTC.

Beginning at 1900 UTC, the two northernmost cells in system 1 produced two cold pools that propagates across the surface, expanding radially (Figure 3.10). These two cells move northward and weaken throughout the 2000 UTC hour.

Evidence of the northernmost cold pool can be seen in the 2040 UTC 19 May sounding at Vici (Figure 3.11) with winds changing to southeasterly very close to the surface, and a cold, moist layer running underneath the warmer, dry air. This layer extends up to 678 meters, and the surface temperature is 18.8°C, whereas (following a dry adiabat) it would have been 27°C. The southernmost cold pool continues to propagate, most strongly in the easterward direction. By 0145 UTC 20 May, however, night has fallen and the cold air is difficult to distinguish.

The line continues to march northeastwards from Texas near the southwestern corner of Oklahoma. This southern portion of the line, aided by cyclical firing of lines in the Texas convergence zone, aligns itself into a bow echo and this echo pushes eastwards across southern Oklahoma (Figure 3.8).

Rotation signatures can be seen in the Frederick, OK WSR-88D radar imagery between 2100 - 0100 UTC in the southern cells in system 1. The cells remain supercells for much of this period, but by 2334 UTC, the cells are aligned roughly SW to NE and the shape becomes bowed, but the leading edge appears "scalloped" from the antecedent supercells that constitute it.

After 0100 UTC 20 May, rotation is no longer evident in the radar imagery. The cells are

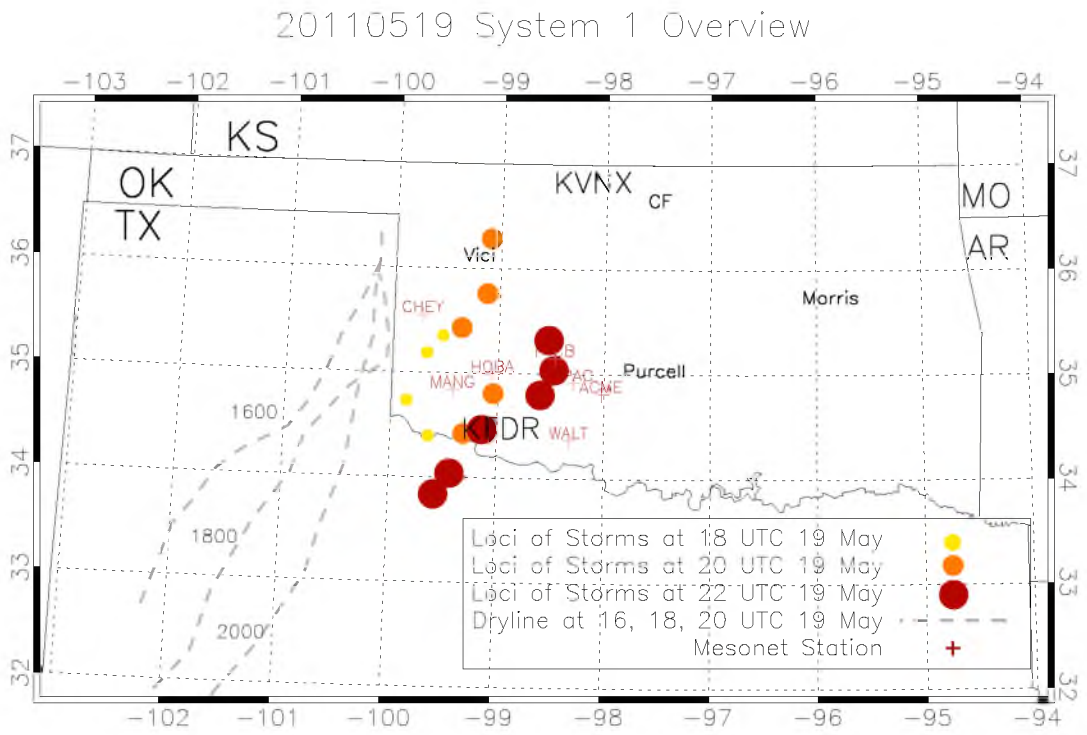

Figure 3.7. Overview of the subjectively determined dryline trajectory and the loci of the convective cells that fired along the dryline (first convection fired at 1705 UTC, positions here shown at 18, 20, and 22 UTC to show the extent of the line's lifecycle).

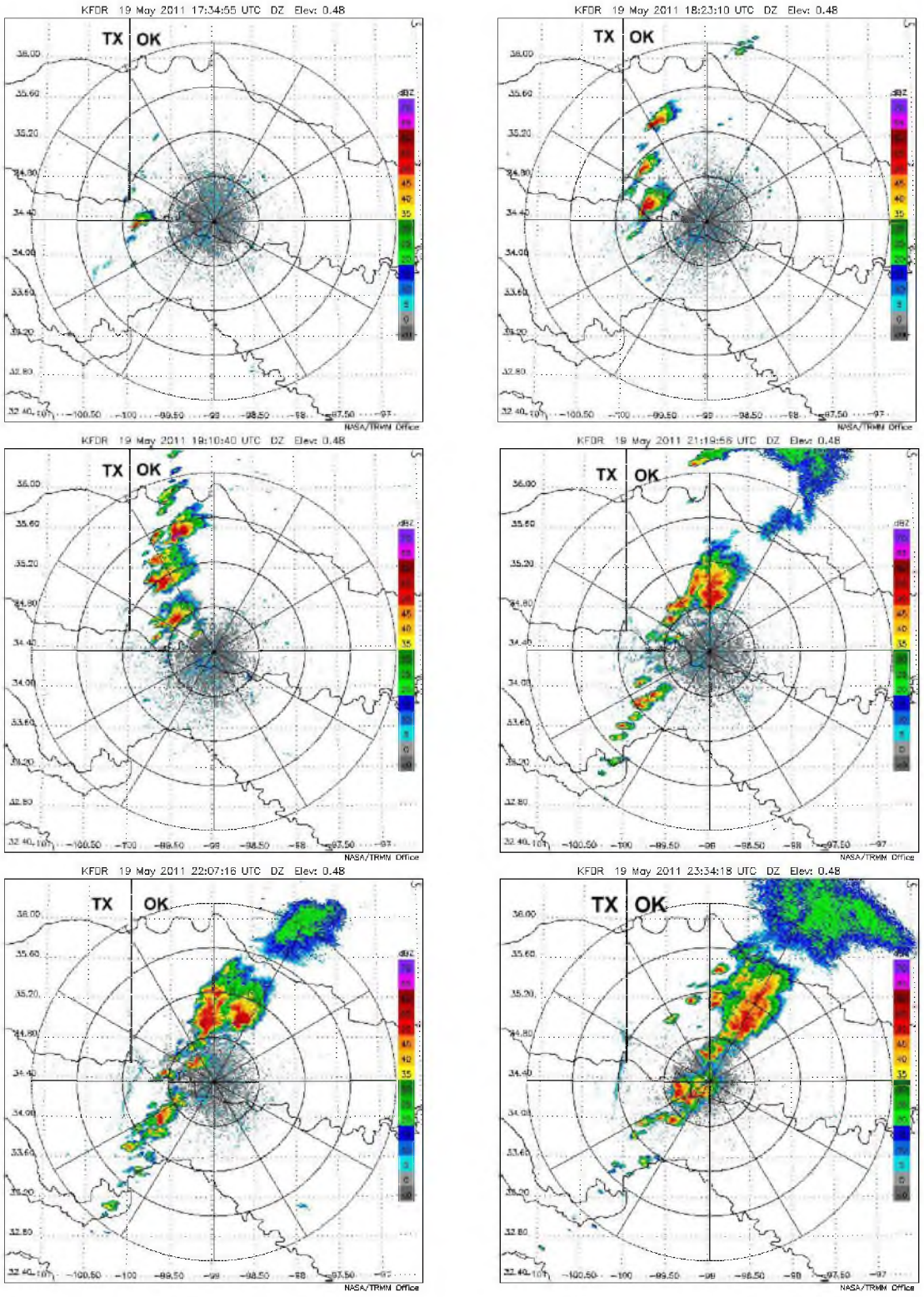

Figure 3.8. Radar timeline of system 1 from the Frederick, OK (KFDR) WSR-88D radar, showing first cells (1734 UTC); hook echoes (1823 UTC); left- and right-movers (1910 UTC); new cells (2119 UTC); secondary supercells (2207 UTC); and the bowing line (2334 UTC).

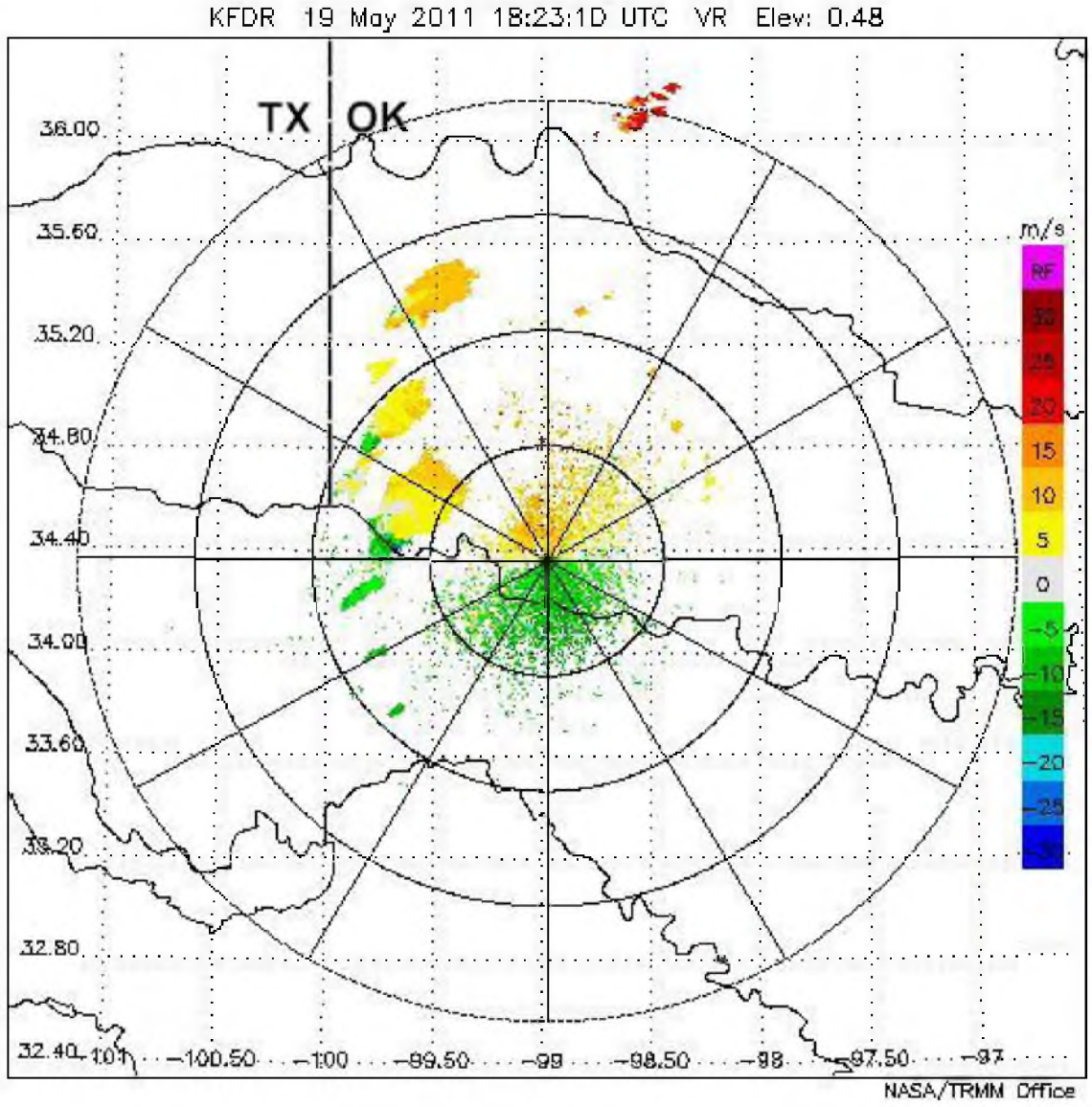

Figure 3.9. Radial velocity as detected by the Frederick, OK (KFDR) radar at 1823 UTC on 19 May 2011. Note the rotation signature at (34.8°N/99.8°W) in the second northernmost supercell.

aligned linearly and propagate northeastwards in a narrow but strong band of reflectivity (Figure 3.8). Throughout the 0200 hour, the line becomes even more distinguished and a trailing stratiform region sets up (Figure 3.8) and remains intact until 0422 UTC, whereupon a bow echo structure forms. This system propagates across central Oklahoma over the morning hours of 20 May, finally dissipating entirely into stratiform by 0715 UTC and eventually dispersing by 0930 UTC (Figure 3.8).

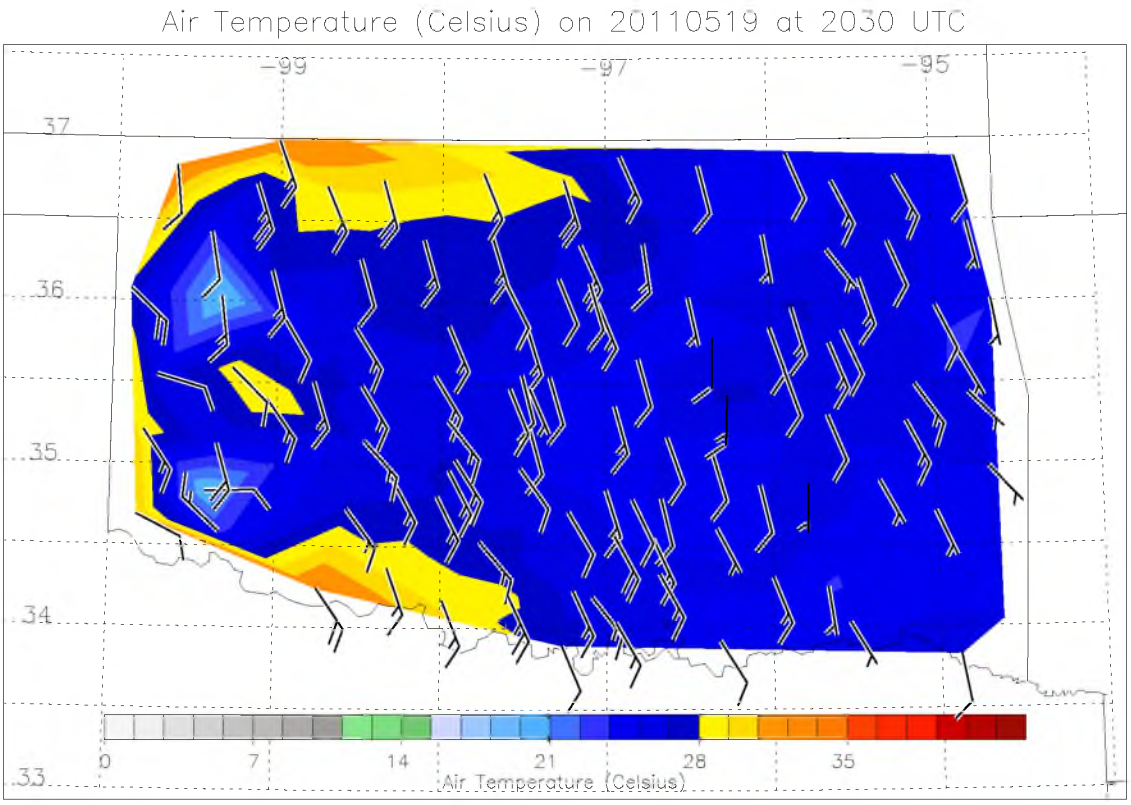

Figure 3.10. Oklahoma Mesonet altitude adjusted air temperature contour plot at 2030 UTC 19 May 2011, overlaid with wind observations (barbs). Note the smal cold pools in western Oklahoma.

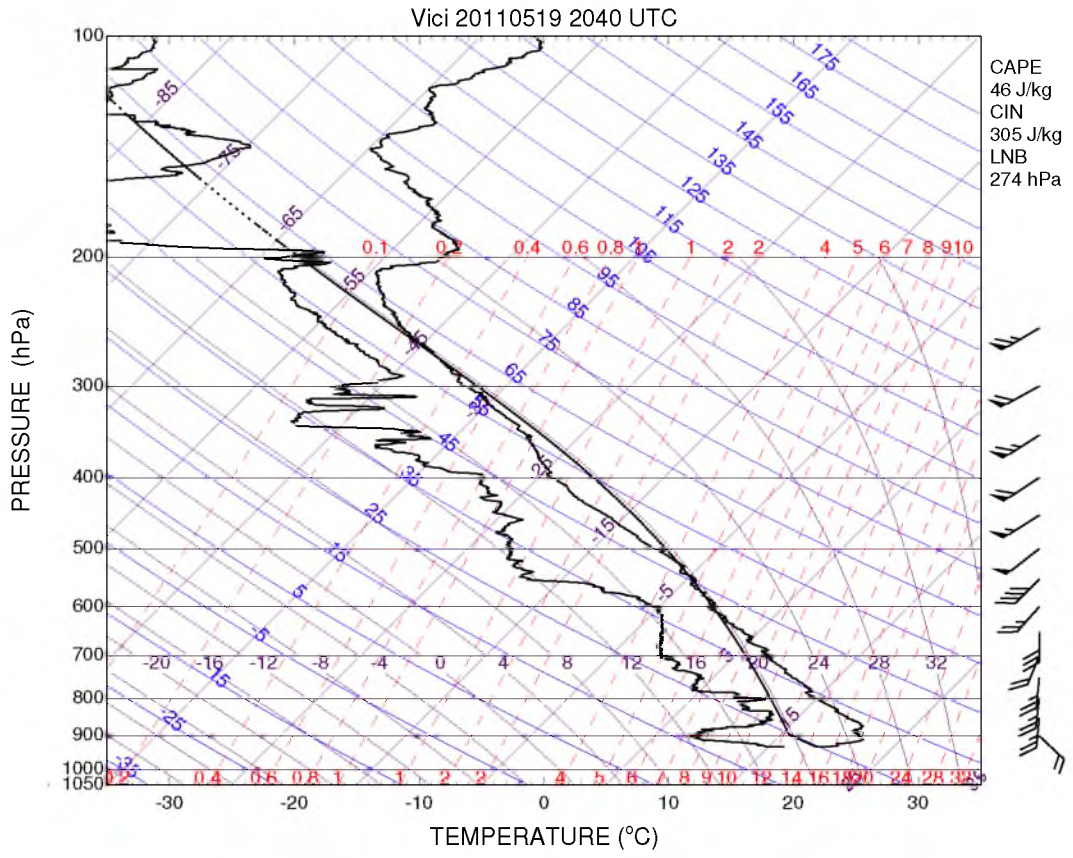

Figure 3.11. Skew-T/Log-P representations of the 2040 UTC sounding launched at Vici, OK (36.15°N,99.3). Radiosonde launch locations are shown in Chapter 2.

3.4 System 2: Narrow Linear Cells

System 2 is constituted of a narrow band of storms that fired ahead of the dryline in northern Texas at 0202 UTC. This line moves northeastward into Oklahoma, and while long-lived, is eventually surpassed by the eastward-pushing system 3. Positions of the eastern extent of the convective line and the dryline position in Texas are shown in Figure 3.12.

At 0202 UTC 20 May, a second system fires in northern Texas, along the same line of moisture convergence, and propagates eastward, the two main cells located at (34°N/100°W) and (34.5°N/99.2°W). This band of cells displays periodic strong reflectivities along a narrow SW-NE oriented line. The line takes on a bowed shape beginning at 0516 UTC (Figure 3.13); however, the cells are disorganized and behave as if in isolation, unlike an MCS.

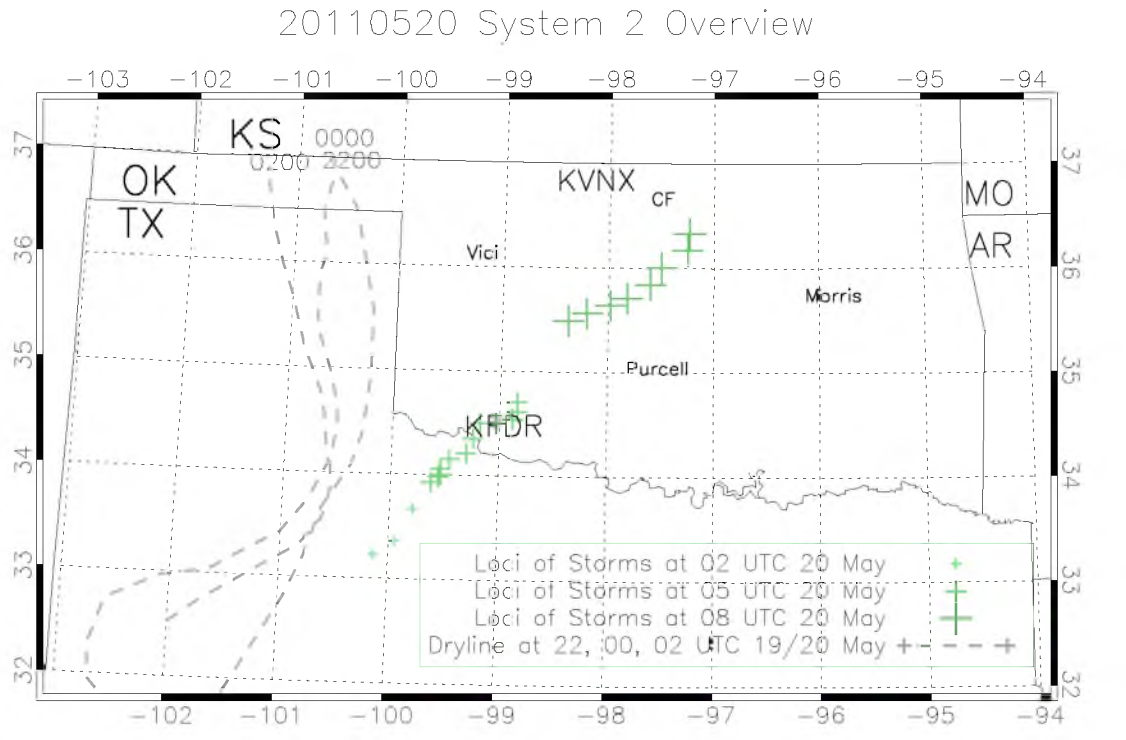

Figure 3.12. Overview of the subjectively determined dryline trajectory and the loci of the easternmost extent of the convective cells that fired along the dryline (first convection fired at 0202 UTC 20 May 2011, positions here shown at 02, 05, and 08 UTC to show the extent of the line's lifecycle).

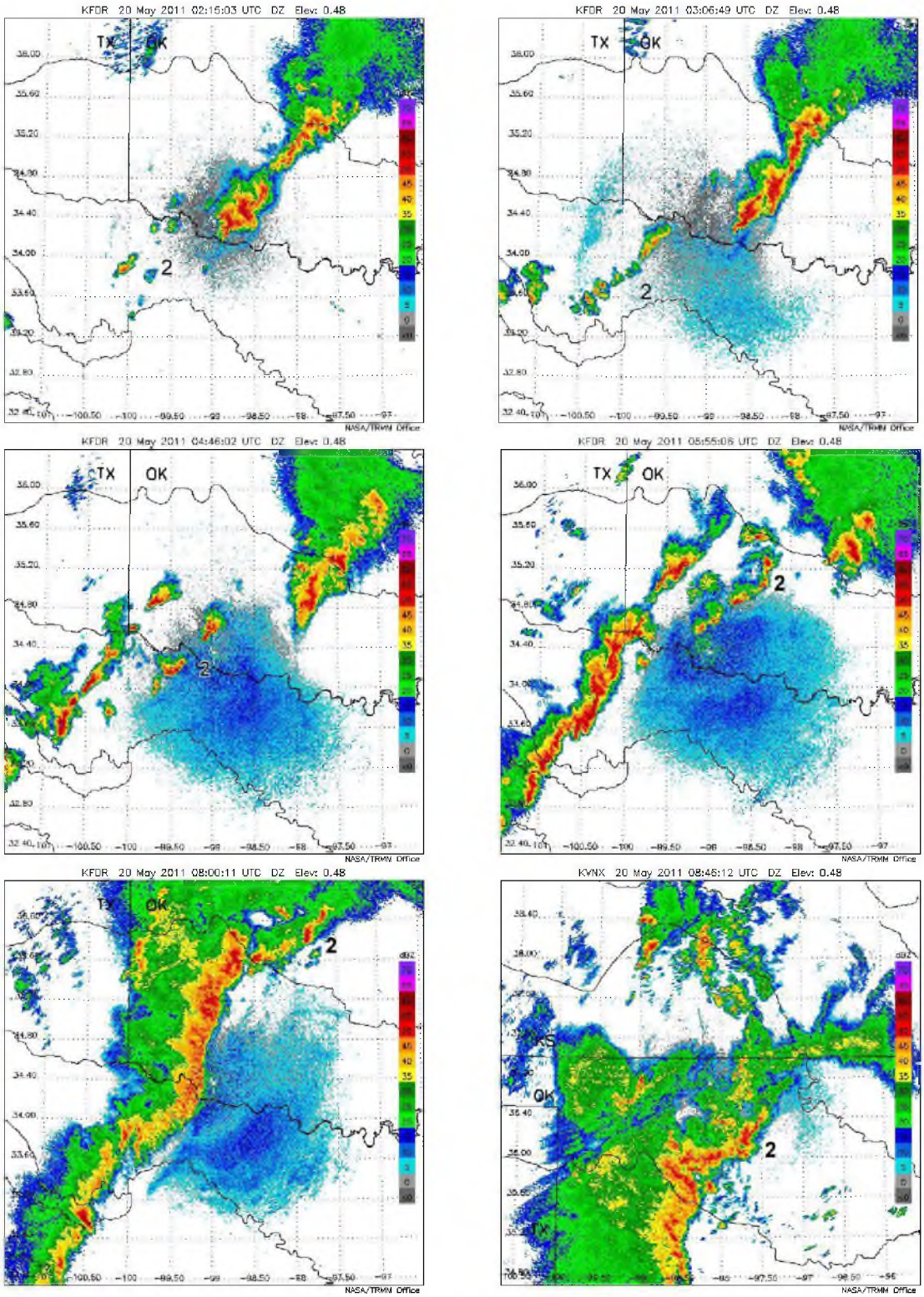

Figure 3.13. Radar timeline of system 2 from the Frederick and Vance radars, showing first cells (0215 UTC); early linearity (0306 UTC); disorganization (0446 UTC); redevelopment (0555 UTC); intersection with system 3 (0800 UTC); and unification (KVNX) (0846 UTC).

A small trailing stratiform structure forms behind system 2 shortly after 0600 UTC, and there is stratiform west of the entirety of system 2 as of 0730 UTC, though it is small in scale and not pronounced. A parallel line of convection develops west of system 2 at 0615 UTC, likely forming at the collision of outflow from lines 2 and 3 (system 3 discussed below).

At 0800 UTC, the system comprises embedded cells of strong convection within a band of stratiform, both still linear in nature. Between 0800 and 0900 UTC, system 2 continues to move northeastward, and new convection develops on its southern edge at the hinge of lines 2 and 3 (near 36°N/98.5°W). The line goes through cycles of a continuous convective leading line and broken up cells, with patchy stratiform trailing it to the north and west (Figure 3.13).

As system 3 progresses eastwards, system 2 diminishes from the west, and by 0930 UTC is indistinguishable from system 3.

3.5 System 3: Leading Line/Trailing Stratiform MCS

System 3 comprises a line of severe cells that fired along the dryline in northern Texas that rapidly developed along this line, increasing in both severity and north-south extent. System 3 moved rapidly eastward and developed into a long-lived leading line/trailing stratiform MCS that propagated across almost the entirety of Oklahoma (excluding the panhandle) for much of the day 20 May. The positions of the easternmost extent of the MCS and the dryline are shown in Figure 3.14.

A third system fired at 0132 UTC 20 May in northern Texas at (33°N/101.7°W). Cells with moderate reflectivities fired along a line extending northeast from the first cell to the southwestern tip of Oklahoma (Figure 3.15). At 0407 UTC, small cells with intense reflectivities begin to gain traction and by 0428 UTC, the cells have a distinct linearity. By 0500 UTC, there is a strong unified band of reflectivity that extends southwestward from the southwestern corner of Oklahoma (Figure 3.15).

Throughout the 0500 and 0600 UTC hours, the line remains strong and the unified band of high reflectivity stretches southwestward down the dryline as new cells form. By 0726 UTC, system 3 has propagated significantly eastwards and strengthened, and by 0754 UTC, the line has a distinct leading-convection/trailing stratiform signature (Figure 3.16) as discussed by Houze et al. (1990).

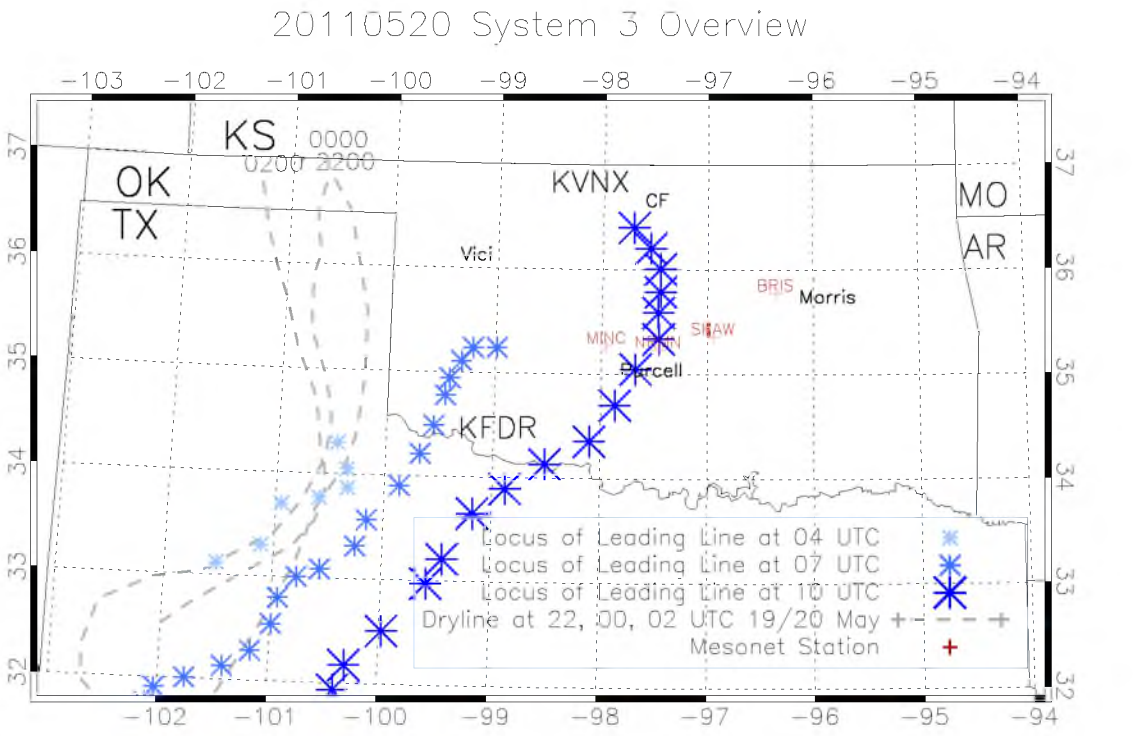

Figure 3.14. Overview of the subjectively determined dryline trajectory and the loci of the westernmost extent of the convective cells that fired along the dryline (first convection fired at 0132 UTC 20 May 2011, positions here shown at 04, 07, and 10 UTC to show the extent of the line's lifecycle).

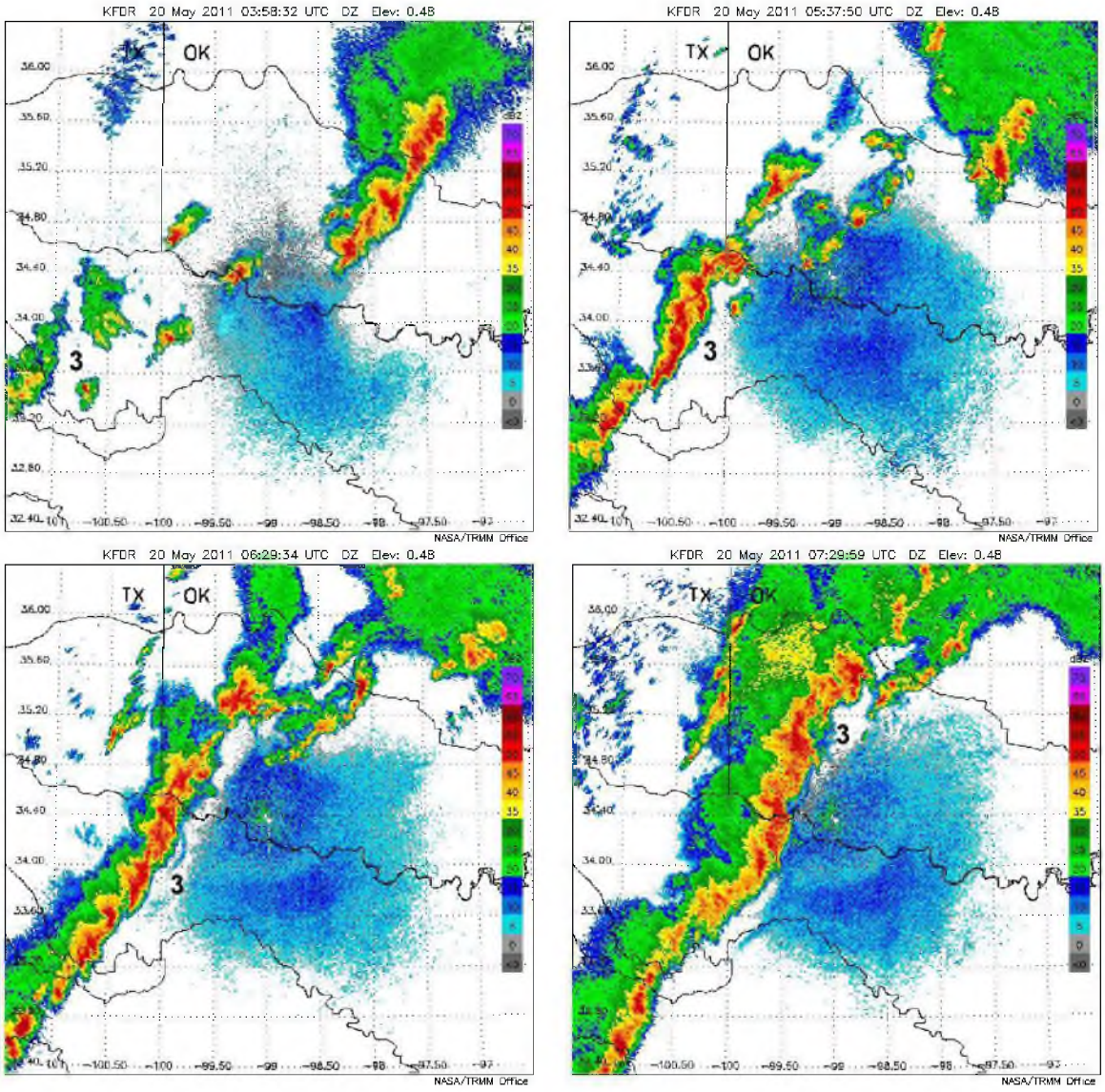

Figure 3.15. Radar timeline of system 3 from the Frederick, OK (KFDR) WSR-88D radar. The timeline illustrates early cells (0358 UTC); early linearity and strong reflectivities (0537 UTC); continued linearity and early trailing stratiform (0629 UTC); maintenance of the strong leading line, and growth of the stratiform region (0729 UTC) (radar timeline continued below).

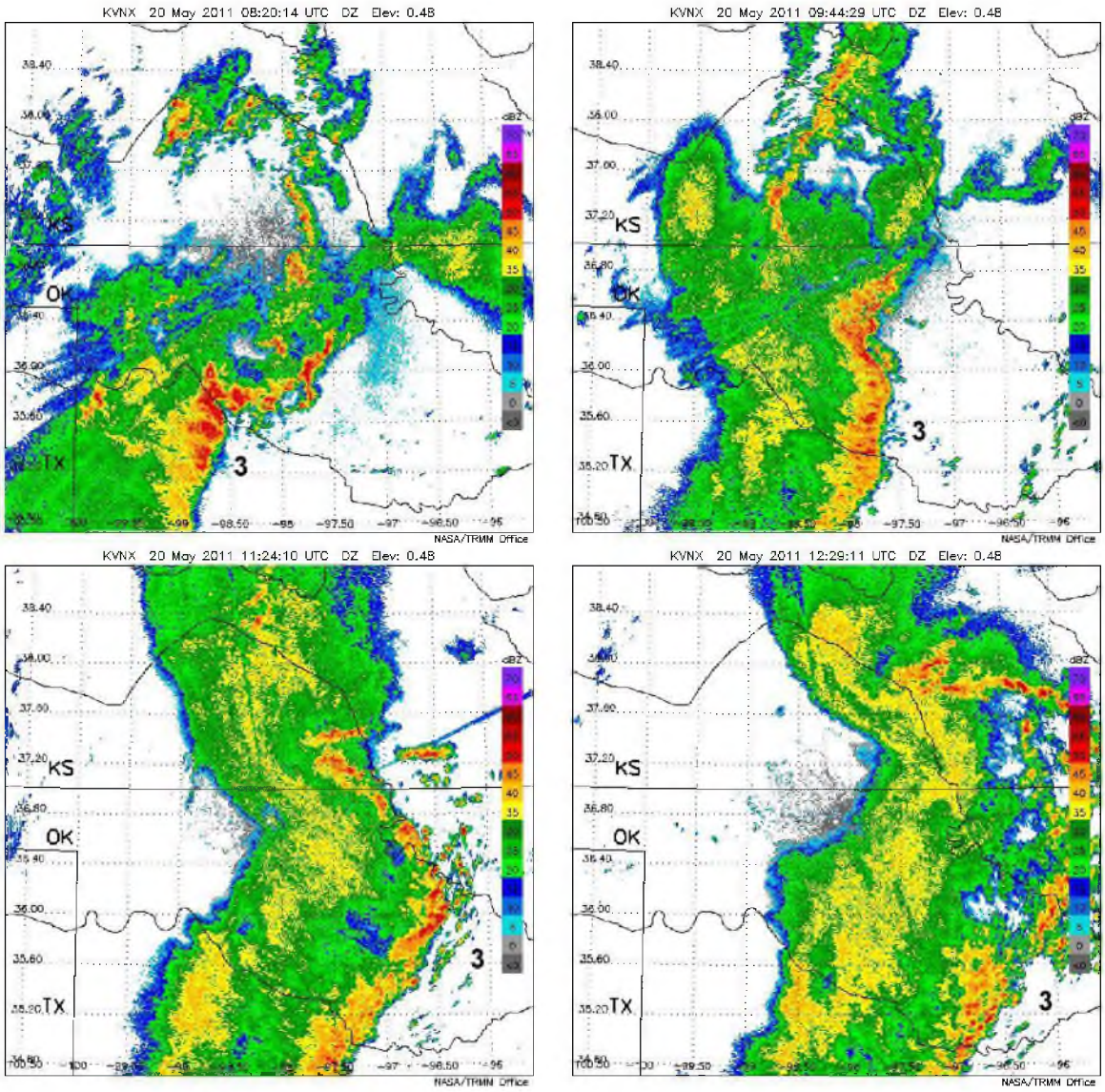

Figure 3.16. Continued Radar timeline of system 3 from the Vance, OK (KVNX) WSR-88D radar. The timeline illustrates intersection with system 3 (0820 UTC); dominance over system 2, bowing, trailing stratiform, and a weak region of reflectivity behind the leading convective line (0944 UTC); mild disorganization and weakening (1124 UTC); initial breakup of the leading convective line (1124 UTC); continued breakup of the convective line and maintenance of the stratiform region (1229 UTC).

By 0855 UTC, system 3 is a dominant LL/TS bow echo, with a northeast portion that arose from the merging of other lines. By 0923 UTC, the line extends from the Oklahoma/Kansas border to the Texas/Mexico border (Figure 3.17). Throughout the 0800 hour, lines 2 and 3 intersect at the northern tip of system 3, the junction found at 35.8°N/98.6°W. By 0955 UTC, system 3 has a strong leading bow echo that propagates eastward, bowing past the remnants of system 2. A weak region directly behind the strong leading line is visible, with a broad, heavy stratiform region trailing the leading line with some areas of embedded convection, and the characteristic weak reflectivity zone situated between the convective line and the stratiform region, indicative of a mature MCS. The leading line begins to break up at 0945 UTC in the southern half of Oklahoma, whereas the northern half of system 3 remains consistent until 1023 UTC, at which point the leading line takes on a fibrous appearance. The system passes over the Central Facility beginning at 1019 UTC. The disintegration of the leading line continues past 1500 UTC; meanwhile the stratiform region remains strong with reflectivities exceeding 40 dBZ until 1800 UTC and finally pushing out of Oklahoma after 2000 UTC (Figure 3.16).

A vertically pointing S-band profiler placed at the Central Facility captures the passage of system 3 from 0000 UTC (anvil) to 1600 UTC. Precipitation first appears at the CF at 0600 UTC and is mostly stratiform, except for some convective rain episodes, the most prominent at 1045 UTC (Figure 3.18). The bright band (as discussed by Houze et al. (1990)) stands out in the stratiform rain for the entirety of the event.

A delayed takeoff of the ER-2 aircraft resulted in its only capturing the stratiform precipitation of system 3. Figure 3.19 shows the ER-2 HIWRAP and CoSMIR cross-sections at 1400 UTC. The bright band is visible at 16 km from the radar, while brightness temperatures remain near 250 K. Later, at 1720 UTC, the ER-2 flew over some embedded convection within the stratiform, as evidenced by the higher reflectivities and echo tops, with CoSMIR 89 GHz (vertical) brightness temperatures nearing 120 K.

3.6 Propagation

The approach of the trough and the associated lifting and change in vertical wind shear are the responsible factors for the change from supercell to MCS development from 19 to 20 May. The Vici, OK soundings throughout the course of the evening and overnight show the change from clockwise turning wind shear to a linear shear profile, especially in the lowest 2 km (Figures 3.4 and 3.5).

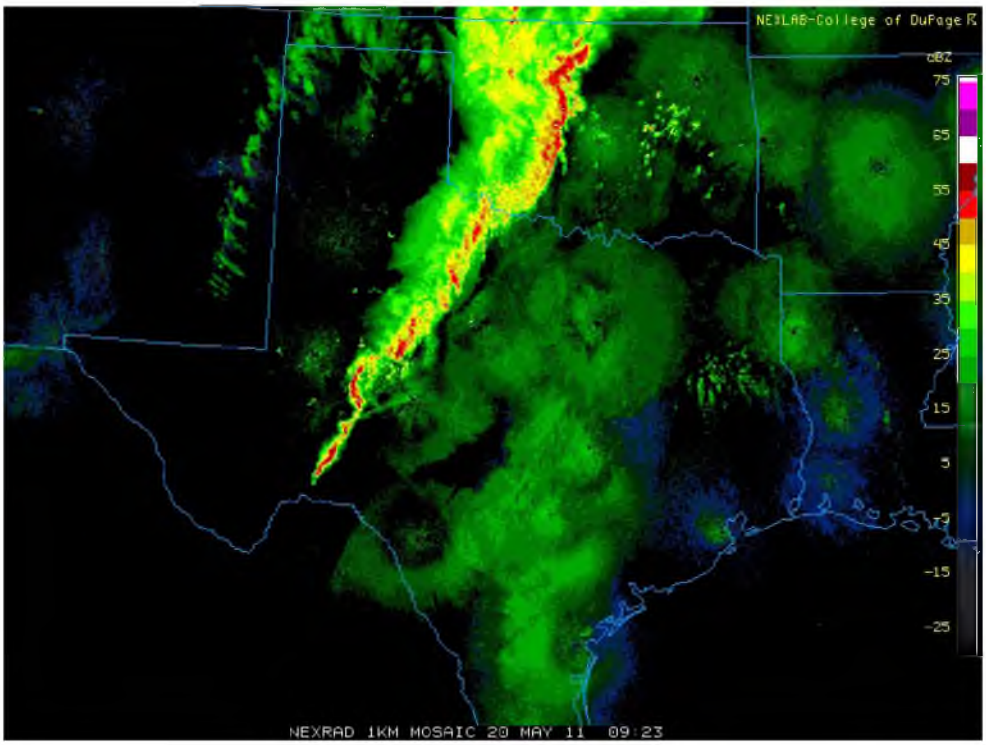

Figure 3.17. Composite WSR-88D radar imagery of the southern plains at 0923 UTC 20 May, 2011, showing the extent of system 3. Courtesy of the National Weather Service.

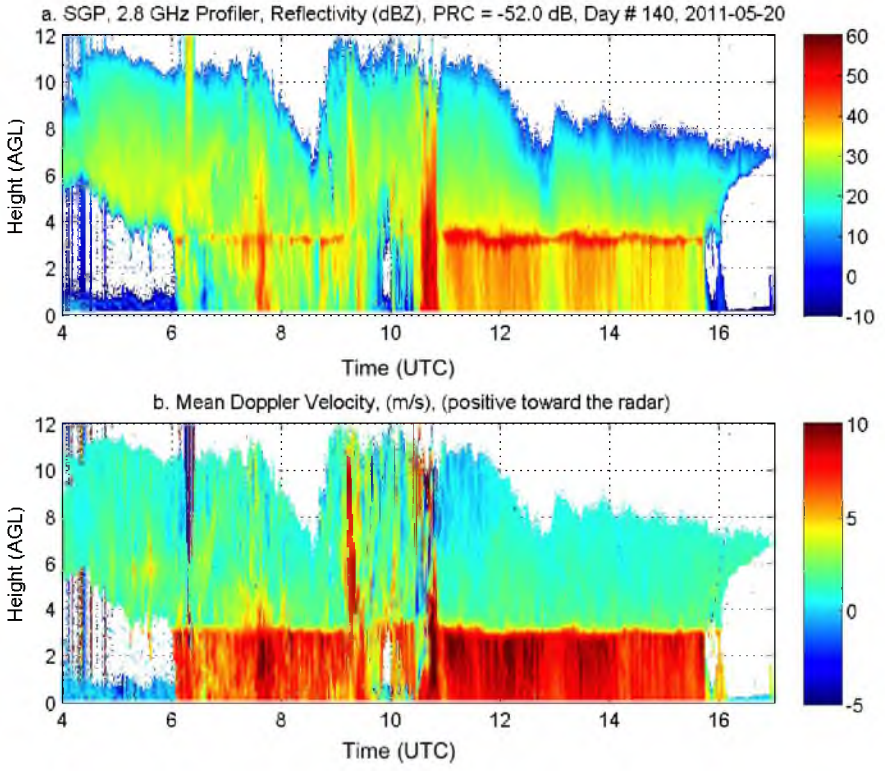

Figure 3.18. Vertically pointing S-band profiler observations (top) Reflectivity (dBZ), (bottom) Doppler Velocity (m s^{-1}) for the duration of the precipitation over the Central Facility.

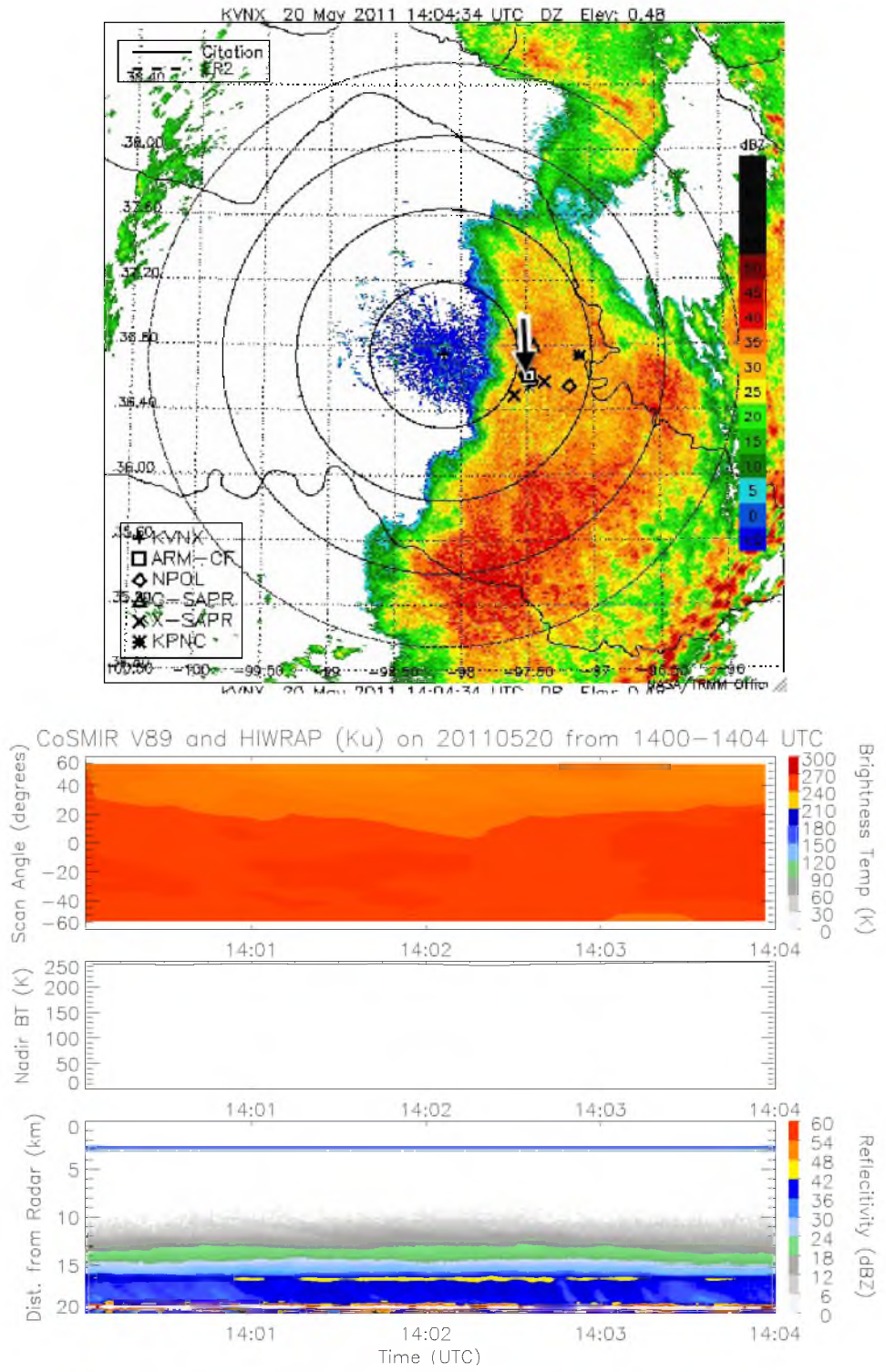

Figure 3.19. Vance, OK (KVNX) WSR-88D PPI scan and ER-2 HIWRAP and CoSMIR cross sections. Top: KVNX radar imagery overlaid with the flight paths of the ER-2 (dashed) and the UND Citation (solid) from 1400 -1404 UTC 20 May 2011. Bottom: CoSMIR 89 GHz (vertical) brightness temperature across the entire swath, 89 GHz (vertical) nadir brightness temperature, HIWRAP Ku-band nadir vertical reflectivity profile.

The supercells developed at 1705 UTC, which coincides with the times when there existed veering shear over Vici, while the linear shear coincides with the maintenance of the MCS (system 3) (veering and linearity established with criteria put forth by Bunkers (2002)), which was sustained between 0100 UTC and 1030 UTC. Following the example of Bluestein and Weisman (2000), the angle of the 1.7 - 5 km AGL shear is rotated 57° from the line of forcing for the supercells. This value exceeds the suggested 45° rotation for optimal supercell performance and avoidance of competition. Shear that is orthogonal to the line of forcing is supportive of squall line development with isolated supercells at the ends, which may explain why a shear value rotated more than 45°, such as these supercells' shear, only supported healthy supercells at either end. Rotation is no longer seen in the supercells after 0100 UTC 20 May.

As the surface trough pushed through Oklahoma over 20 May, winds ahead of the trough were southerly (Figure 3.6), winds in in the Texas panhandle shifted slightly from south/southeasterly to southwesterly around 1800 UTC. Later, the surface winds show a brief change to northwesterly in the western Oklahoma Mesonet stations around 0300 UTC 20 May. In the southwest corner of Oklahoma, particularly at the Apache, Acme, Fort Cobb, and Walters stations (for example), winds shifted abruptly to the northwesterly and temperatures dropped approximately 8°C (Figure 3.20). The shift to northwesterly in the western Mesonet stations is coincident with the arrival of outflow from the storm cells in system 1, not with the arrival of a forcing boundary, as there is no accompanying wind shift west of these stations, at Mangum, for example (Figure 3.21).

Beginning at 0720 UTC at the Cheyenne Mesonet station, winds shifted to westerly and this pattern continues across the western half of the state between 720 and 0900 UTC (Figure 3.22). The shift to westerly/southwesterly is matched in the upper levels throughout the early morning and thus, the veering profile in the lower levels at Vici is eliminated.

As the MCS (system 3) moves across Oklahoma, abrupt temperature drops on the order of 5°C, moderate pressure spikes, and shifts to westerly/southwesterly winds coincide with the arrival of the MCS on radar imagery (Figure 3.16 0944 UTC) and its location over Oklahoma (Figure 3.23). The timeseries from Minco, Norman, Shawnee, and Bristow (shown in west to east order) show this arrival plainly (Figure 3.24) as the MCS progresses across the state. The temperature drops and pressure spikes suggest the convective downdraft is over the stations mentioned above, and the corresponding wind shifts indicate that the MCS is maintained by its own outflow and cold pool.

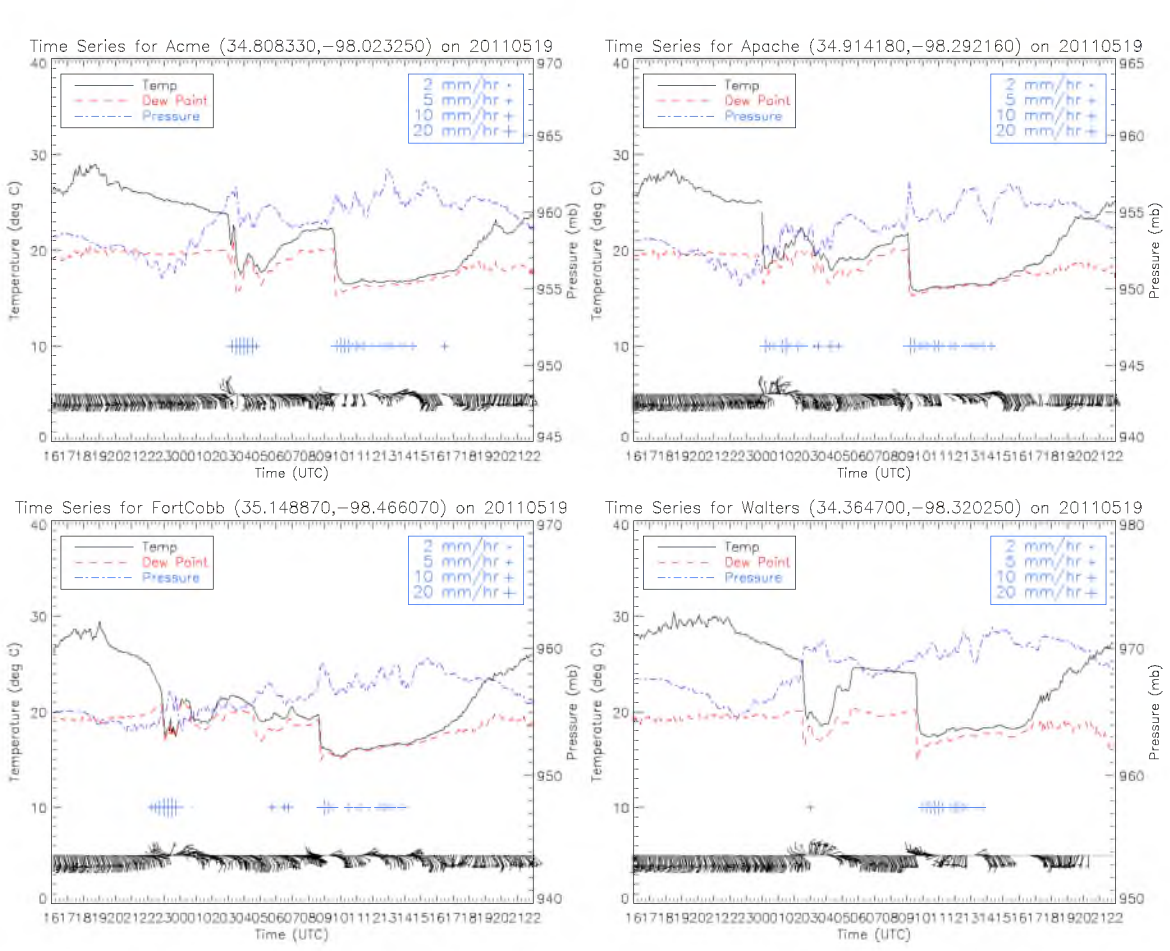

Figure 3.20. Timeseries of temperature, dew point, pressure, winds, and precipitation overnight from 1600 UTC 19 May 2011 to 2200 UTC 20 May 2011 at the Acme, Apache, Fort Cobb and Walters Mesonet Stations (locations are shown in Figure 3.7).

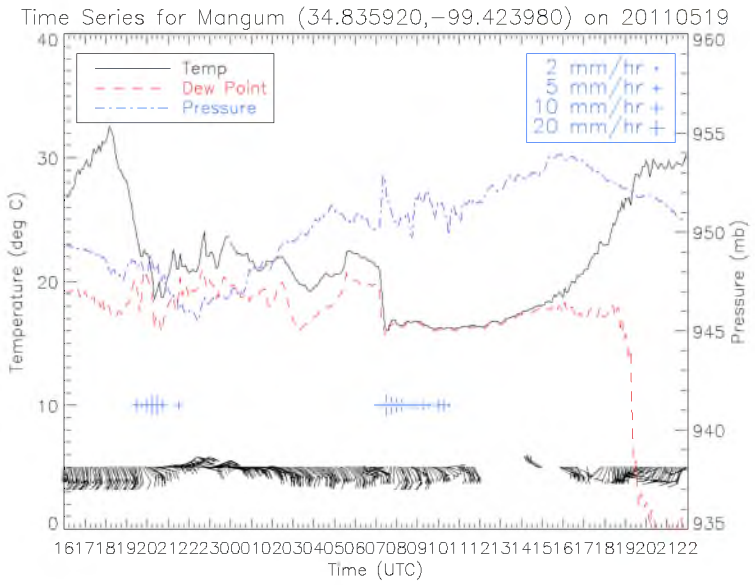

Figure 3.21. Timeseries of temperature, dew point, pressure, winds, and precipitation overnight from 1600 UTC 19 May 2011 to 2200 UTC 20 May 2011 at the Hobart and Mangum Mesonet Stations (locations are shown in Figure 3.7).

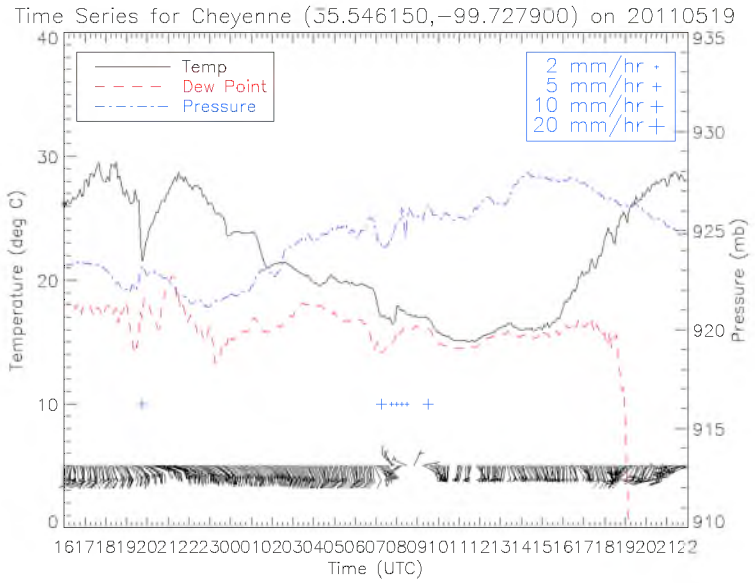

Figure 3.22. Timeseries of temperature, dew point, pressure, winds, and precipitation overnight from 1600 UTC 19 May 2011 to 2200 UTC 20 May 2011 at the Cheyenne Mesonet Station (location is shown in Figure 3.7).

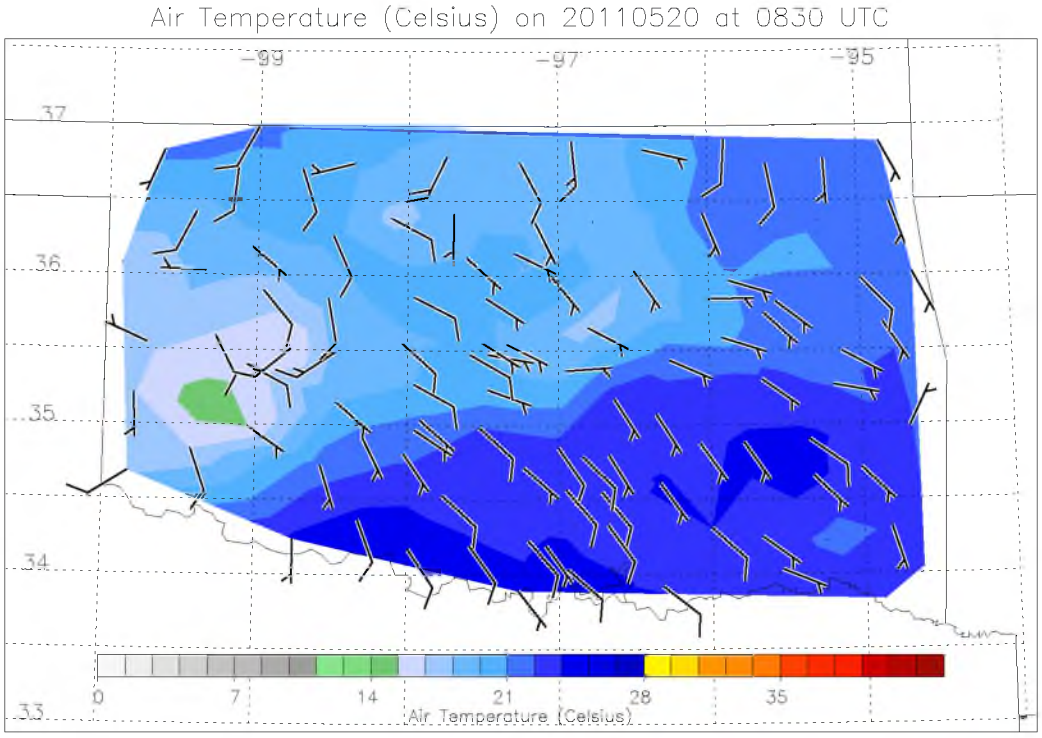

Figure 3.23. Oklahoma Mesonet altitude adjusted air temperature contour plot at 0830 UTC 20 May 2011. Overlaid with wind observations (barbs).

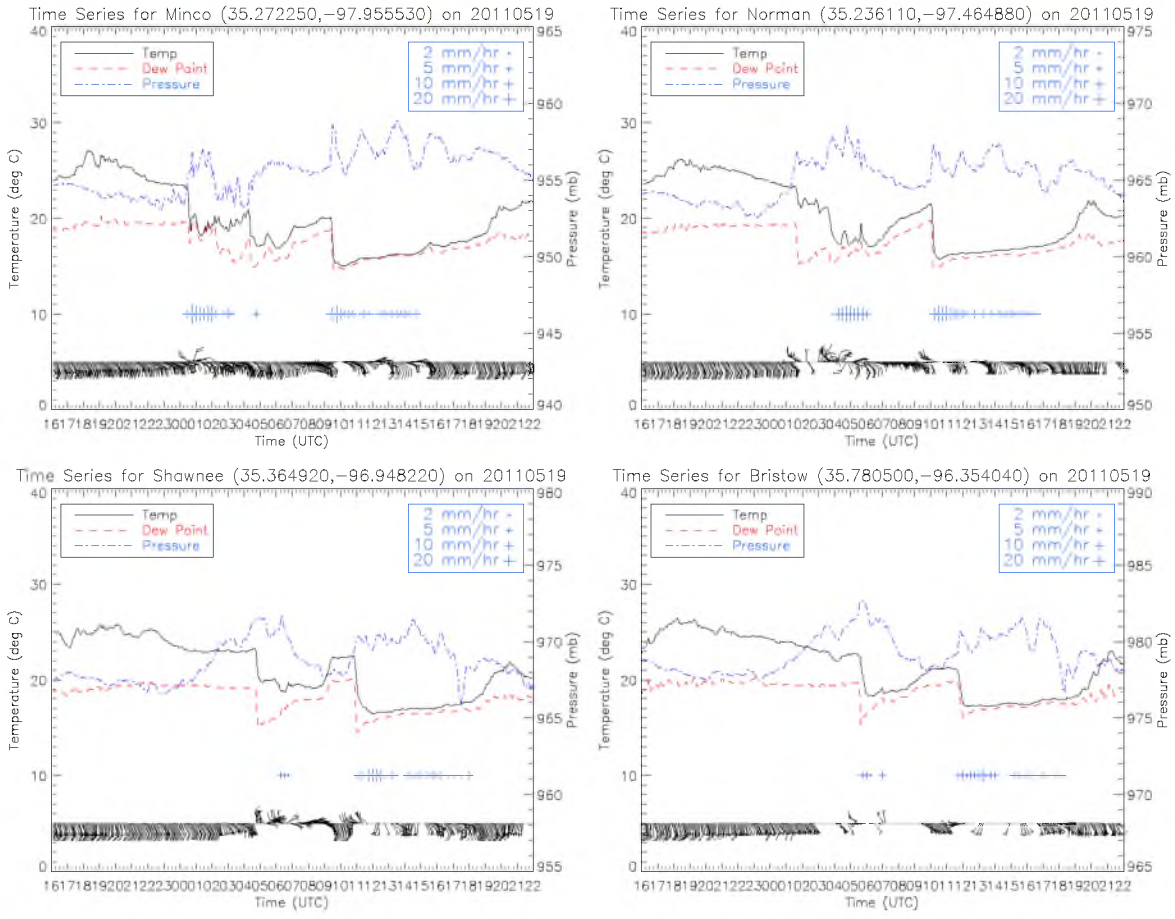

Figure 3.24. Timeseries of temperature, dew point, pressure, winds, and precipitation overnight from 1600 UTC 19 May 2011 to 2200 UTC 20 May 2011 at the Minco, Norman, Shawnee, and Bristow Mesonet Stations (locations are shown in Figure 3.14).

CHAPTER 4

EVOLUTION OF THE CONVECTION ON 23 MAY 2011

The several waves of convection on 23 May 2011 are described as follows:

- **System 0:** An MCC stalled northeast of Oklahoma and created a large cold pool.
- **System 1:** Supercells fired along the dryline at 1913 UTC.
- **System 2:** Supercells fired on the MCC's cold pool boundary at 2020 UTC.
- **System 3:** Outflow from a system 1 supercell allowed the supercell above it to back-build on the dryline from 2135 UTC to 2300 UTC, after which the dryline retreated and the cell continued to back-build via discrete propagation until 0300 UTC 24 May.

A map of the various systems and their boundaries is shown in Figure 4.1.

4.1 Prestorm Environment

4.1.1 Synoptic and Large Scale

On 22 May 2011, a low-pressure system deepened in the northwestern U.S., and a second low-pressure center was situated over the Dakotas. The troughs sat on either side of a ridge over the Rocky Mountains that built as the lows deepened. Over the course of May 23, the westernmost trough deepened and pushed eastwards, with the trough axis finally crossing the MC3E region near 0000 UTC May 24 (Figure 4.2). The trough brought with it a split upper-level jet that stretched across the central part of the continental U.S.. The jet's exit region was located at the western border of Oklahoma and Texas.

The trough generated a shortwave impulse that crossed the western U.S. over the course of 23 May. The 1145 UTC GOES-13 water vapor satellite imagery (Figure 4.3) indicates a shortwave impulse over New Mexico in the morning hours of 23 May 2011. Figure 4.4 shows Oklahoma Mesonet surface pressure data for Camargo, Minco, and Hectorville, OK (Mesonet station positions are shown in Figure 4.1), which show the progression of the

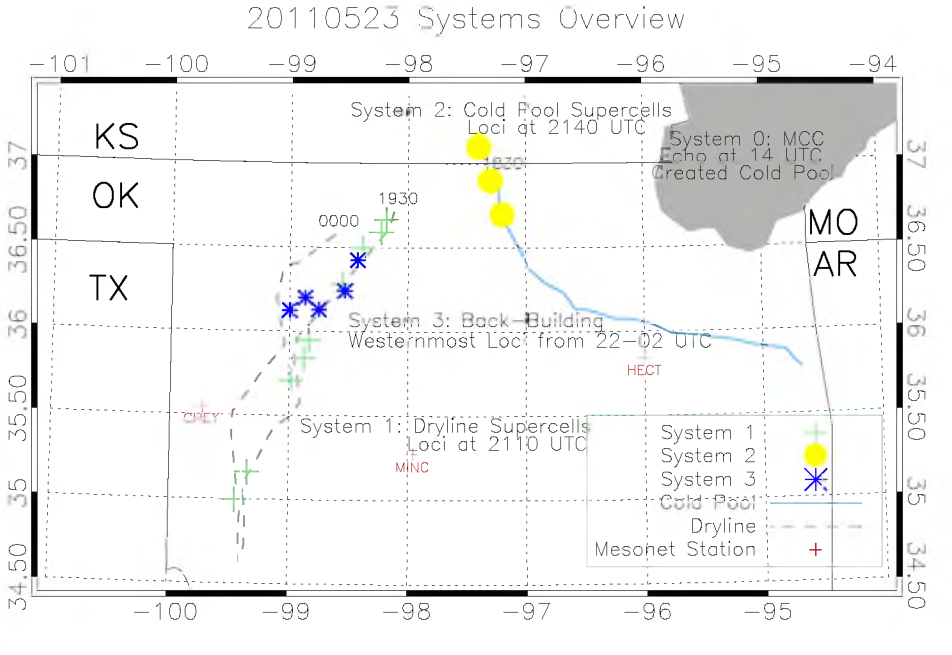

Figure 4.1. Overview of the prominent boundaries and convective systems that occurred on 23 May, 2011 in Central Oklahoma

shortwave across the northern half of Oklahoma. The time lapsed between the passage of the trough axis at each station is short, indicating a quick-moving trough. The 1728 and 2019 UTC soundings from the Central Facility are shown in Figure 4.5. The cap at 1728 UTC is near 770 hPa, whereas by 2019, the cap is at 700 hPa, suggesting that shortwave trough forced ascent as it crossed Oklahoma.

The Central Facility (CF) and Purcell, OK soundings are used as examples of the convective environment, as initiation occurred towards the center of the state. In both locations, environmental conditions were indicative of supercell development. Both the CF and Purcell exhibited significant capping at 800 hPa, which eroded substantially between 1130 UTC and 1730 UTC. By 1730 UTC, CAPE values had increased to 4696 J kg^{-1} and 4082 J kg^{-1} at the CF and Purcell, respectively. Also, throughout the course of the day, the low-level winds backed to become progressively more southerly, which in tandem with the dominant westerly flow aloft provided the veering wind profile supportive of supercell development. The hodograph from the CF at 1730 UTC shows the strong veering of the winds up to 812 hPa (Figure 4.6).

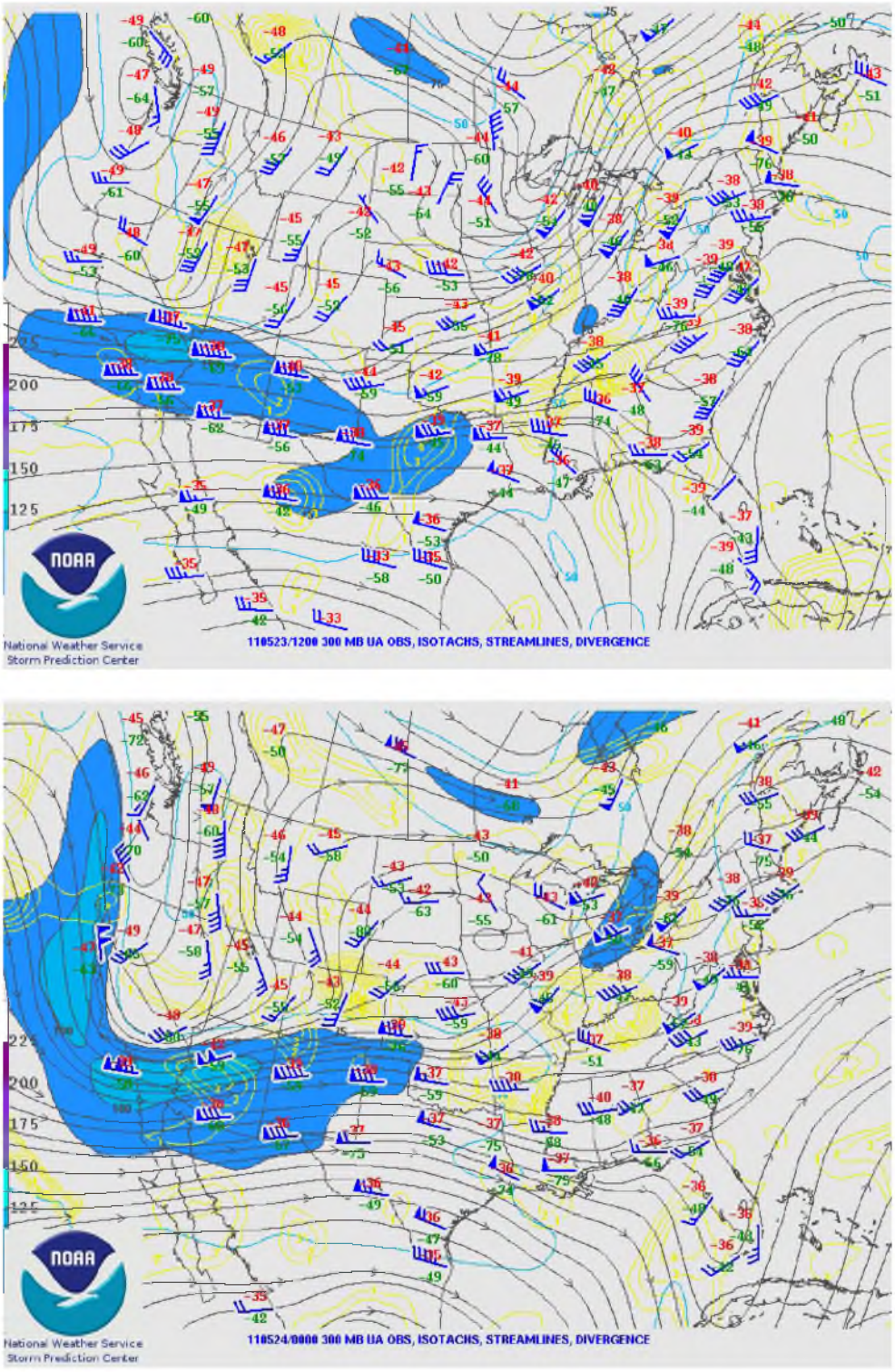

Figure 4.2. 300 hPa analysis at 1200 UTC 23 May 2011 (top) and 0000 UTC 24 May 2011 (bottom). Rawinsonde retrieved temperature, dew point, and wind observations (wind barbs coincident with numbers) and RUC Analysis streamlines, isotachs (fill), and divergence (contours). Courtesy of the National Weather Service.

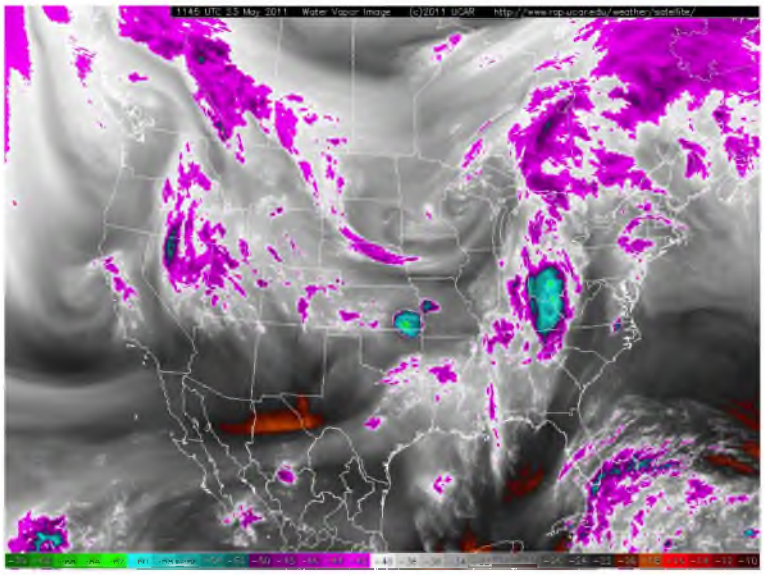

Figure 4.3. GOES 13 Water Vapor channel imagery at 1154 UTC 23 May 2011

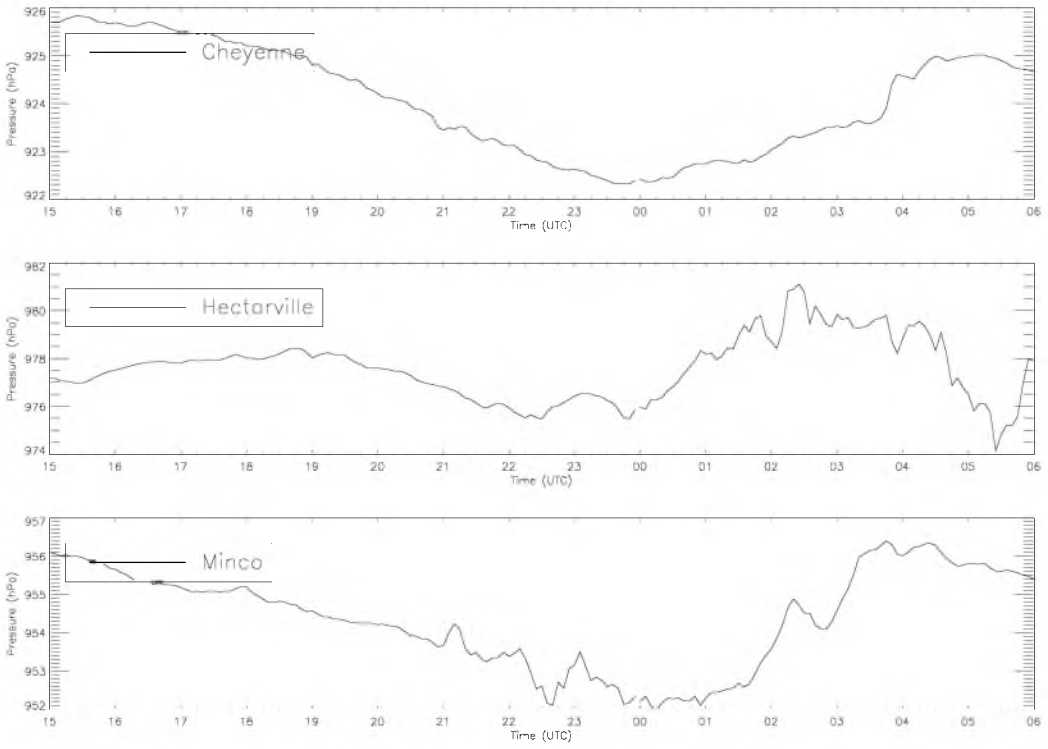

Figure 4.4. Time plot of surface pressure on 23 May 2011 at the Cheyenne, Minco, and Hectorville Oklahoma Mesonet stations. The locations of these three stations can be found in Figure 4.1.

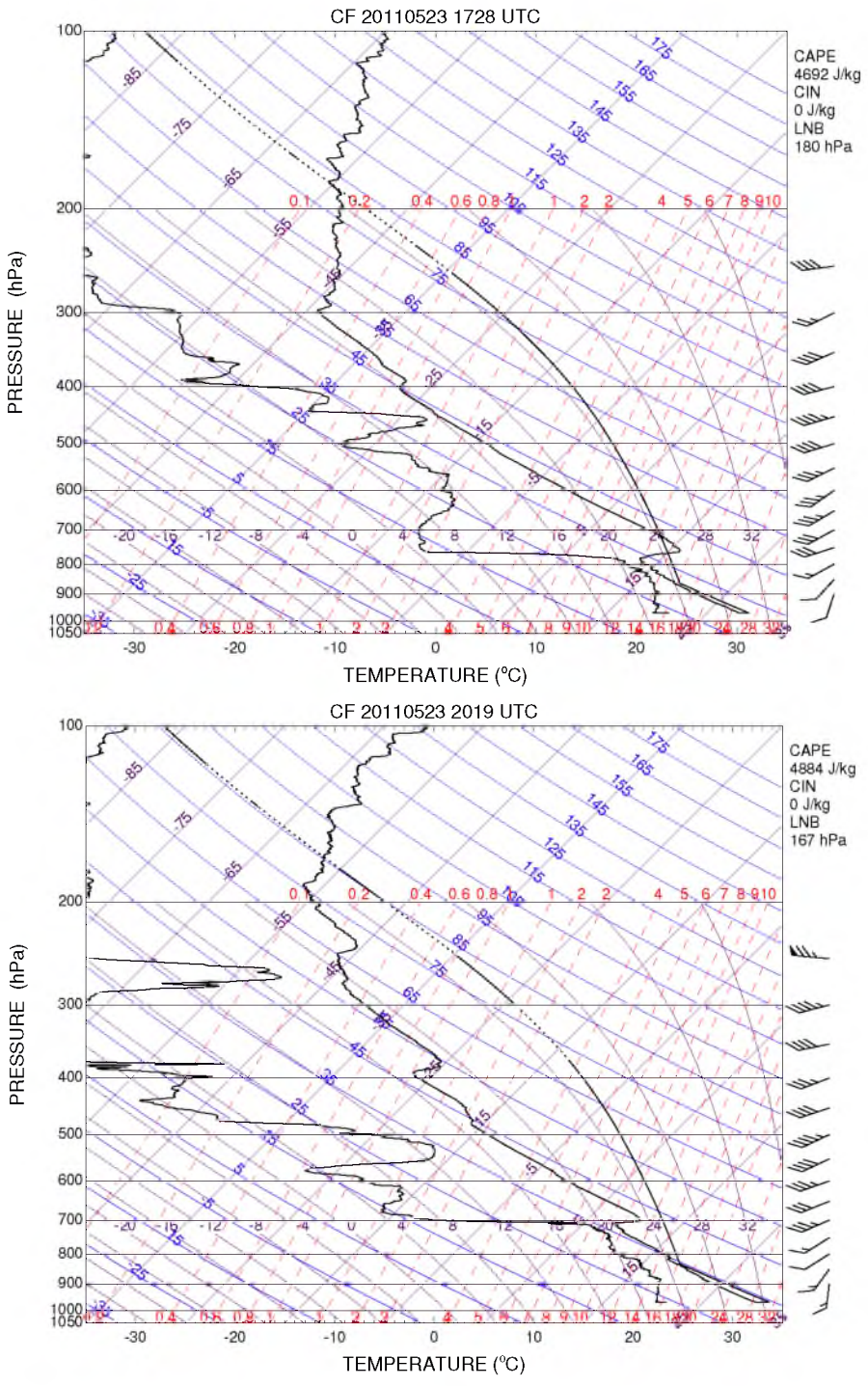

Figure 4.5. Skew-T/Log-P representations of the 1728 UTC (top) and 2019 UTC (bottom) soundings launched at the Central Facility (36.6°N/97.49°W). Radiosonde launch locations are shown in Chapter 2.

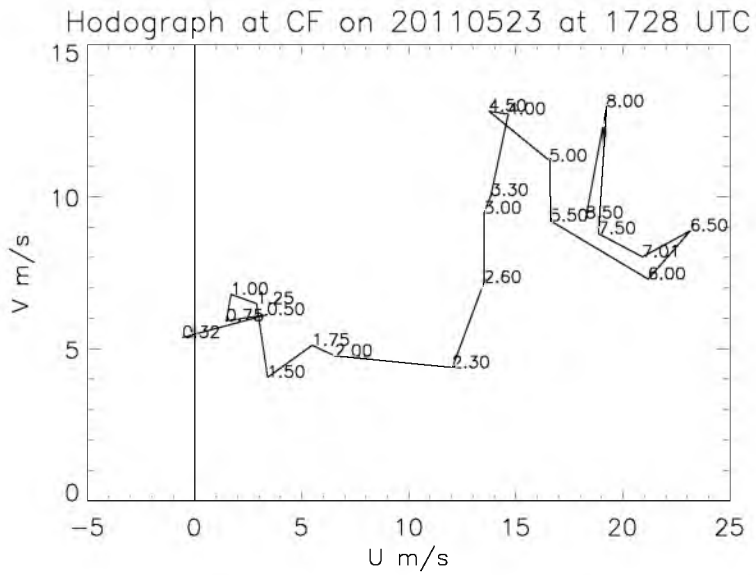

Figure 4.6. Hodograph created from the 1728 UTC 23 May 2011 Central Facility (36.6°N/97.49°W) radiosonde data.

4.2 System 0: Overnight and Early Morning Convection

The first wave of convection associated with the events of 23 May 2011 occurred on 22 May, when convection fired at 1830 UTC near the central KS-OK border at the intersection of the dryline and a cold front. The storms moved eastward as part of a large linear system that by 2330 UTC extended from Wisconsin to Texas, through Illinois, Oklahoma, and Kansas (this system ultimately caused the tragic Joplin, MO tornado) (Figure 4.7).

At 1000 UTC, convection fired in southern Kansas along a stationary front, well west of the line depicted in Figure 4.7. The system rapidly developed into a mesoscale convective complex (MCC), propagated eastwards, and stalled at the KS-OK-MO junction. The cold, massive cold shield is shown in the visible satellite imagery in (Figure 4.8). Strong, cold outflow propagated radially from this system at the surface.

4.3 System 1: Dryline Supercells

Ahead of the low, southerly flow dominated the lower levels of the atmosphere above the Great Plains, advecting warm moist air into Oklahoma throughout the course of 22 May. A dryline fluctuated over Oklahoma, Kansas, and Texas throughout May 22 and 23. As of 1830 UTC on May 23, the dryline stretched across western Oklahoma (Figures 4.9 and

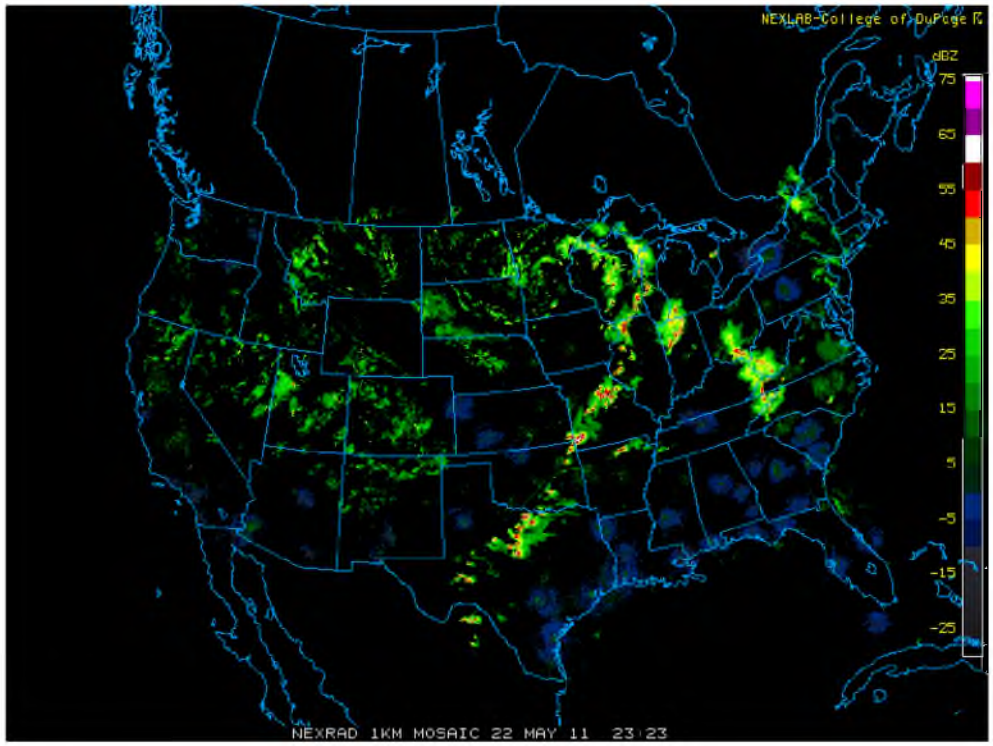

Figure 4.7. Composite WSR-88D radar imagery for the continental United States at 2330 UTC 22 May 2011. Courtesy of the National Weather Service.

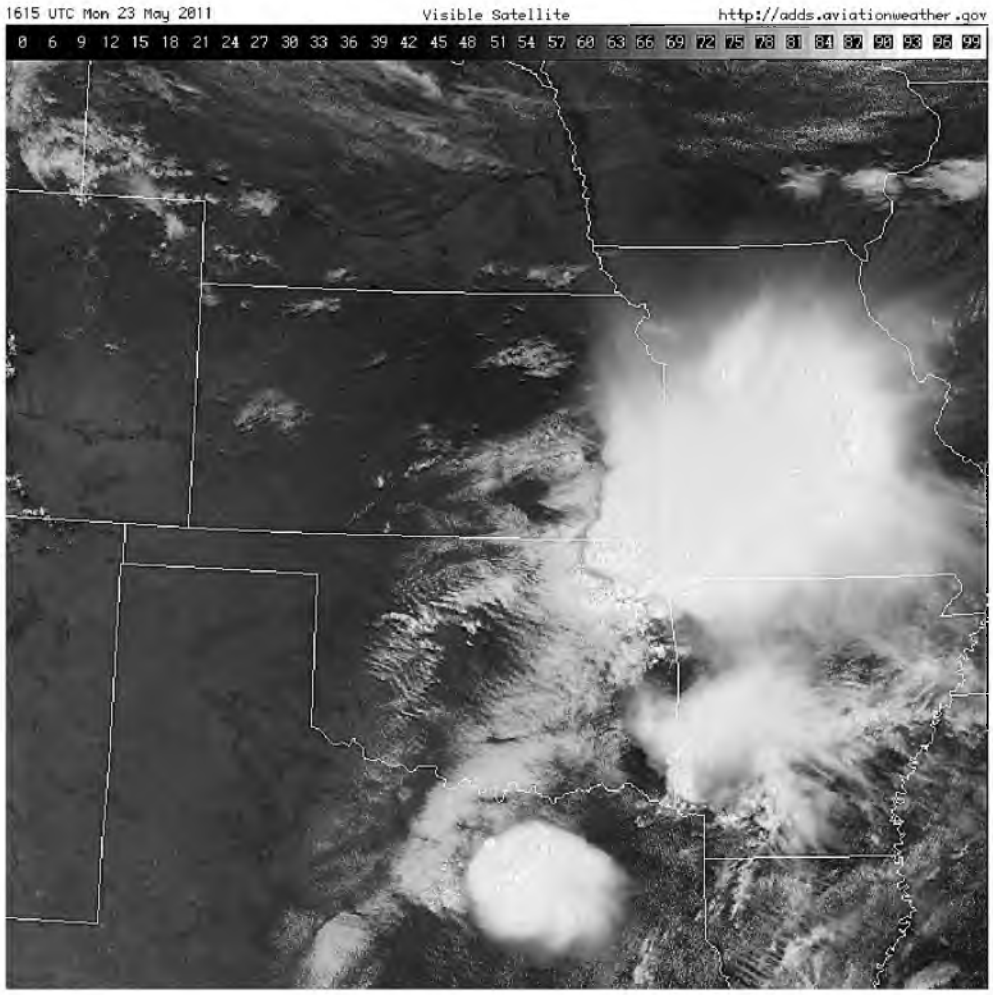

Figure 4.8. Visible satellite imagery from 1630 UTC 23 May 2011. Courtesy of the National Weather Service.

4.10).

A shortwave trough moved across New Mexico into Oklahoma and Texas during the day, and as it crossed the dryline may have contributed to lifting the air mass to its east, already extremely convectively unstable. The first cells formed along the dryline at 1913 UTC. The cells that fired on the dryline rapidly became intense, with supercell structure first visible at 2040 UTC (Figure 4.11b). The dryline cells continued to propagate eastwards in a SW-NE line from 1913 to 2136 UTC. As the cells from the dryline propagated eastwards, there is evidence of competition and merging among the supercells. The final cell in the line dissipated by 0125 UTC May 24.

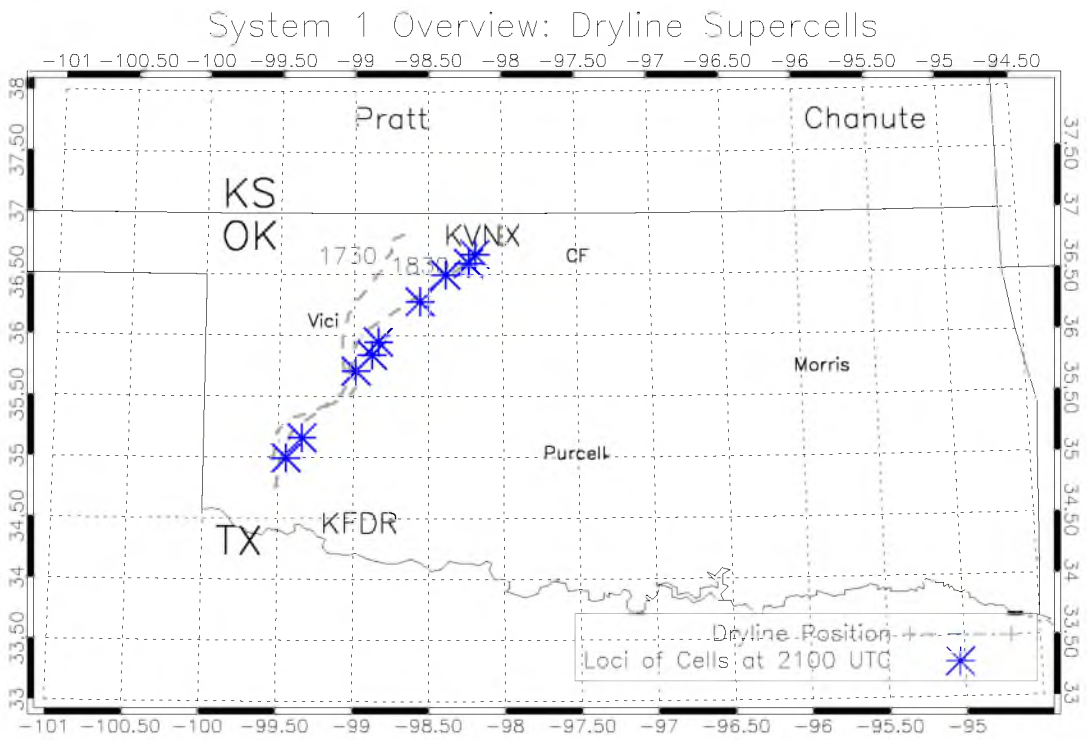

Figure 4.9. Overview of the subjectively analyzed dryline trajectory and the loci of the convective cells that fired along the dryline (first convection fired at 1913 UTC, positions here shown at 2100 UTC to show the full extent of the line).

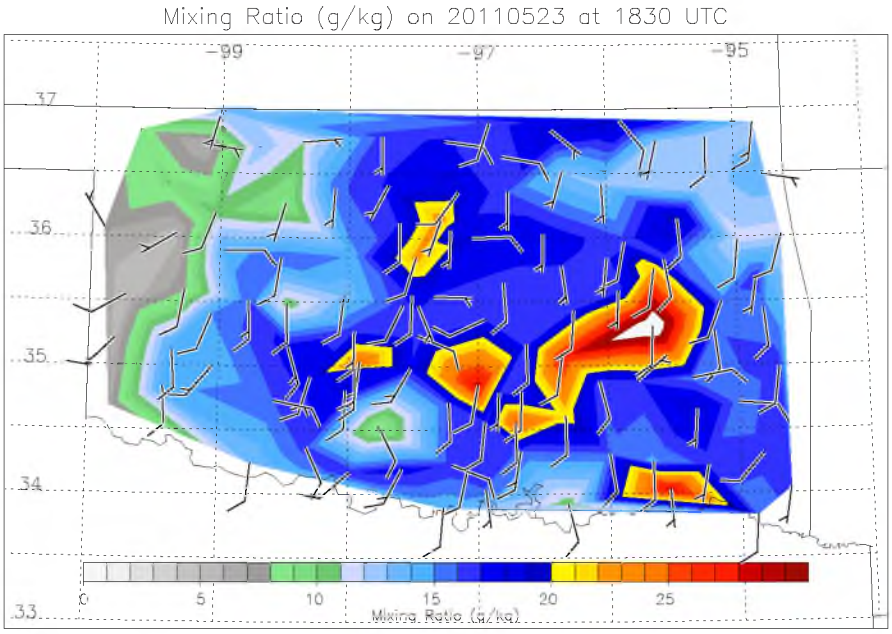

Figure 4.10. Surface water vapor mixing ratio (g kg^{-1}) calculated from Oklahoma Mesonet data at 1830 UTC 23 May 2011

4.4 System 2: Cold Pool Supercells

The MCC at the OK-KS-MO junction (System 0) created substantial outflow; bow echoes formed at the eastern and southeastern periphery of the storm. An overview of the relevant boundaries and positions of convective cells is shown in Figure 4.12. At 1330 UTC at Chanute, KS (37.68°N/95.46°W), the convection was developing to the southwest when the sounding was taken (Figure 4.13). Figure 4.14a shows a shallow layer of cold, moist air (607 m thickness) and southwesterly low-level winds. This suggests that the convection early on was creating a cold pool.

The next sounding (Figure 4.14b), taken at 1730 UTC, shows a shallow, cold layer of air at the surface that is 651 meters deep. The lower level winds are from the south/southeast, suggesting that the near surface air is still within the cold pool generated by the MCC. The temperature at the surface would have been 28°C (following a dry adiabat); however, within the cold pool, the surface temperature is 18°C.

The extent of the western edge of the outflow boundary is evident in the Oklahoma Mesonet data, with air temperatures dropping several degrees, winds often shifting to east northeasterly, and pressure spikes at the stations in the northeastern corner of the state as the cold pool propagated into Oklahoma (Figure 4.15). The isochrone plot (Figure 4.12)

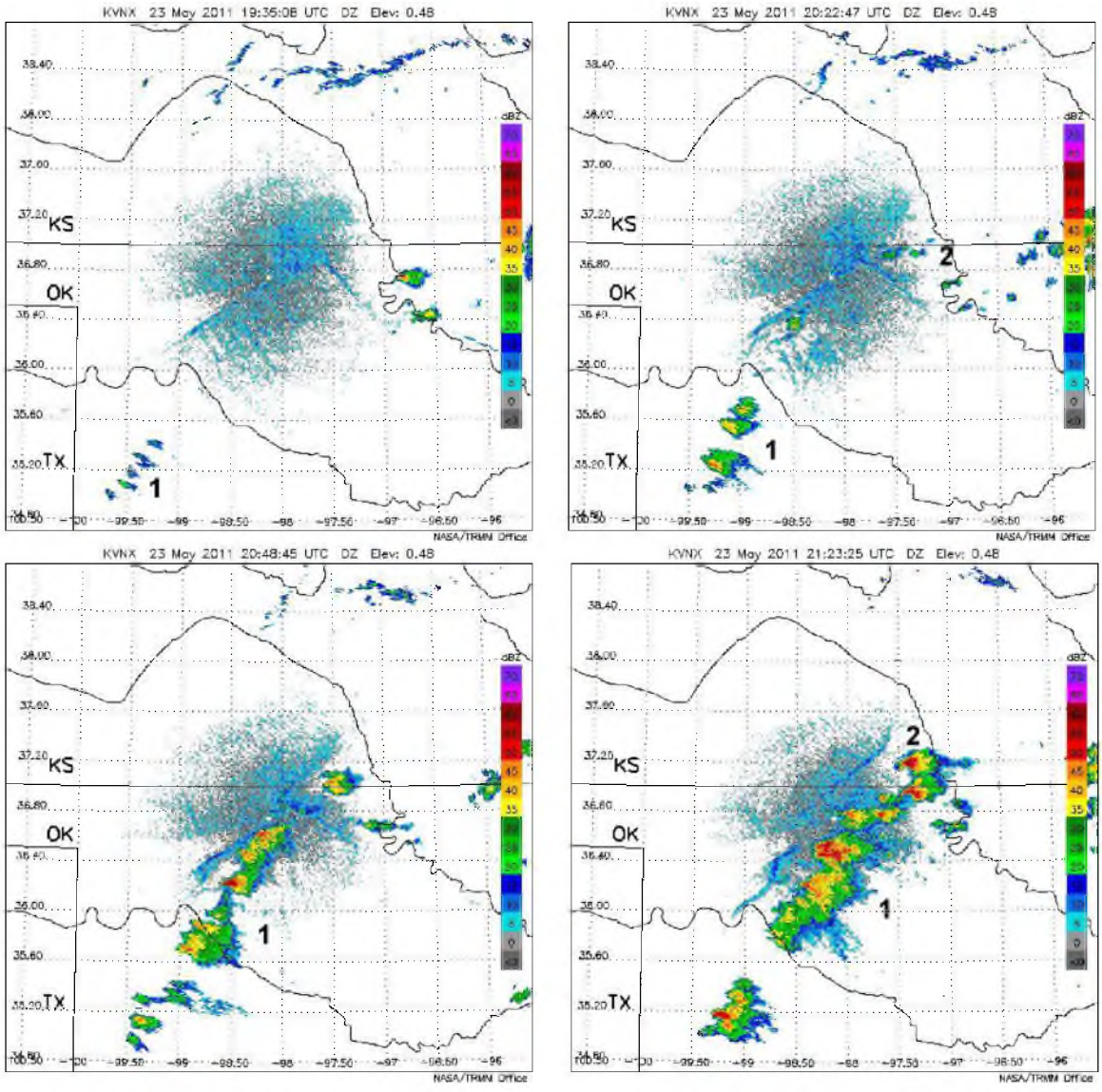

Figure 4.11. Radar timeline of system 1 from the Vance, OK (KVNX) WSR-88D radar. The timeline illustrates first cells (1935 UTC); linear extent of the initiation (2022 UTC); supercell structure (2048 UTC); and severe appearance of the northernmost cells (2123 UTC).

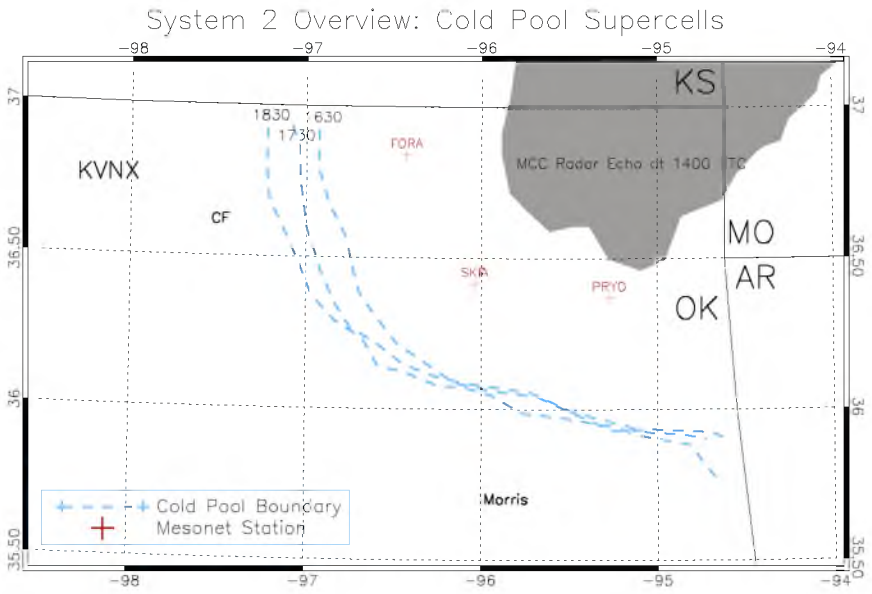

Figure 4.12. Overview of the subjectively analyzed cold pool trajectory, the loci of the convective cells that fired along the cold pool's western boundary, and the locations of the relevant Oklahoma Mesonet stations.

shows the western boundary of the cold pool as determined subjectively from the Mesonet data, using the criteria listed above.

While the effects of this cold pool on the propagation of the MCC will not be discussed, this cold pool was able to initiate strong convection at its western boundary, which lifted the moist southerly flow (Figure 4.5) that persisted for most of the day.

Storms fired along the western cold pool boundary, and can be detected in radar imagery at 2020 UTC along the western edge of this boundary and exhibited supercell structure by 2110 UTC (Figure 4.13b). A well-developed hook echo can be seen in the centermost cell at (37°N/97.4°W). Four distinguishable cells formed on this boundary within 100 km. By 2245 UTC, it becomes difficult to isolate one cell in particular due to the interaction between the storms, and after 2300 UTC, the storms have evolved into a large stratiform region with intense embedded convection and they move eastward away from the locus of convective initiation (Figure 4.13d).

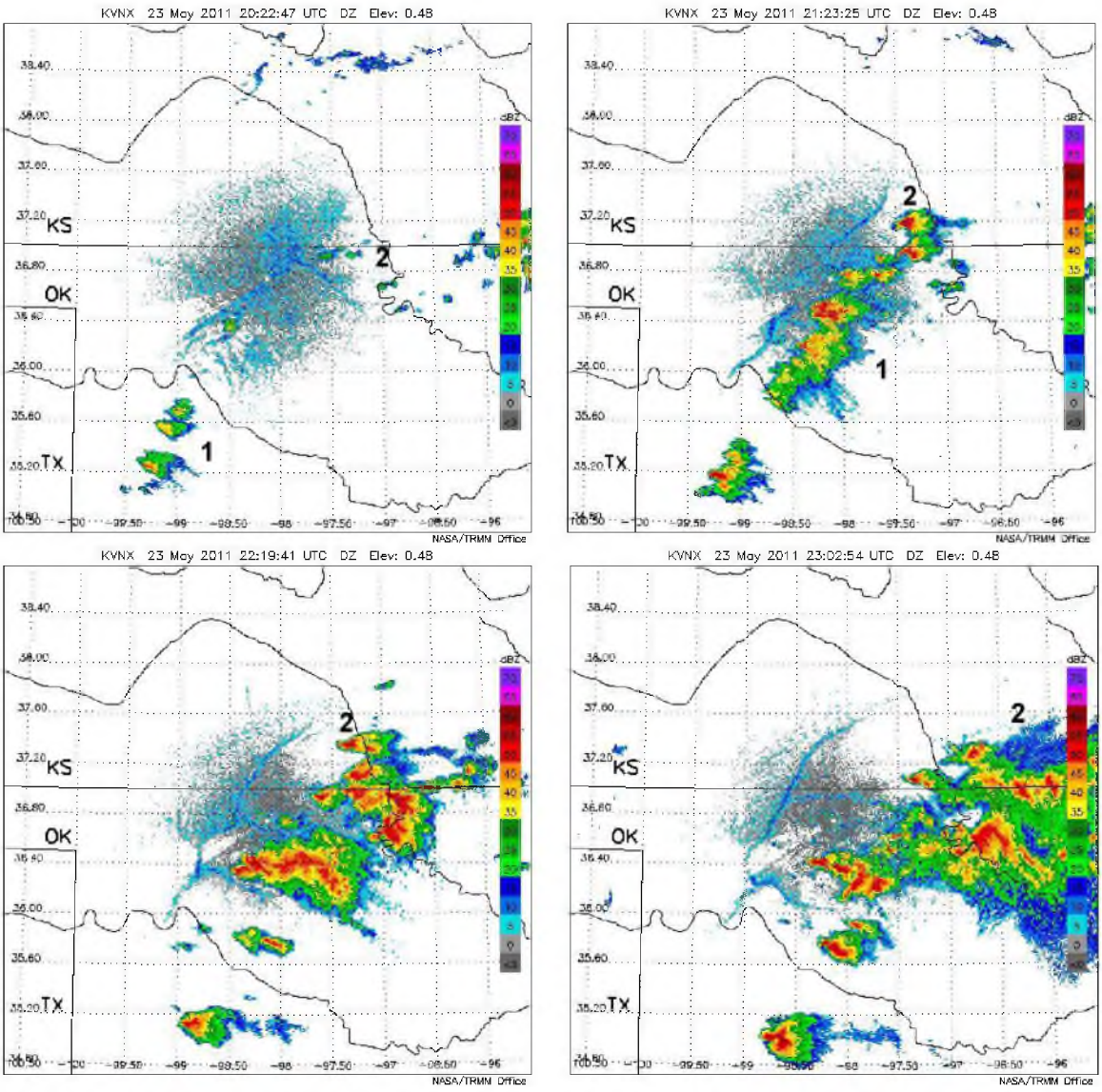

Figure 4.13. Radar timeline of system 2 from the Vance, OK (KVNX) WSR-88D radar. The timeline illustrates first cells (2022 UTC); the appearance of hook echoes (2123 UTC); the loss of organization (2219 UTC); and the dissipation into stratiform (2302 UTC).

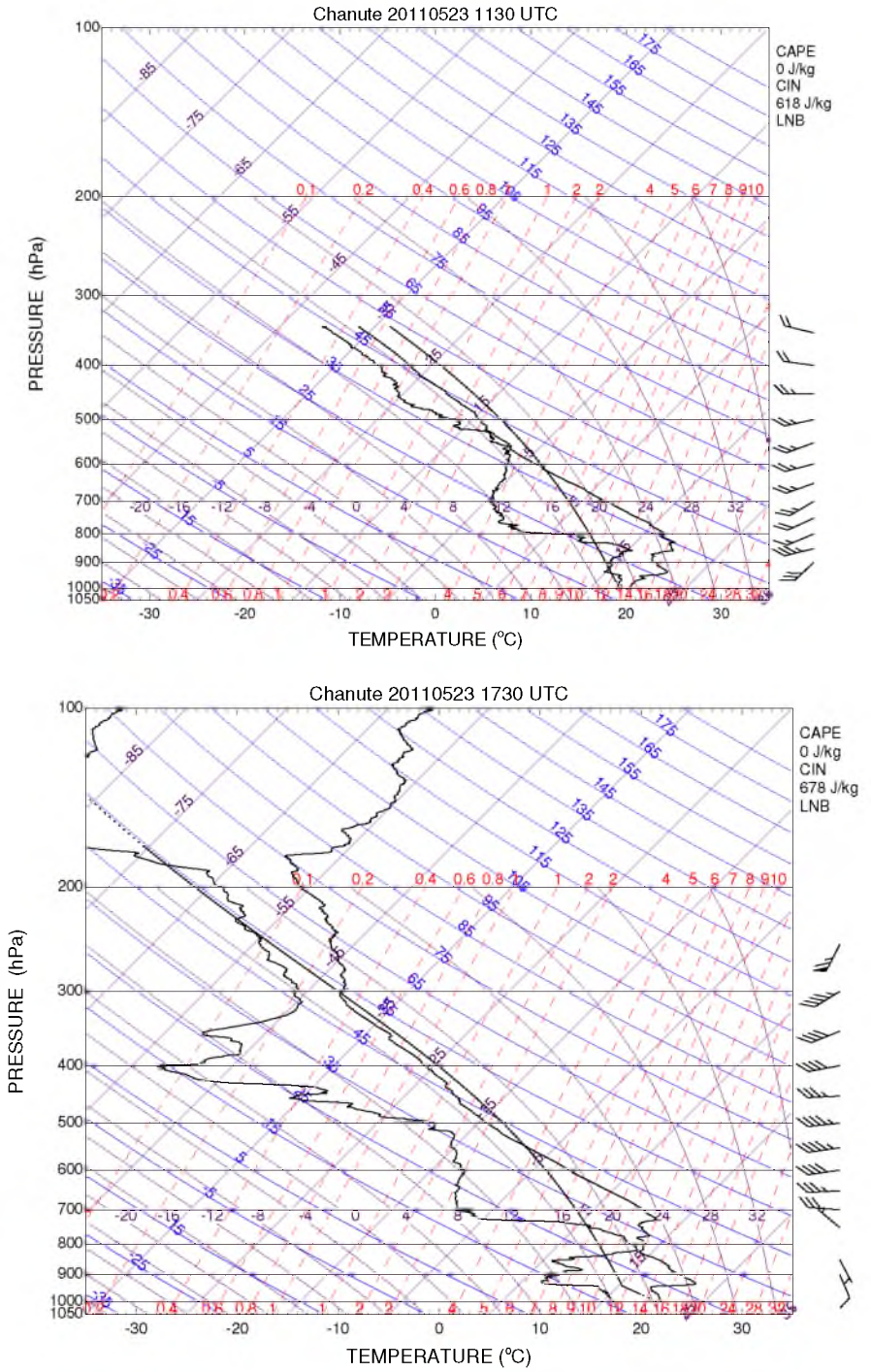

Figure 4.14. Skew-T/Log-P representations of the 1130 UTC (top) and 1730 UTC (bottom) soundings launched at Chanute, KS (37.68°N/95.46°W). Radiosonde launch locations are shown in Chapter 2.

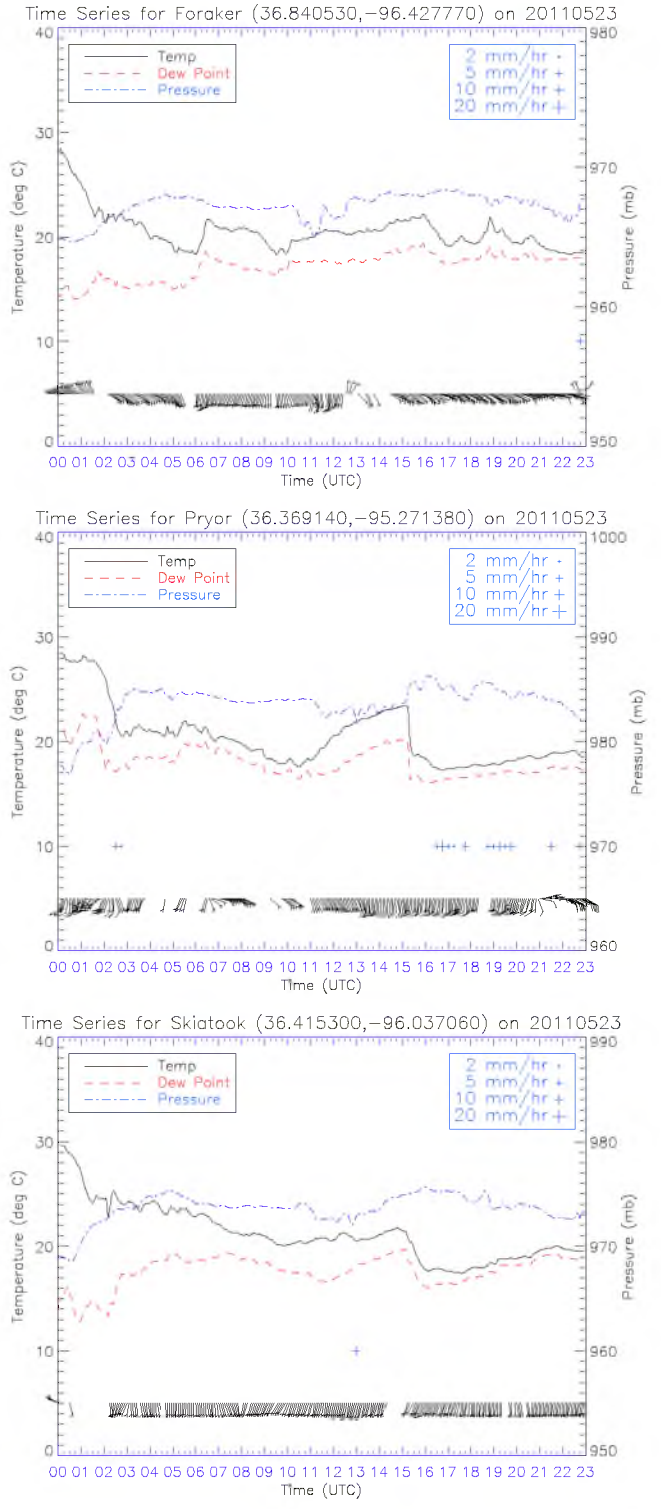

Figure 4.15. Timeseries of the Foraker, Pryor, and Skiatook Oklahoma Mesonet station data for the course of the day on 23 May 2011. Station locations are shown in Figure 4.12.

4.5 System 3: Back-Building Convection

At 2132 UTC, the second northernmost cell (36.4°N/98.3°W) in the dryline-forced line began to back-build, with new cells developing on its western flank at the intersection of dryline and outflow from the supercell south of the back-builder (the orientation suggests it is the rear flank downdraft). An overview of the relevant system boundaries is shown in Figure 4.16 and a timeline of the reflectivities of system 3 is shown in Figure 4.17.

Cells spawned by the back-building system maintained updrafts strong enough to produce a weak echo region (WER) (Figure 4.18) and were responsible for large hail. The slightly negative differential reflectivity signature (Figure 4.18) suggests the presence of hail aloft in the NPOL radar imagery. These signatures are discernible for several hours throughout the second (discrete) phase of the back-builder's lifecycle (Figure 4.19), and are discussed below and in section 6.

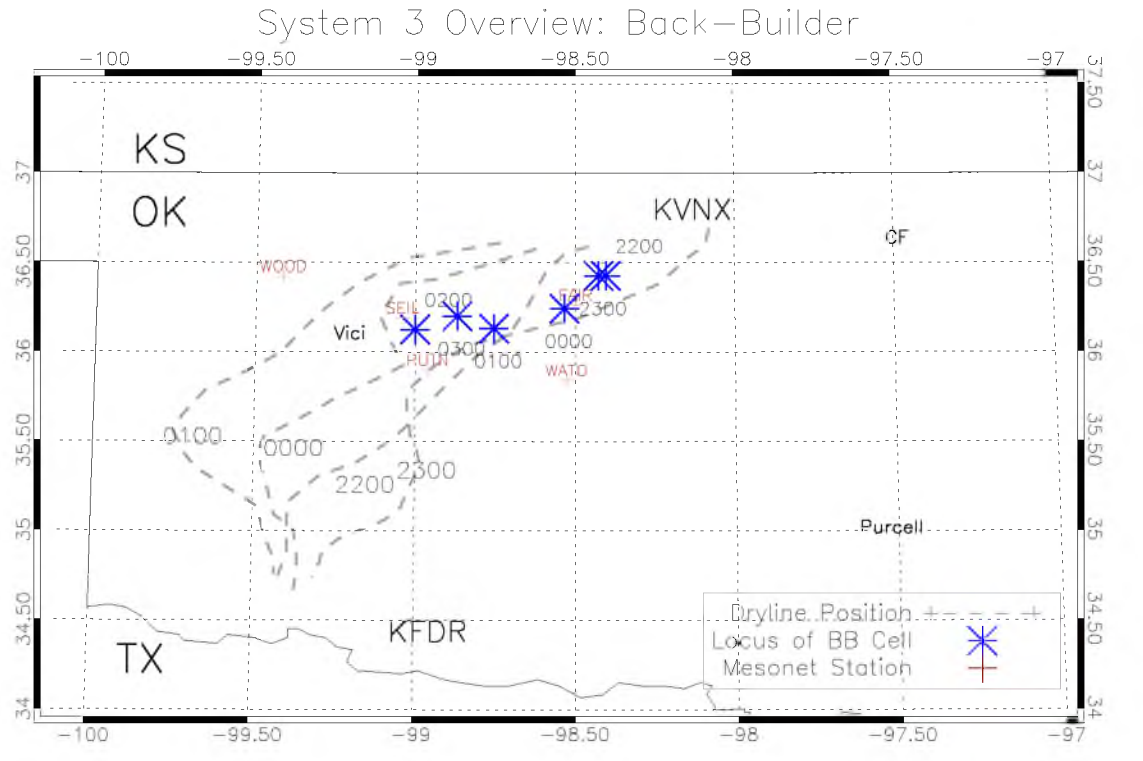

Figure 4.16. Overview of the subjectively analyzed dryline trajectory, the loci of the convective cells (westernmost extent) that back-built between 2130 UTC 23 May 2011 and 0400 UTC 24 May 2011, and the relevant Oklahoma Mesonet stations.

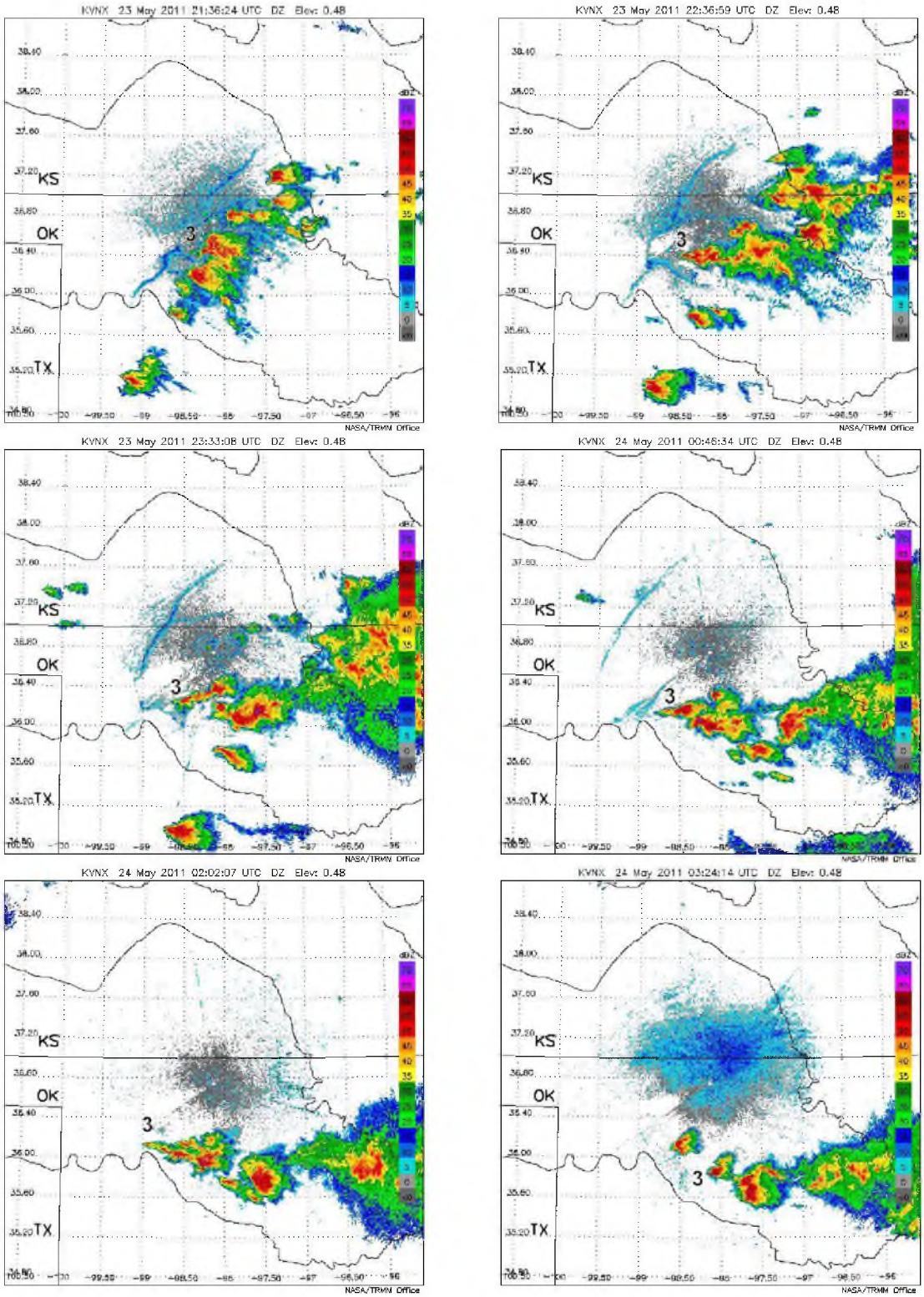

Figure 4.17. Radar timeline of system 3 from the Vance radar, showing the first back-building (2136 UTC); quasi-stationary growth (2236 UTC); continuation (2333 UTC); new SW cells (0046 UTC); SW growth (0202 UTC); and dissipation (0324 UTC).

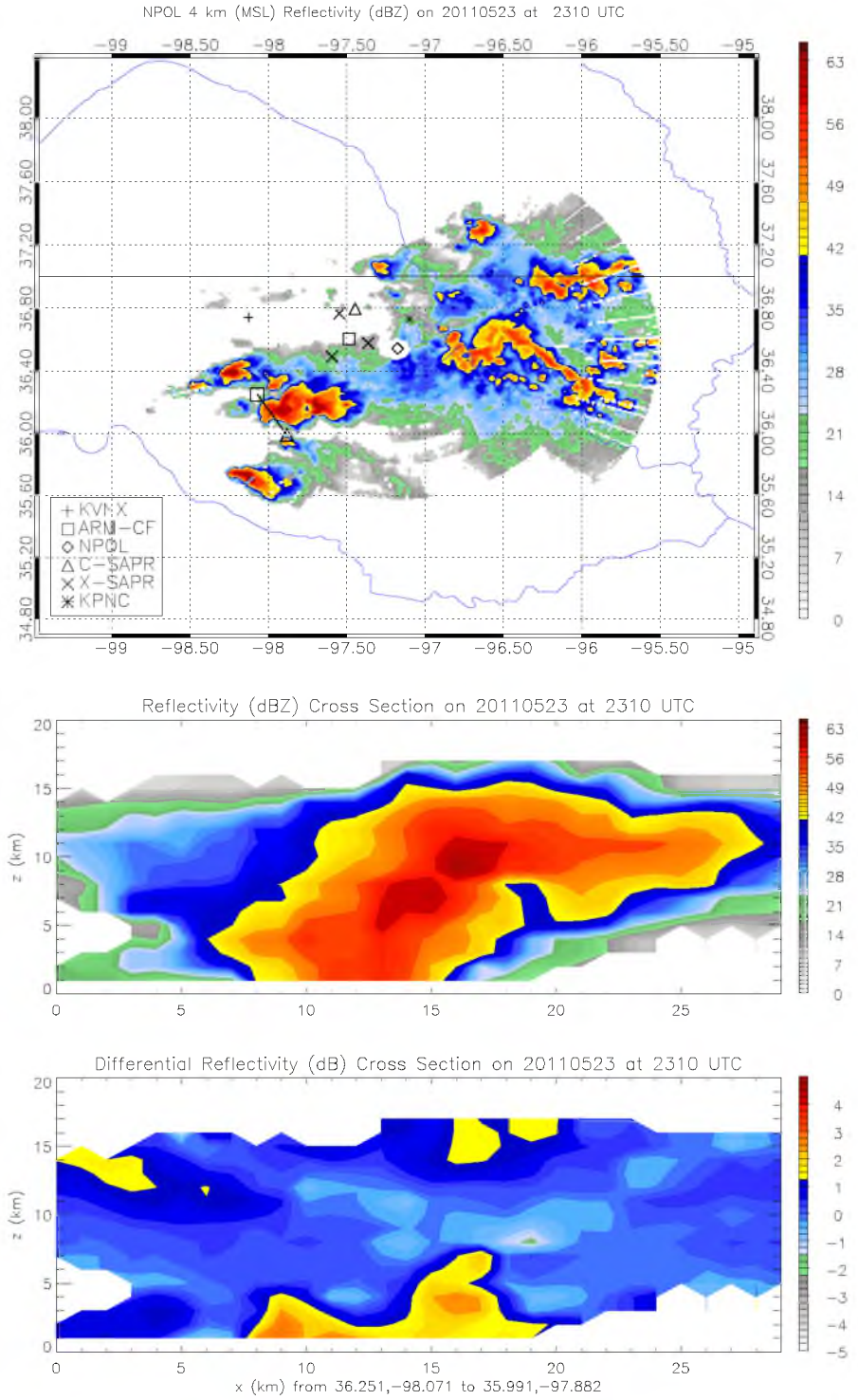

Figure 4.18. NPOL 4 km CAPPI overlaid with the path of the cross-section shown underneath. NPOL reflectivity (middle) and differential reflectivity (bottom) cross-sections at 2310 UTC 23 May 2011.

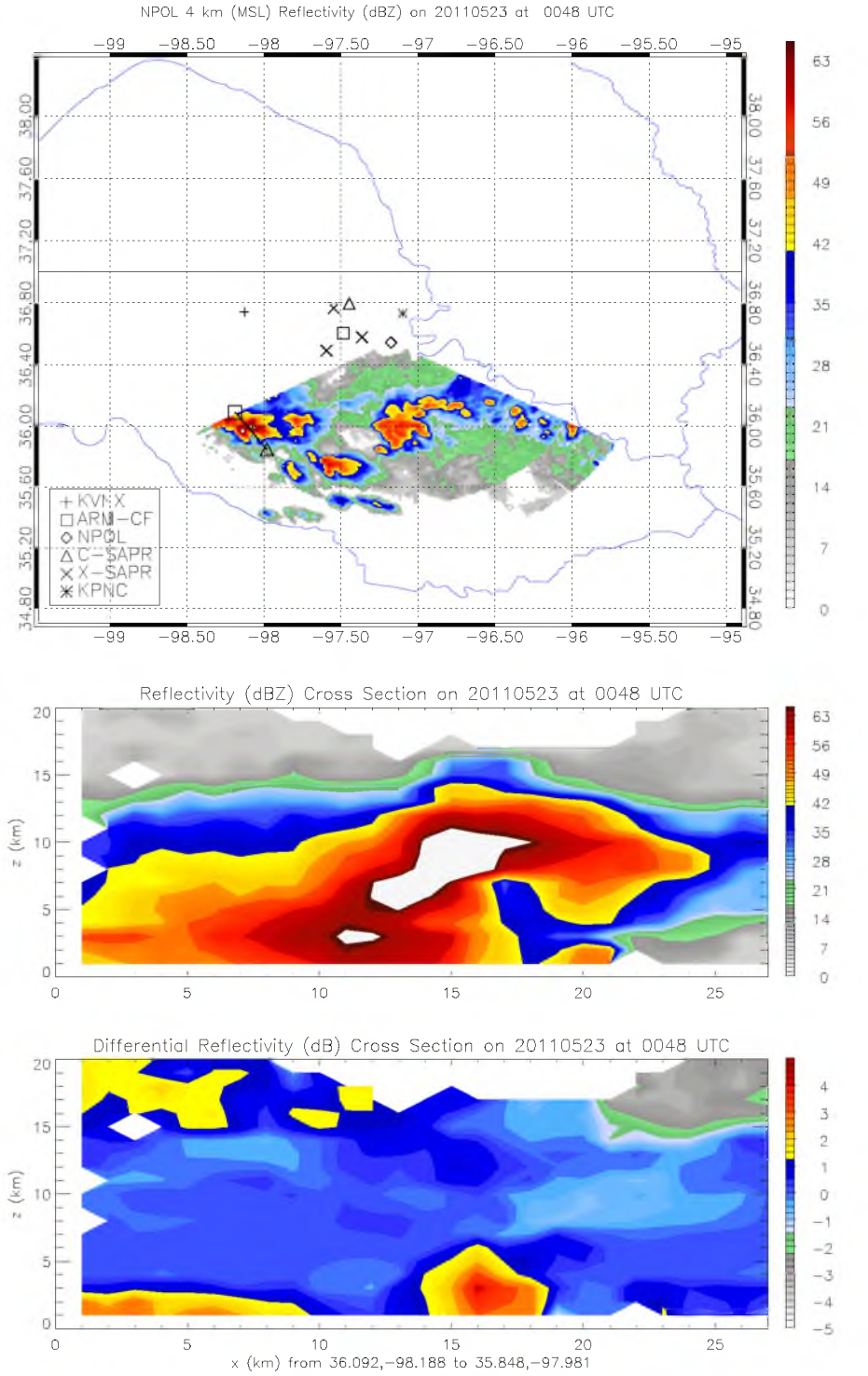

Figure 4.19. NPOL 4 km CAPPI overlaid with the path of the cross-section shown underneath. NPOL reflectivity (middle) and differential reflectivity (bottom) cross-sections at 0048 UTC 24 May 2011.

The back-building system remained quasi-stationary from 2135 to approximately 2300 UTC, its new cells forming in the same location during this period; therefore, its propagation was continuous. However, after 2300 UTC, new cells began to form southwest of the parent cell, the final cell developing at (36.15°N/98.8°W). The traveling loci of the back-building cells can be seen in Figure 4.16 and the Vance, OK radar timeline (Figure 4.17). This method of propagation is more reminiscent of the discrete propagation discussed by Houze (2004).

The ER-2 aircraft flew over the system early in its back-building lifecycle at 2145 UTC. Figure 4.20b shows the vertical Ku-band reflectivity (HIWRAP) and CoSMIR brightness temperatures, and Figure 4.20a shows the position of the ER-2 during this segment. Radar echoes reach 15 km in altitude. The 89 GHz (vertical channel) brightness temperatures reach 100 K at their lowest point in the overpass, indicating very strong ice scattering.

Later in the lifecycle of the back-builder, at 0125 UTC 24 May, the ER-2 flew over an intense convective cell at (36°N/98.4°W). Echoes in this overpass exceeded 17 km, and the CoSMIR 89 GHz brightness temperatures dropped below 70 K (Figure 4.21). The HIWRAP Ku-band radar recorded radar echoes that exceeded 16.8 km; however, the measurements make it impossible to know by how much. We will use 16.8 km as the echo height. A level of neutral buoyancy (LNB) of 13.4 km is estimated from the 2030 UTC Purcell sounding (Figure 4.22).

In order to reach (at least) 3.4 km above the LNB, if this sounding represents the environment of this storm, the negative buoyancy would be approximately 2380 J kg^{-1}, requiring the maximum speed of the updraft at the tropopause to be 69 m s^{-1}. There is direct evidence from the EDOP radar of particle updraft speeds of at least 39 m s^{-1} (Heymsfield et al. 2013). Clearly, this cell and many of the other cells in this system were extremely intense, as evidenced by the hail reports made on this day, with hail sizes exceeding 3 inches (23 cm) (Figure 4.23).

4.6 Propagation

The three convective events of 23 May were very different in nature; their morphologies included supercells, MCCs, and back-building. While the events of 22 May and the MCC that fired at 1000 UTC on 23 May are pertinent, we will focus on the convection that took place within the MC3E domain, those being the outflow-forced supercells on the western edge of the MCC's cold pool, the dryline-forced supercells, and the back-builder.

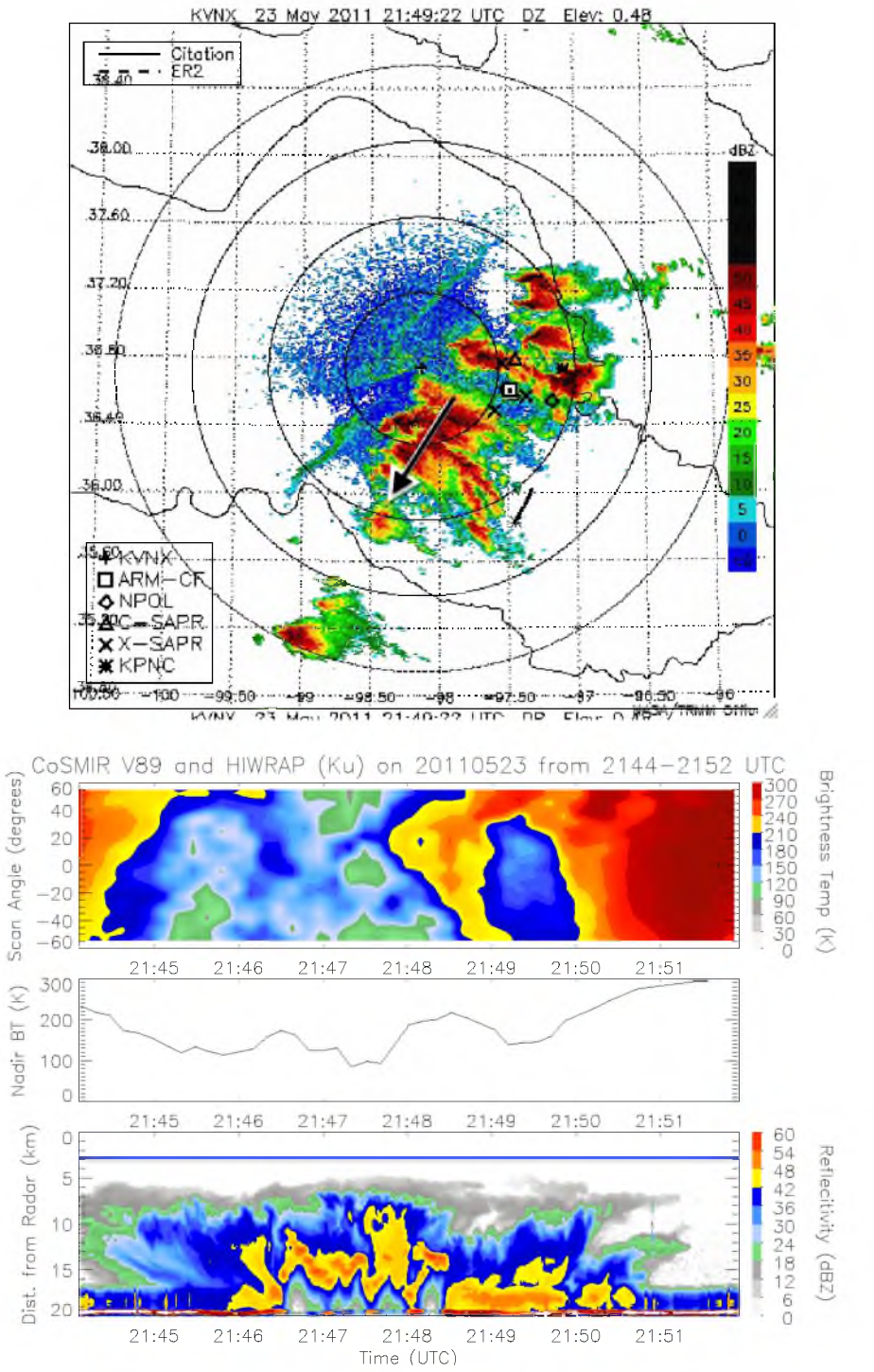

Figure 4.20. Vance, OK (KVNX) WSR-88D PPI scan and ER-2 HIWRAP and CoSMIR cross sections. Top: KVNX radar imagery overlaid with the flight paths of the ER-2 (dashed) and the UND Citation (solid) from 2145 - 2149 UTC 23 May 2011. Bottom: CoSMIR 89 GHz (vertical) brightness temperature across the entire swath, 89 GHz (vertical) nadir brightness temperature, HIWRAP Ku-band nadir vertical reflectivity profile.

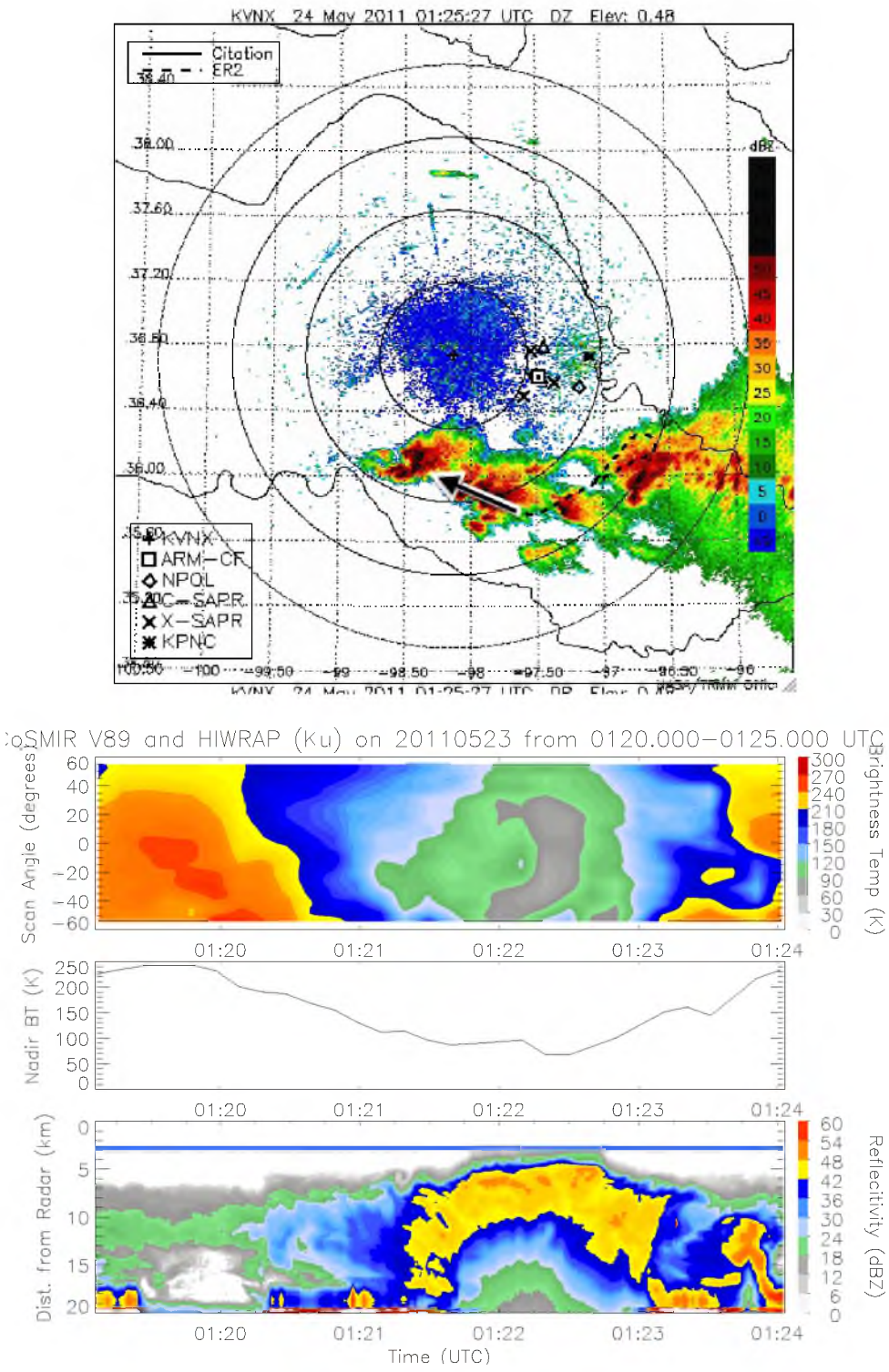

Figure 4.21. As in Figure 4.20 from 0125 - 0129 UTC 24 May 2011

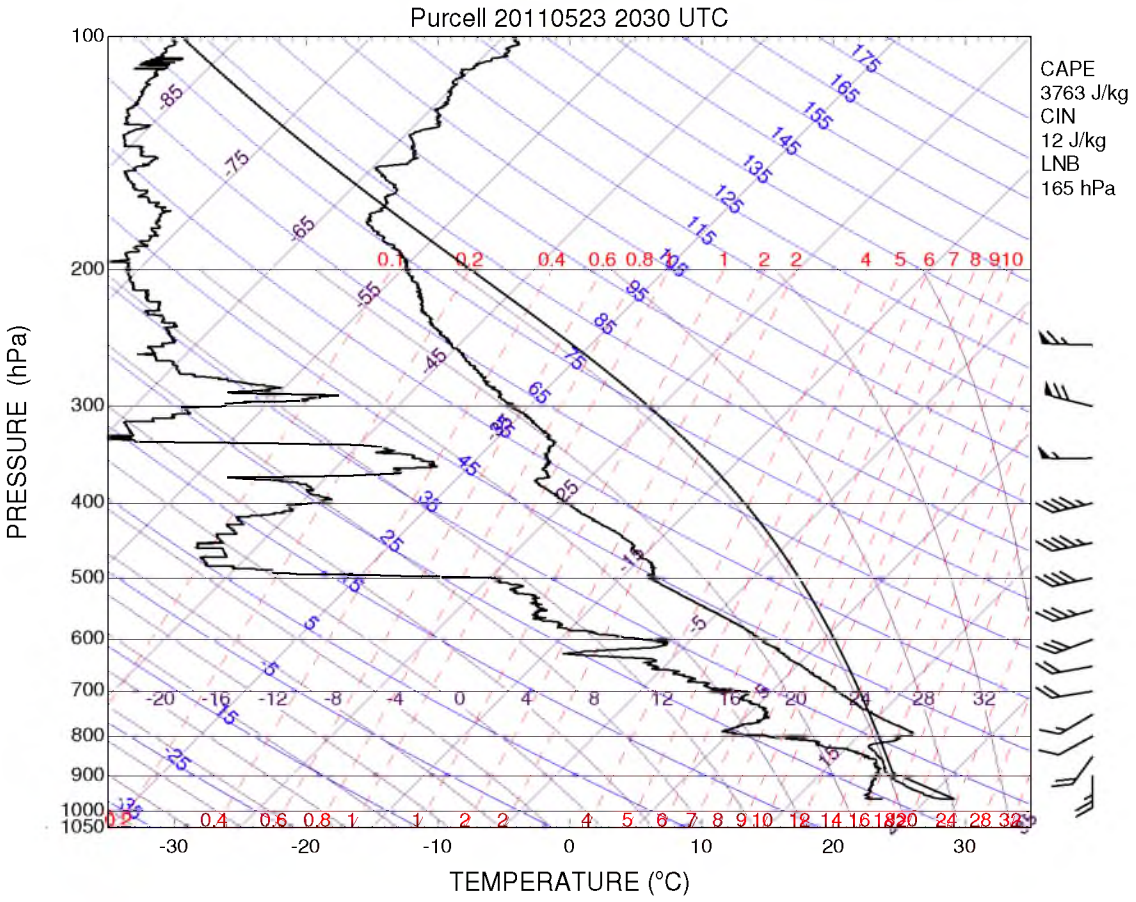

Figure 4.22. 2030 UTC 23 May 2011 skew-T/log-P representation of the sounding taken at Purcell, OK (35.02°N/97.37°W). Radiosonde launch locations are shown in Chapter 2.

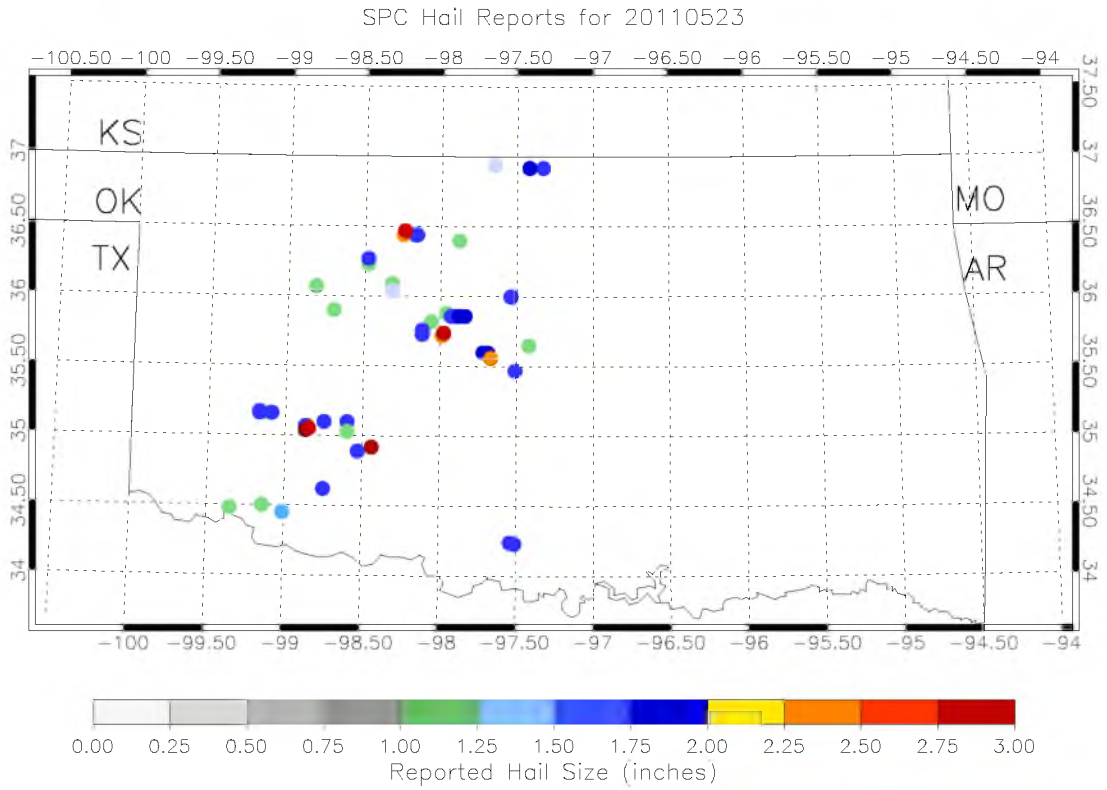

Figure 4.23. Locations of hail reports collected by the Storm Prediction Center (SPC) for the events of 23-24 May 2011. Color indicates reported hail size.

The cold pool that propagated into northeastern Oklahoma had a strong temperature depression (10°C), and in the presence of the strong southerly flow in the middle of the state, created strong convergence, resulting in supercell convection. The appearance of radar echoes coincides directly with the arrival of the cold pool at the locus of new cell growth. The northeasterly winds at the surface in combination with the southerly to westerly veering winds aloft (Figure 4.5) would have provided strong wind shear and maintained the veering of the winds with height. At the CF at 2030 UTC, just south and west of the line, there was 4888 J kg^{-1} of CAPE, which in combination with the strong wind shear could easily support supercell development. However, the supercells grew along a curved boundary roughly aligned SE-NW, moving quickly to locations deep within the cold air pool, and thus, they could not be maintained as if they could still tap the moist southerly air flow, and very shortly after their first hour of growth, they lost their supercell structure and weakened, evolving quickly into an MCS with mostly stratiform precipitation.

The dryline cells, conversely, fired in a SW-NE line, and were oriented in such a way that the updrafts on their southeast flank retained access to the southerly moist flow. The 1730 UTC CF sounding reveals that the above 1.7 AGL shear (1.7 km - 5 km) is rotated clockwise 24° from the line on which the supercells fired. Bluestein and Weisman (2000) found that 45° is ideal, whereas 0° causes destructive competition among the cells. A rotation of 24°, however, is suboptimal, and thus, this alignment of the shear to the forcing boundary may be responsible for the short-lived nature of the southern portion of the line.

The back-building convection that began at 2135 UTC was aligned roughly horizontally along the 36.4°N latitude. The back-building was initiated by outflow from the supercell at (36.2°N/98.4°W), perhaps initially from its rear flank downdraft. The outflow propagated northwest until it reached the junction of the rear flank of the cell at (36.4°N/98.5°W) and the dryline. The dryline can be seen on the Vance radar reflectivity imagery as a faint green boundary (Figure 4.24).

There existed a continual source of fuel for the back-building convection, as winds over

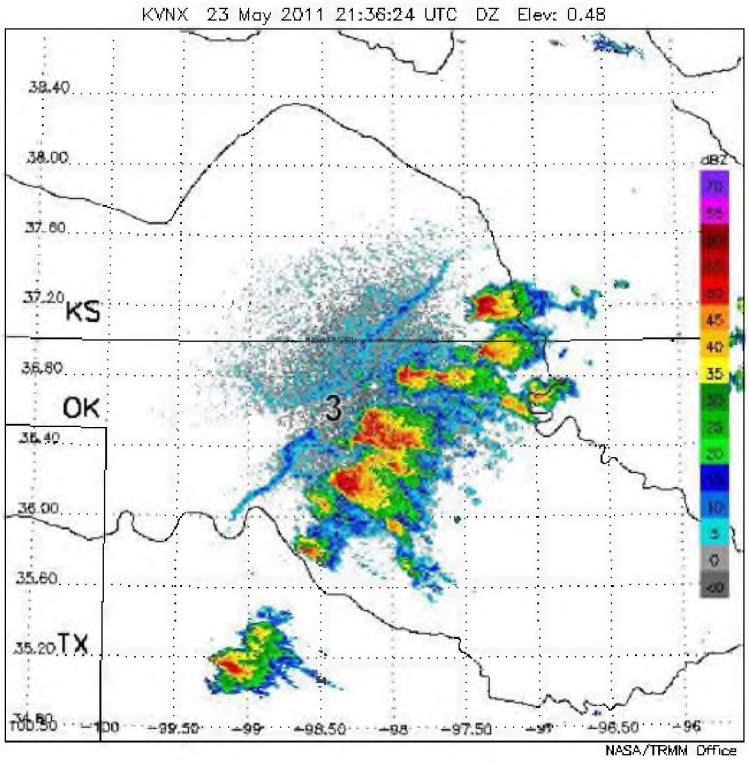

Figure 4.24. Vance, OK (KVNX) WSR-88D radar imagery at 2136 UTC. The dryline appears near (36.4°N/98.5°W) as a faint, curvy, green line.

Oklahoma remained southerly, even after the passage of the shortwave trough. Thus, the back-builder has access to moisture and instability throughout its lifecycle (the Purcell sounding had over 2000 J kg^{-1} of CAPE at 2300 and 0220 UTC). Its propagation from 2135 to 2300 UTC is reminiscent of the "continuous propagation" discussed in Chapter 1, as the locus of new cells remains at (36.4°N/98.5°W) until 2300 UTC, seemingly stationary.

The dryline, however, did not remain in the same position throughout the lifecycle of the back-builder. At 2245 UTC, the dryline begins to retreat westwards, and the back-building continues despite the retreat of the dryline. By this time, the cells to the south have also moved eastwards and their outflow is no longer interacting with the dryline (Figure 4.25). Mesonet timeseries analyses of the Woodward and Seiling stations show a characteristic rapid moistening at 2330 and 2350 UTC, respectively, showing the westward retreat of the dryline (Figure 4.26). The back-building continues, however, until 0345 UTC in the same location, spawning severe cells that overshoot the tropopause and produce hail.

After 2300 UTC, when the support of the dryline retreated to the west, the back-building convection was maintained by its own gust front propagating southward into the persistent ambient southerly flow. The locus of back-building can be seen to drift southwest (Figures 4.16 and 4.17), as the new cells are created as the cold outflow forces the environmental air

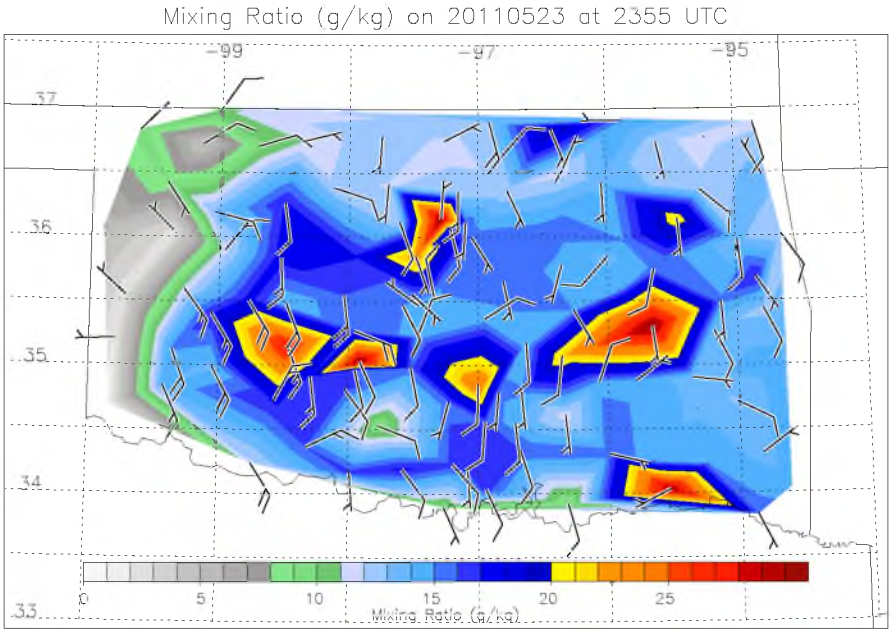

Figure 4.25. Water vapor mixing ratio (g kg^{-1}) calculated from Oklahoma Mesonet data at 2355 UTC 23 May 2011.

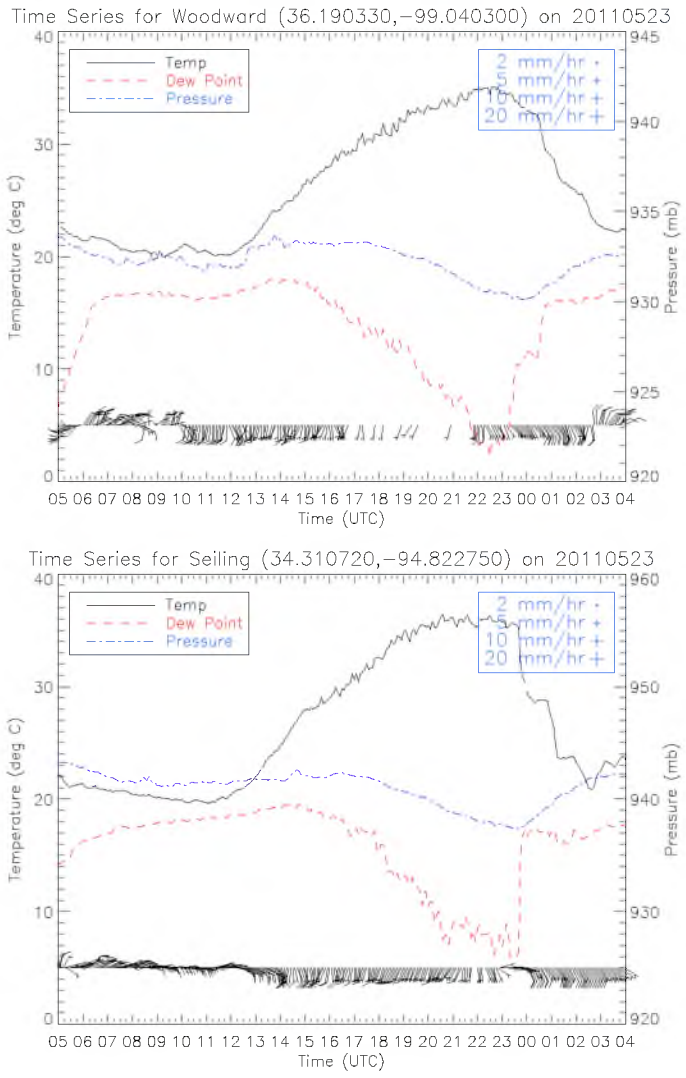

Figure 4.26. Timeseries of temperature, dew point, pressure, winds, and precipitation overnight from 0500 UTC 23 May 2011 to 0400 UTC 24 May 2011 at the Woodward and Seiling Mesonet stations (locations are shown in Figure 4.16).

to rise. The outflow boundary can be seen pushing away (both north and south) from the back-builder as a faint reflectivity line crossing the 98.5°W longitude at 36.2°N.

The Fairview and Putnam Oklahoma Mesonet station register a sharp temperature drop exceeding 10°C, a shift to northerly winds, and a mild pressure spike at 2300 and 00 UTC, respectively signifying the arrival of the back-builder's outflow (Figure 4.27). The Fairview station is along the track of the site of new growth as it propagates discretely southwestward; thus, the winds quickly veer to southerly, though the temperature continues to drop and the pressure continues to rise, corresponding with registered precipitation, also, shortly before 00 UTC.

Despite the strong convergence at the western boundary of the cold pool and the approach of the stationary front from the north, the back-building did not interact with either of these boundaries. The stationary front reaches neither the Lahoma nor the Woodward Mesonet stations, both of which were north of the back-building development.

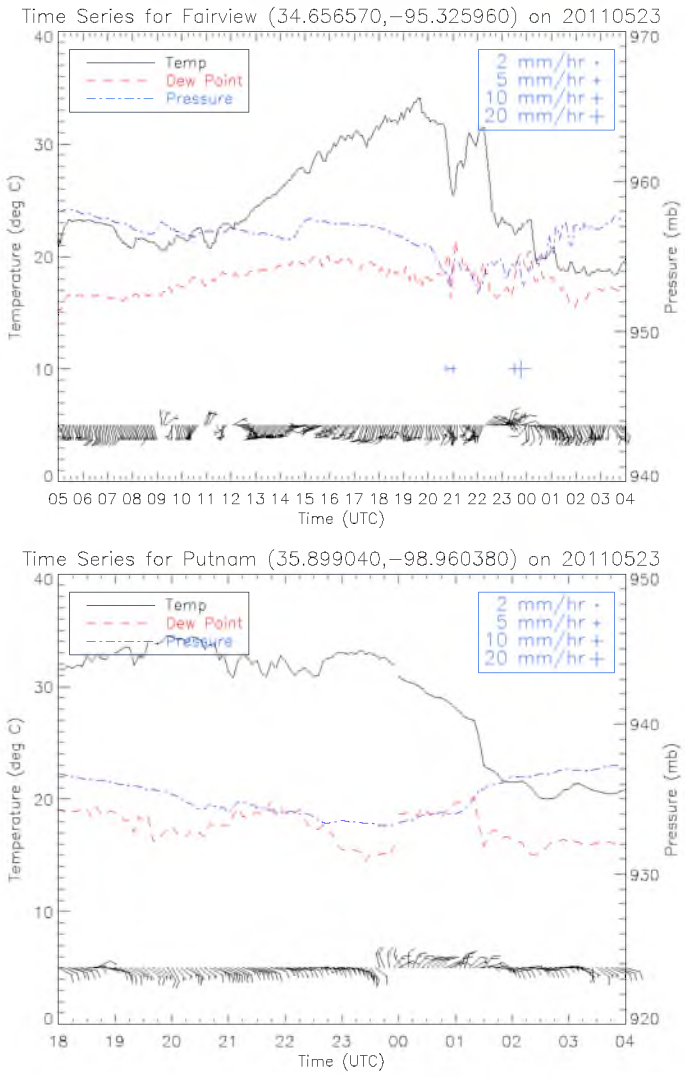

Figure 4.27. Timeseries of temperature, dew point, pressure, winds, and precipitation overnight from 0500 UTC 23 May 2011 to 0400 UTC 24 May 2011 at the Fairview and Putnam Mesonet stations (locations are shown in Figure 4.16).

CHAPTER 5

EVOLUTION OF THE CONVECTION ON 24 MAY 2011

The convection on 24 May 2011 was dominated by the supercellular and multicellular convective morphologies and produced violent tornadoes and large hail over its lifetime. Figure 5.1 provides an overview of the prevalent boundaries and locations of the most important convective cells throughout their lifecycles.

As a trough crossed over the dryline in western Oklahoma, supercells fired throughout the afternoon of 24 May beginning at 1843 UTC along the dryline in western Oklahoma. The supercells intensified rapidly, with rotation signatures appearing by 1947 UTC. This line of supercells spawned 11 confirmed tornadoes, one of which was fatal. There were 19 associated tornado reports and reports of hail up to golf ball size. The official survey conducted by the Storm Prediction Center confirmed 12 tornadoes, one of which was rated at EF-5 and caused 9 fatalities. Both left- and right-moving supercells fired on the dryline and interacted with each other. After 2100 UTC, the cells began to evolve into a solid north-south band of reflectivity with leading anvil. Other cells fired behind the original dryline-forced storms and propagated eastwards. By 0421 UTC 25 May, the dryline-forced supercell storm system was out of Oklahoma and by 0622 UTC 25 May, all convection was out of Oklahoma. Figure 5.1 provides an overview of the prevalent boundaries and locations of convective cells throughout their lifetimes.

5.1 Prestorm Environment

Throughout the daytime hours of 24 May, an upper-level trough lay draped over the Rocky Mountains (Figure 5.2), its surface low-pressure center located at Oklahoma's western border. The upper air contour plots show the path of the trough overnight into the early hours of 25 May. The GOES-13 water vapor imagery (Figure 5.3) shows the location of the trough at 1145 UTC 24 May over the western United States and demarcates clearly the dryline over central Oklahoma.

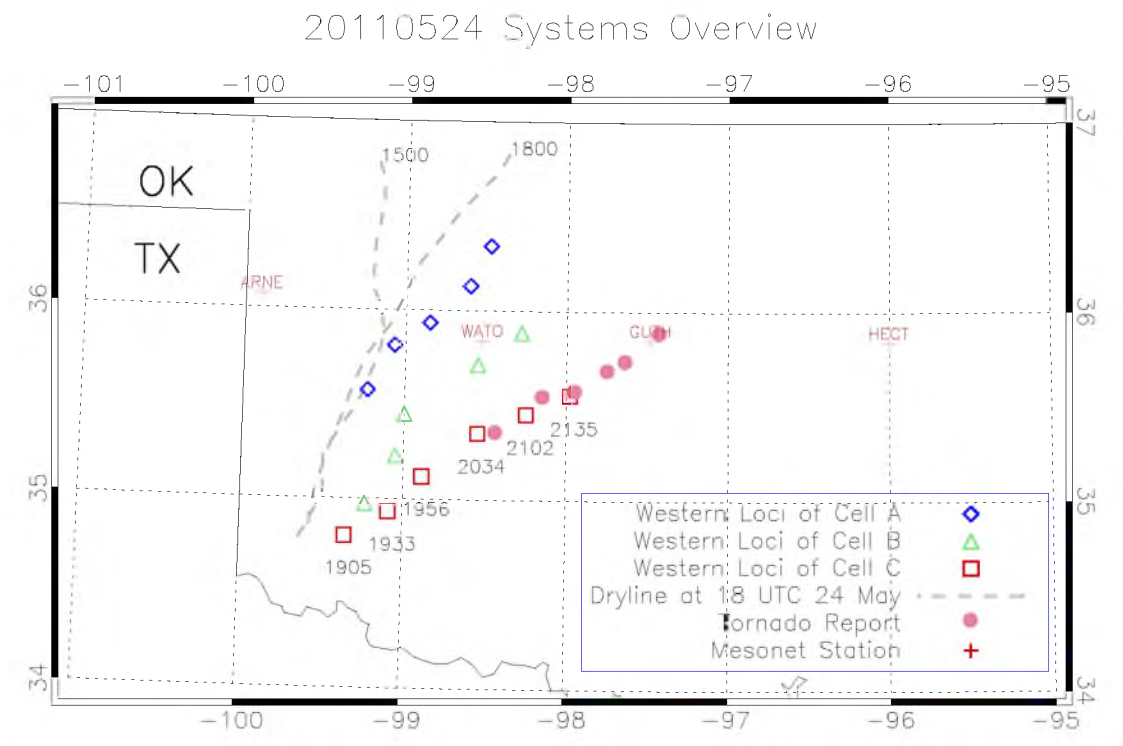

Figure 5.1. Overview of the prominent boundaries and convective systems that occurred on 24 May, 2011 in Western and Central Oklahoma

The low pushed over Oklahoma from about 1600 UTC 24 May to 0400 UTC 25 May. The surface trough axis reached the Arnett, OK Mesonet Station on the western border of Oklahoma (excluding the panhandle) at 2230 UTC 24 May and pushed eastwards over the course of the day. Its passage can be seen at the Watonga, Guthrie, and Hectorville Mesonet sites (Figure 5.4).

The dryline seen in Figure 5.5 fluctuates across the state throughout the day (positions can be seen in Figure 5.1). By 18 UTC, the dryline had progressed eastward and was draped in a SSW-NNE line slightly west of central Oklahoma. Figure 5.5 shows the mixing ratio calculated from Oklahoma Mesonet data. Dew points east of the dryline exceeded 22°C.

The 1730 UTC sounding taken at the Central Facility (Figure 5.6) shows a sizeable capping inversion at 850 hPa and 4602 J kg^{-1} of possible convective available potential energy (CAPE). There are strong south/southwesterly winds with slight clockwise shear in the lower 5 km.

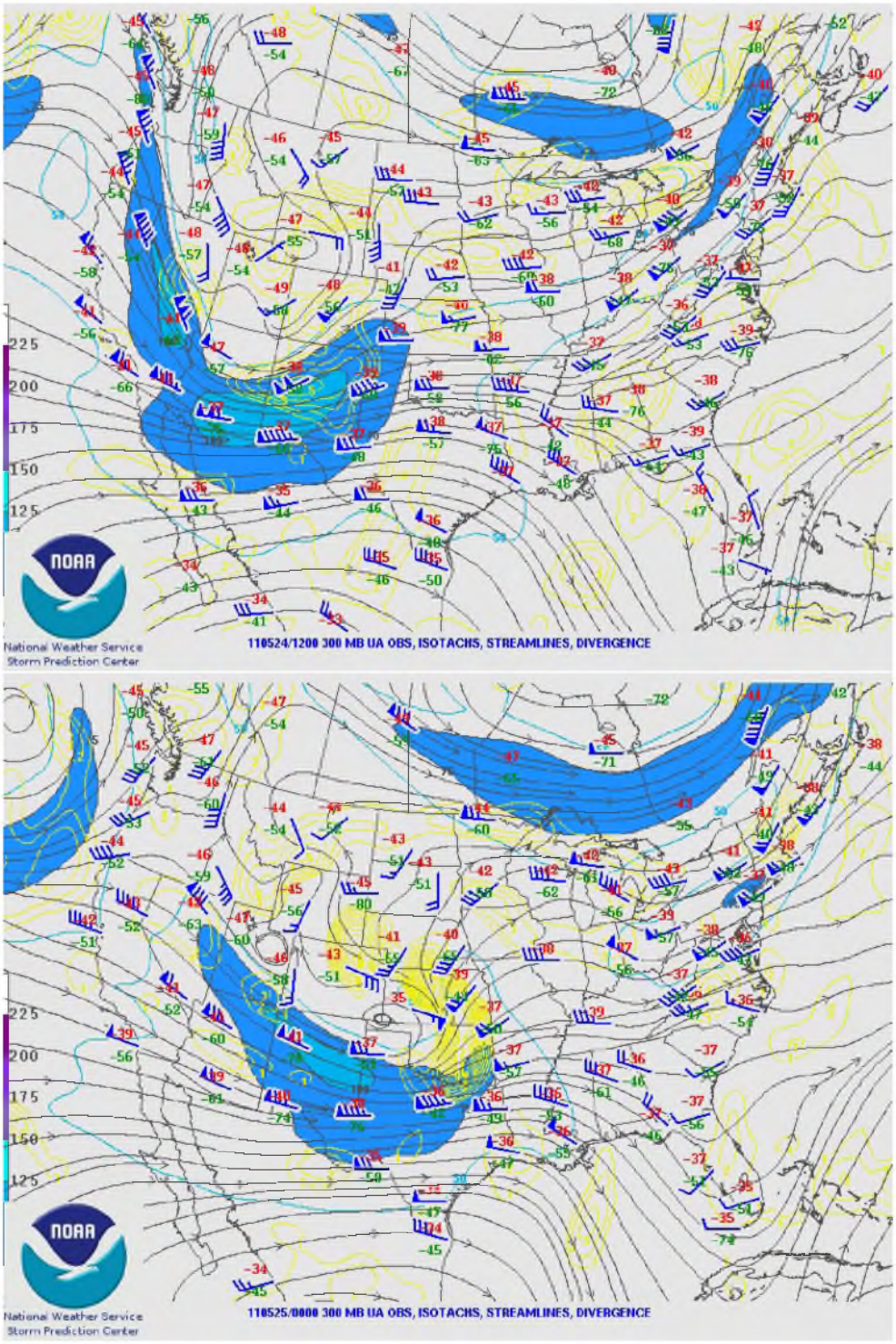

Figure 5.2. 300 mb analysis at 12 UTC 24 May and 00 UTC 25 May 2011. Rawinsonde retrieved temperature, dew point, and wind observations (wind barbs coincident with numbers) and RUC Analysis streamlines, isotachs (fill), and divergence (contours). Courtesy of the National Weather Service.

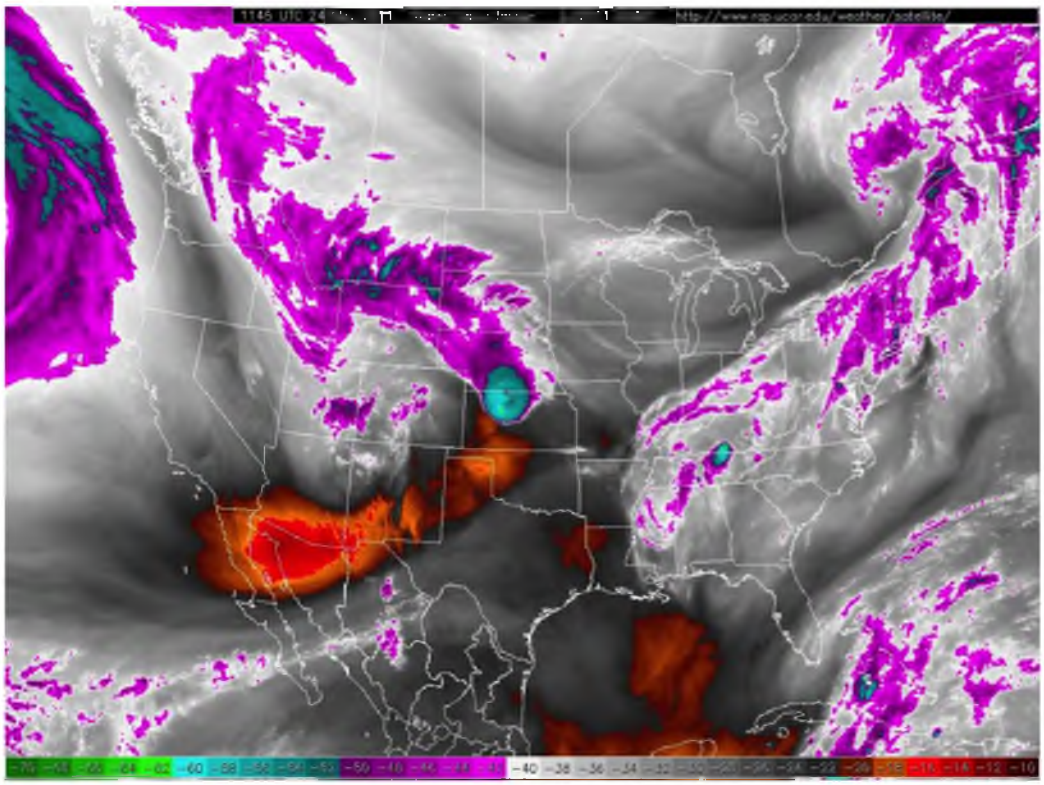

Figure 5.3. GOES-13 water vapor satellite imagery at 1145 UTC 24 May 2011

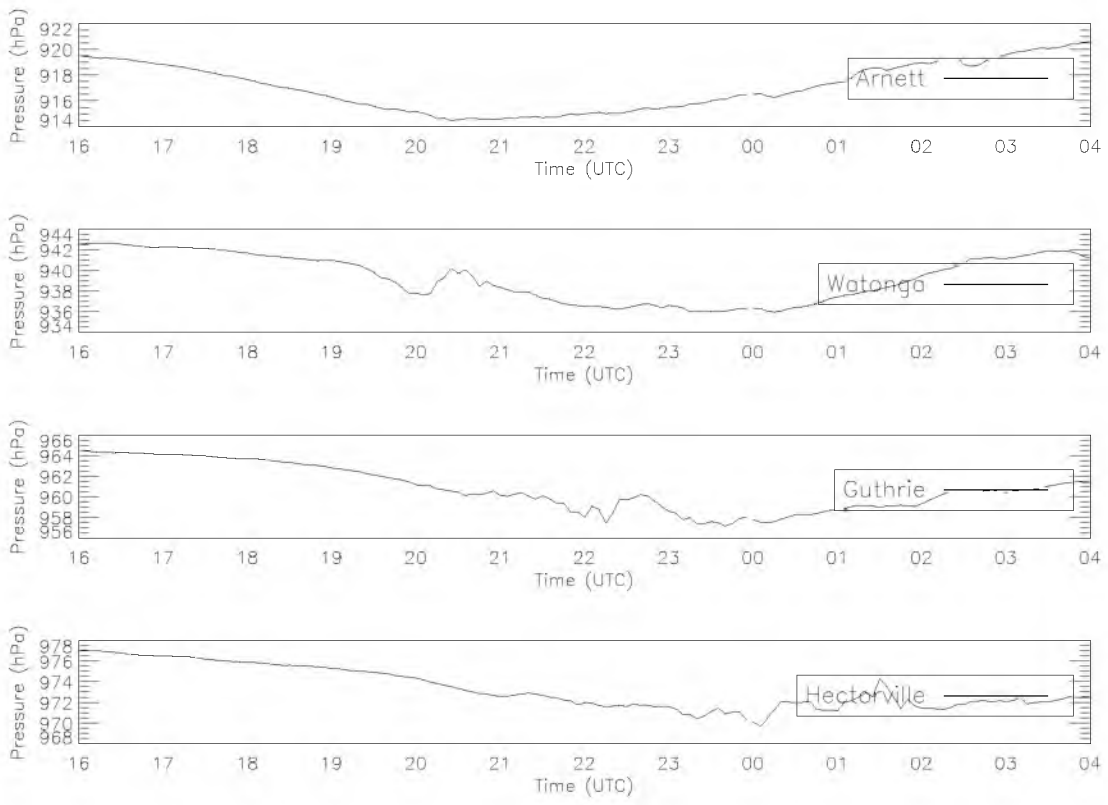

Figure 5.4. Surface pressure as measured at the Arnett, Watonga, Guthrie, and Hectorville Oklahoma Mesonet Stations from 16 UTC 24 May to 04 UTC 25 May. Note the sequential dip in pressure as you progress across the state. Stations are presented in west-east order. Station locations are shown in Figure 5.1

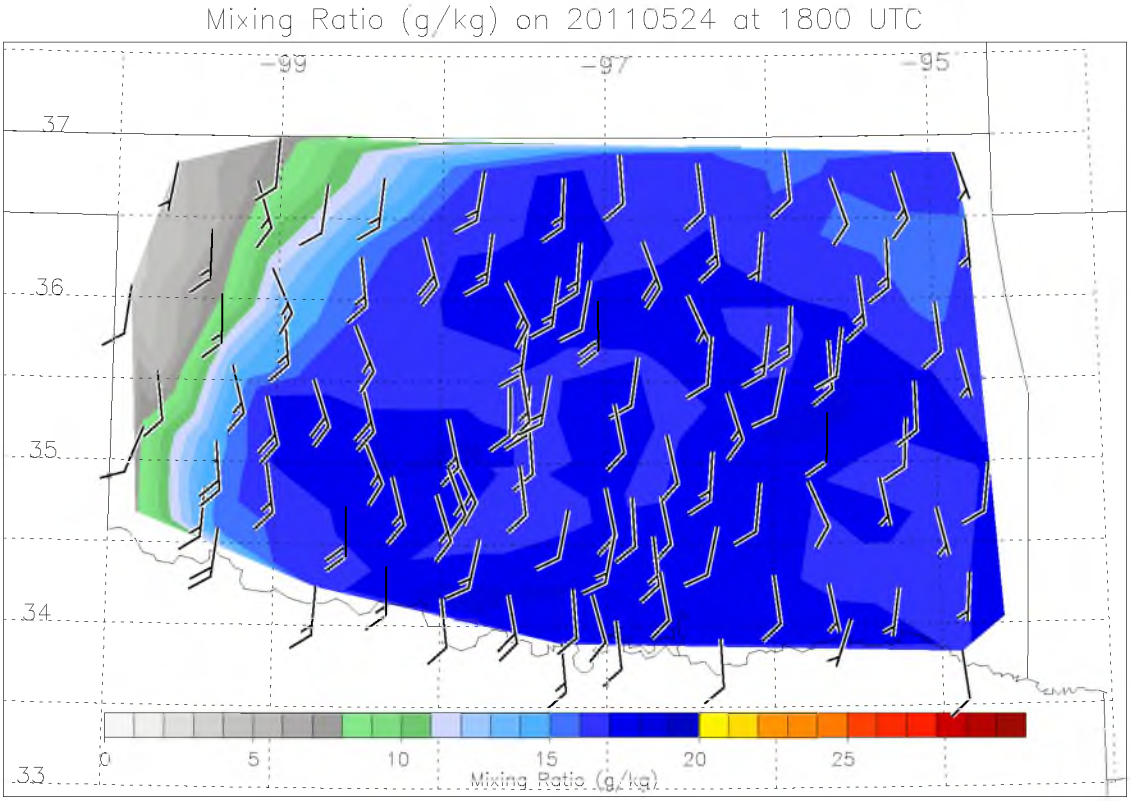

Figure 5.5. Mixing ratio (g kg^{-1}) as calculated from Oklahoma Mesonet data at 1800 UTC 24 May, overlaid with wind speed and direction (barbs), temperature (upper left), and dew point temperature (lower left) observations.

By 2022 UTC (Figure 5.7), the cap is significantly reduced in size and has been lifted to 800 hPa, and convective inhibition is now one quarter of what it was 3 hours prior. Shear has increased in magnitude; however, the clockwise component at lower levels is no longer. Instead, the hodograph looks more indicative of multicell convection, which does not suppress as much the persistence of left-movers. Winds from the south have increased, suggesting the approach of the strong low-level jet, which supplies the area with large amounts of moisture. During these 3 hours, the lapse rate steepens; the temperatures at 400 hPa dropped from -22°C to -25°C at 400 hPa, with a 2°C drop at 500 hPa, while the temperature at 600 hPa remains relatively constant, all of which is clear evidence of lifting of the air mass during this 3-hour period.

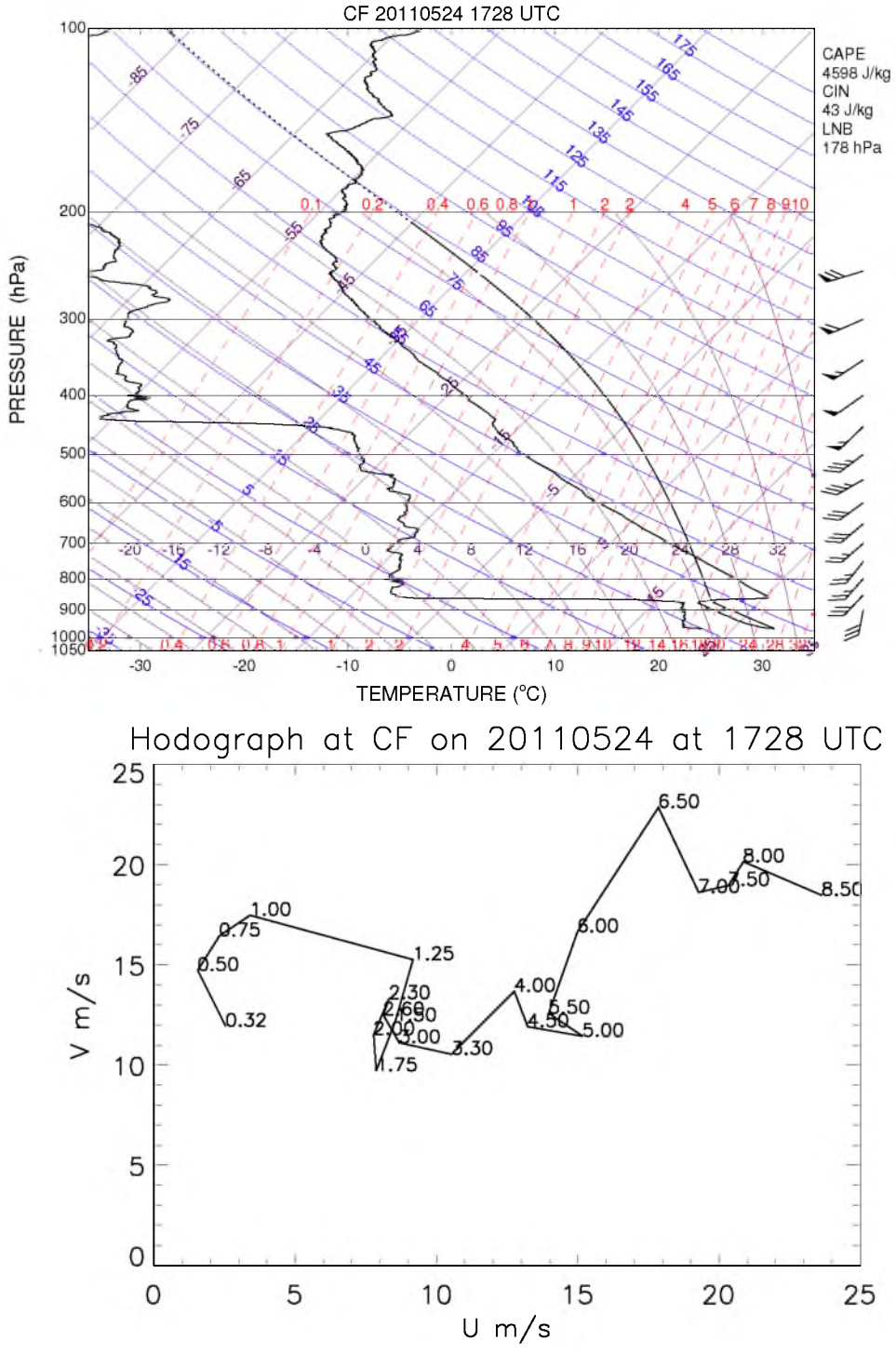

Figure 5.6. Skew-T/Log-P (top) and hodograph (bottom) representations of the 1728 UTC sounding launched at the Central Facility (36.6°N/97.49°W). Radiosonde launch locations are shown in Chapter 2.

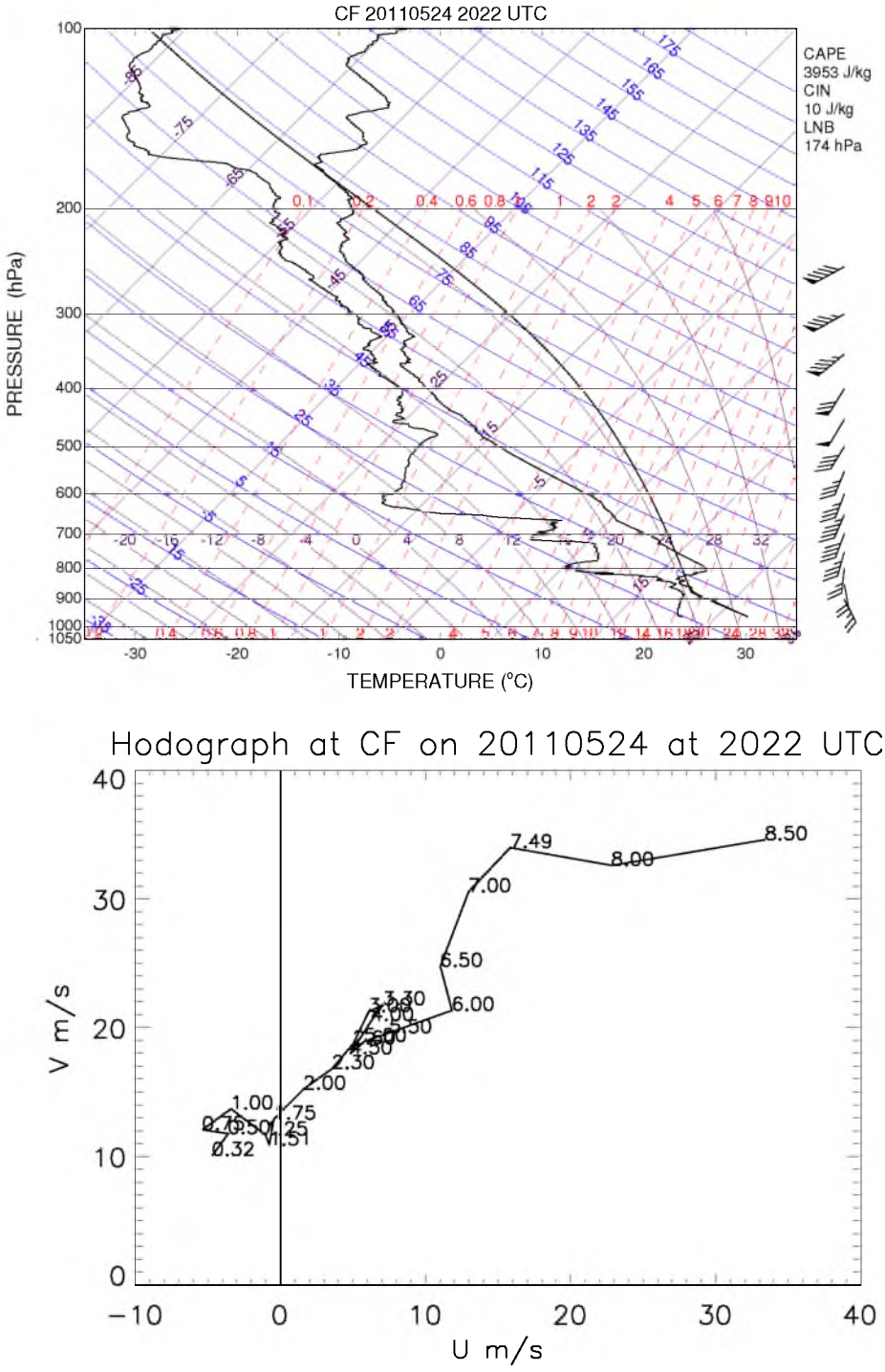

Figure 5.7. Skew-T/Log-P (top) and hodograph (bottom) representations of the 2022 UTC sounding launched at the Central Facility (36.6°N/97.49°W). Radiosonde launch locations are shown in Chapter 2.

5.2 Dryline Supercells

The first convective cells fired at 1841 UTC in southwestern Oklahoma along the dryline (Figure 5.8a). The first cell to fire (A) exhibited radar echoes over 50 dBZ by 1905 UTC and supercellular characteristics by 1910 UTC. The cells fired in isolation (Figure 5.8a,b), and formed a north-south line of nearly continuous precipitation by $\sim$ 21 UTC (Figure 5.8b,c). Note the existence of the left-moving cell B. By 22 UTC, the line of storms superficially resembles a squall line (5.8c,d) and the northern portion begins to form a forward anvil. By 2330 UTC, the whole line has forward anvil components, the northern half with higher anvil reflectivities, and no trailing stratiform precipitation.

5.2.1 Cell A

The first cell to fire on the dryline is labeled Cell "A". An overview of the dryline position and cell trajectory is shown in Figure 5.9. Figure 5.10 shows the stages of A's development. Cell A fired at 1841 UTC at 35.3°N and 99.4°W on the dryline. Other cells fired to the south (most notably B and C). At 1933 UTC, a left-mover splits from A and propagates northwestward. A is henceforth referencing the right-mover as the left-moving component propagates away and dissipates.

The cell to the south of A fired at 1848 UTC and strengthened throughout the 1900 UTC hour. At 1947 UTC, the cell starts to split and its left-mover moves northward directly into the path of A, reaching A's rear flank by 2015 UTC, resulting in a very strong velocity signature (Figures 5.10 and 5.11).

At 2008 UTC, the NPOL radar shows a weak echo region at 20 km into the cross-section; a strong indicator of an intense updraft (Figure 5.12). At the lowest part of the updraft, the strong positive oblate signature is likely heavy rain reaching the surface. Cell A also shows a mesocyclone in the velocity radar imagery (Figure 5.10) now classifying A as a supercell. Using the 2008 UTC NPOL radar sweep to find an echo top height, a conservative estimate of the maximum height of the radar echo is 16 km (Figure 5.12). Using the 2029 UTC Purcell, OK sounding, the level of neutral buoyancy (LNB) is found at 12.9 km (Figure 5.13). In order to reach a height of 16 km, a convective parcel would need to overcome 1570 J kg^{-1} of stability, which corresponds to an estimated vertical velocity of 56 m s^{-1}. Heymsfield et al. (2013) retrieved a maximum upward particle velocity of 30 m s^{-1} using HIWRAP Doppler velocity data to observe cells on this day, though long after they had reached the linear stage.

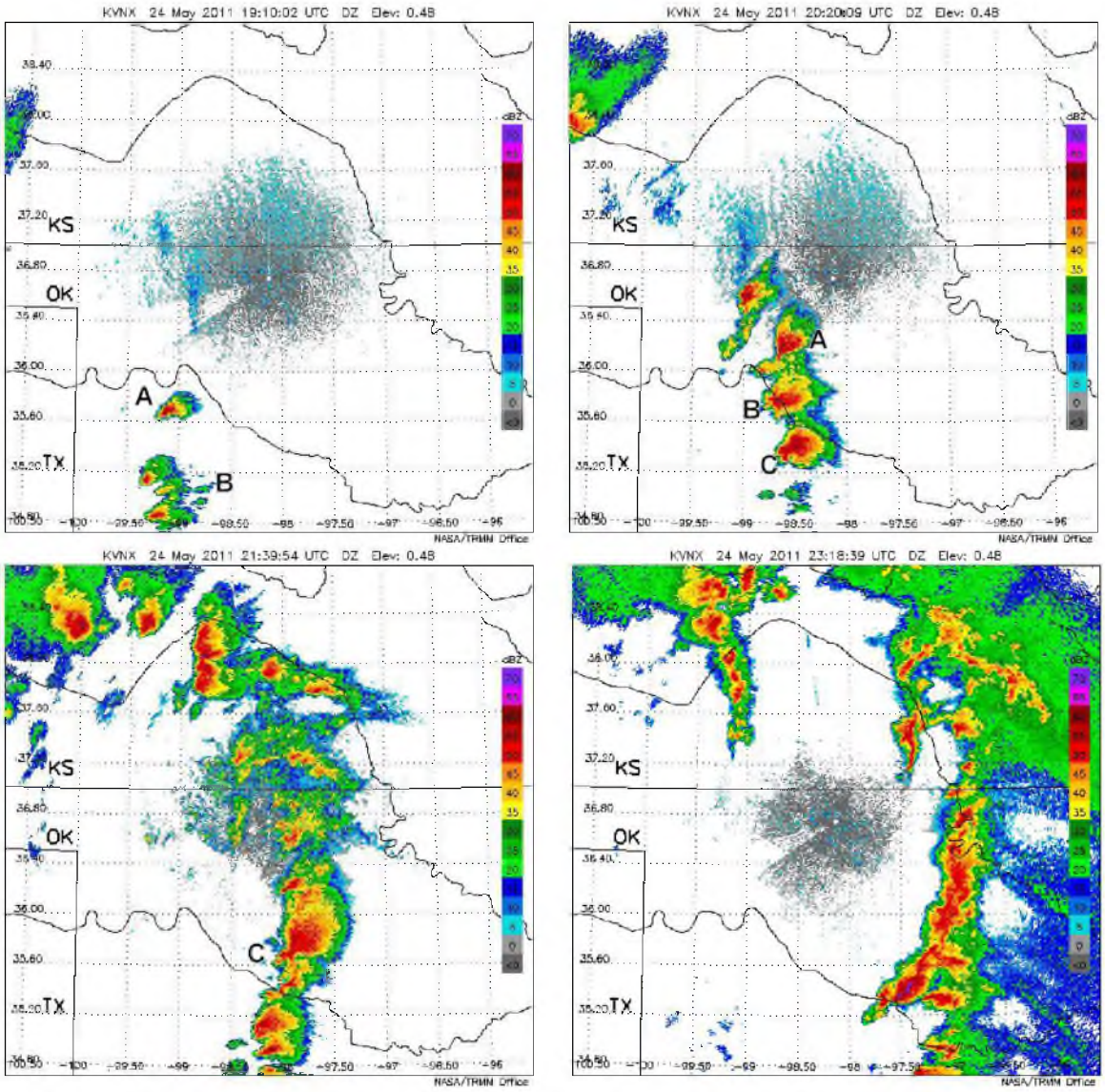

Figure 5.8. Radar timeline of 24 May 2011 from Vance, OK (KVNX). The timeline illustrates early cells (1910 UTC); supercell character of cells A and C (2020 UTC); the now linear arrangement of A and B, and the continued strong supercell C (2139 UTC); final line (2318 UTC). Cell labels are indicated.

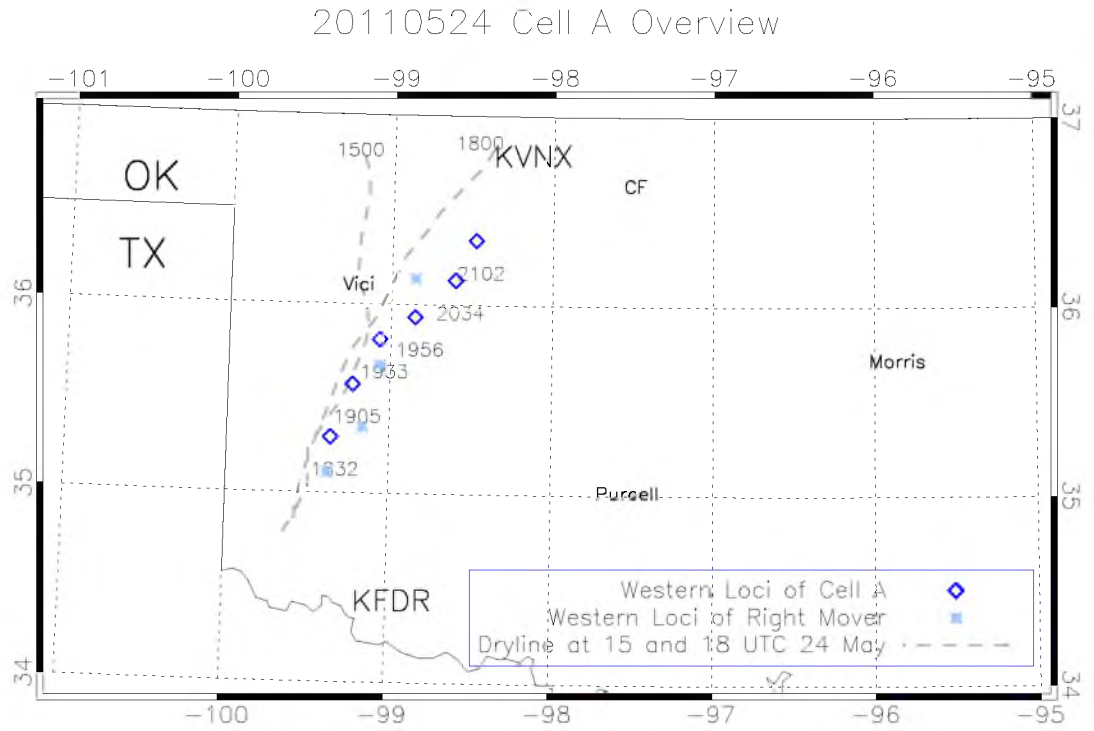

Figure 5.9. Overview of the subjectively determined dryline location and the loci of the westernmost extent of the convective cell A that fired along the dryline (convection fired at 1841 UTC 24 May 2011, positions here shown at several times to show the extent of the cell's lifecycle).

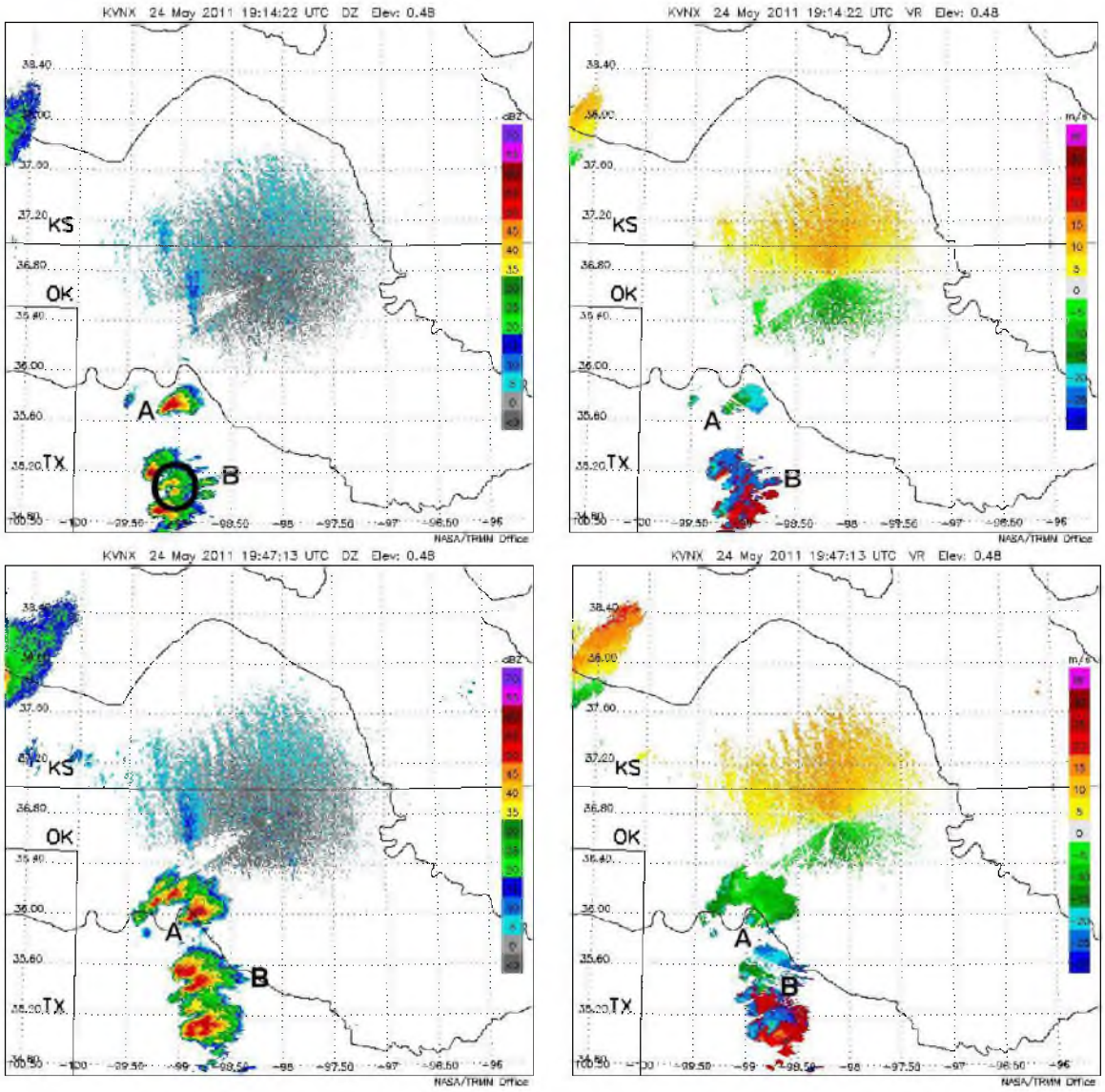

Figure 5.10. Radar timeline of Cell A from the Vance, OK (KVNX) WSR-88D radar. Reflectivity (dBZ) is on the left, velocity (m s^{-1}) is on the right. The timeline illustrates early cells (1914 UTC) and northward advance of the left-mover to the south (2001 UTC) (radar timeline continued on next page).

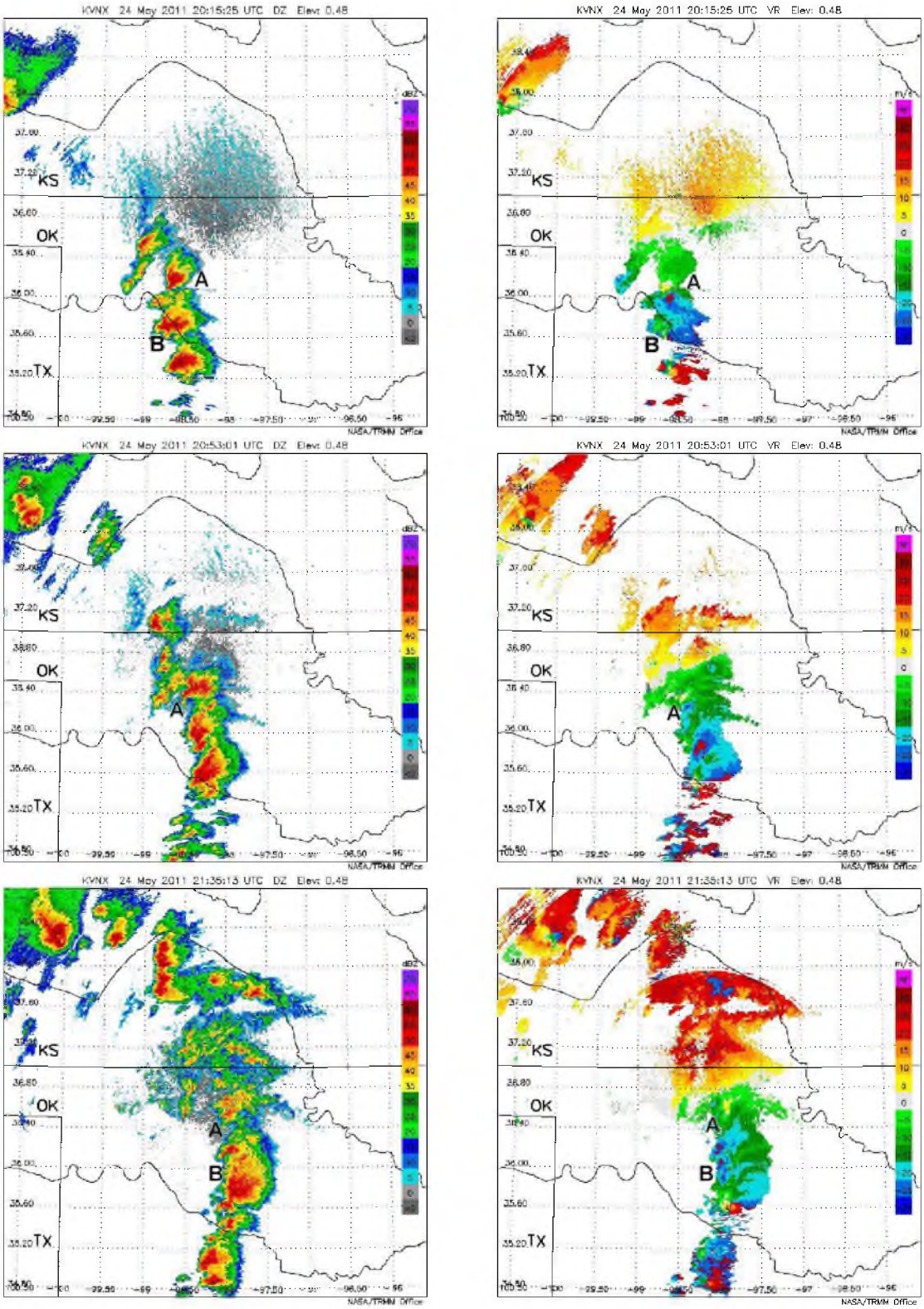

Figure 5.11. Radar timeline of Cell A continued, illustrating the strong mesocyclone (2015 UTC); weakening mesocyclone (2053 UTC); and linear evolution (2135 UTC).

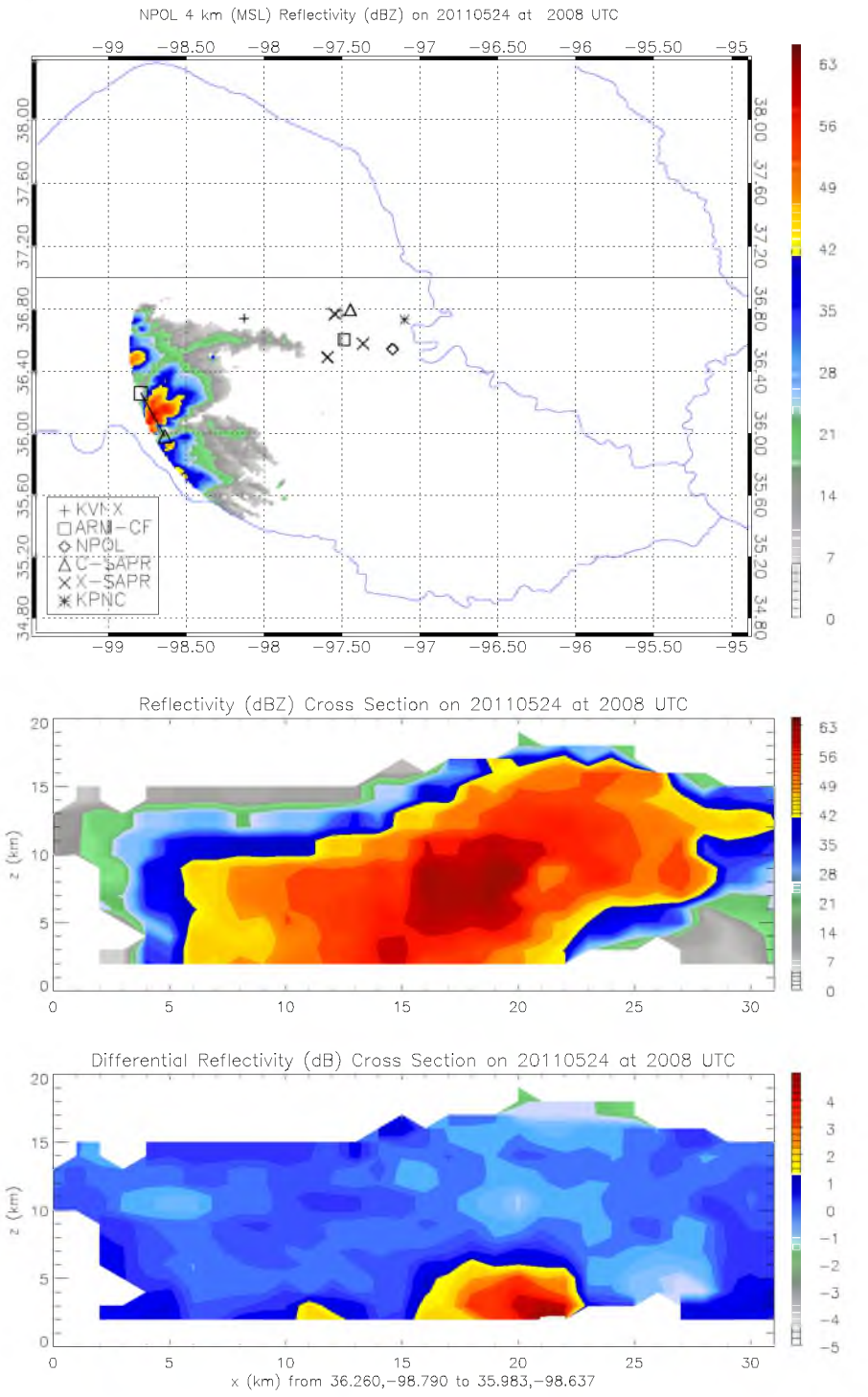

Figure 5.12. NPOL 4 km CAPPI at 2008 UTC 24 May (top). The cross-section transect is shown in black and goes from square to triangle. NPOL reflectivity (dBZ) cross-section (middle) NPOL differential reflectivity (dB) cross-section (bottom).

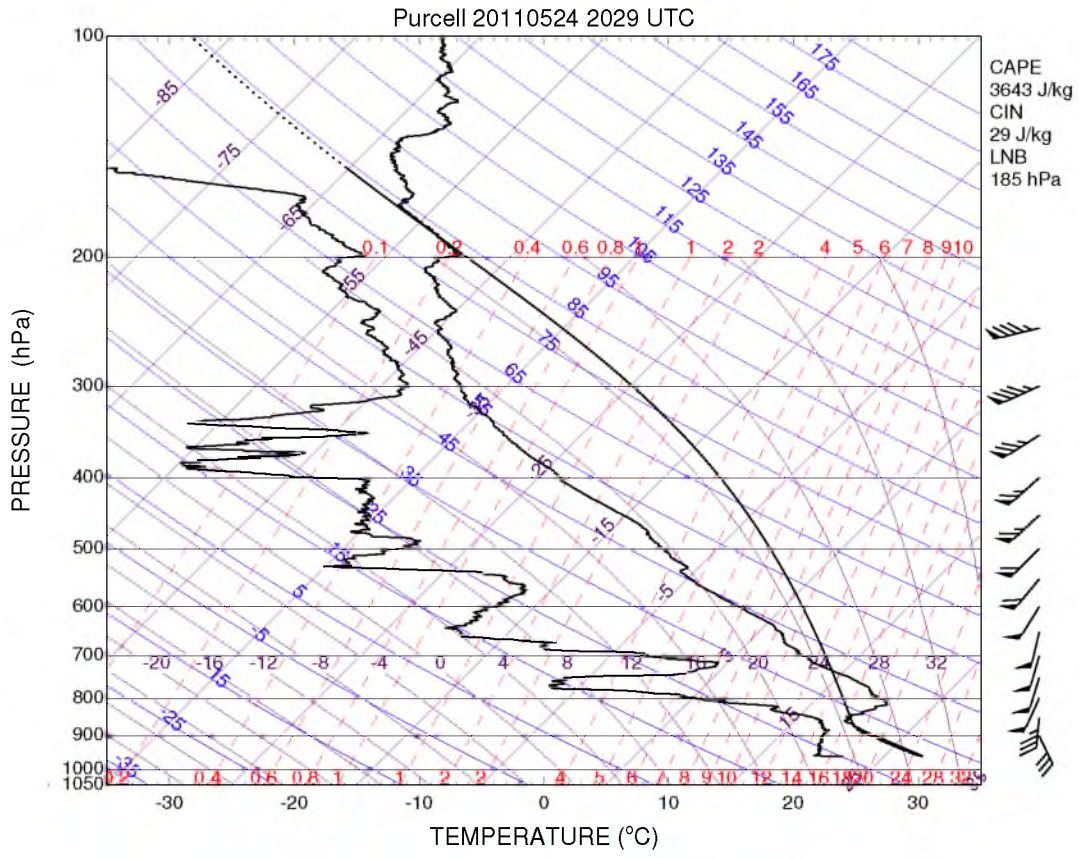

Figure 5.13. Skew-T/Log-P diagram of the 1731 UTC sounding launched at Purcell, OK (35.0°N/97.4°W). Radiosonde launch locations are shown in Chapter 2.

By 2017 UTC (Figure 5.14), the WER is more characteristic of a bounded-WER as the overhang becomes more pronounced. The hail is indicated by slightly negative differential reflectivity (Zrnic and Ryzhkov 1999) becoming stronger and at the base of the updraft, it appears likely that hail is reaching the ground. This cross-section suggests that the 30 dBZ echo is reaching heights of 17 km (note: the beam width is 2.5 km at this point). Around 2030 UTC, a left-moving cell, (A's neighbor to the south) progresses northward towards A (Figure 5.10). It is plausible to speculate that new updrafts could compete with the existing structure and disrupt the mesocyclone. With the strong B cell to the south, perhaps this event weakened A as by 2042 UTC (Figure 5.15), the updraft has weakened, and while there are still high reflectivities and it is still tall, the weak echo region is gone, and there is not much of a hail signature in the differential reflectivity profile. The velocity timeline (Figure 5.11) shows the weakening of the mesocyclone after the left-mover has intersected cell A.

Although the cell has weakened by 2042 UTC, it persists until about 2115 UTC, whereupon it becomes difficult to distinguish in isolation from the other cells in the line (Figure 5.11). All cells in the linear phase have high reflectivities that persist for hours; however, rotation is not seen again once a cell has entered into the linear phase and no longer resembles a supercell.

5.2.2 Cell B

Cell "B" seems to result from the merging of several cells between 1902 UTC and 2024 UTC. An overview of this cell's trajectory is shown in Figure 5.16, starting at 1902 UTC at 35°N/99.2°W along the dryline in southern Oklahoma (Figure 5.17). Several cells fired in close proximity (less than .4° of latitude) from 1902 to 2003 UTC and development of left- and right-movers is evident. Cell B begins to resemble a supercell at 2020 UTC and there are hints of a hook echo from 2020 to 2043 UTC; however, there is no evidence of a mesocyclone in the radar velocity imagery. Reflectivities exceed 65 dBZ at 2045 UTC (Figure 5.18). Cell B ceases to be identifiable in isolation after 2116 UTC and strong cells that may have originated in the "B" cluster remain strong (reflectivities exceed 50 dBZ until shortly before the entire system dissipates after 0900 UTC on 25 May) (Figure 5.18).

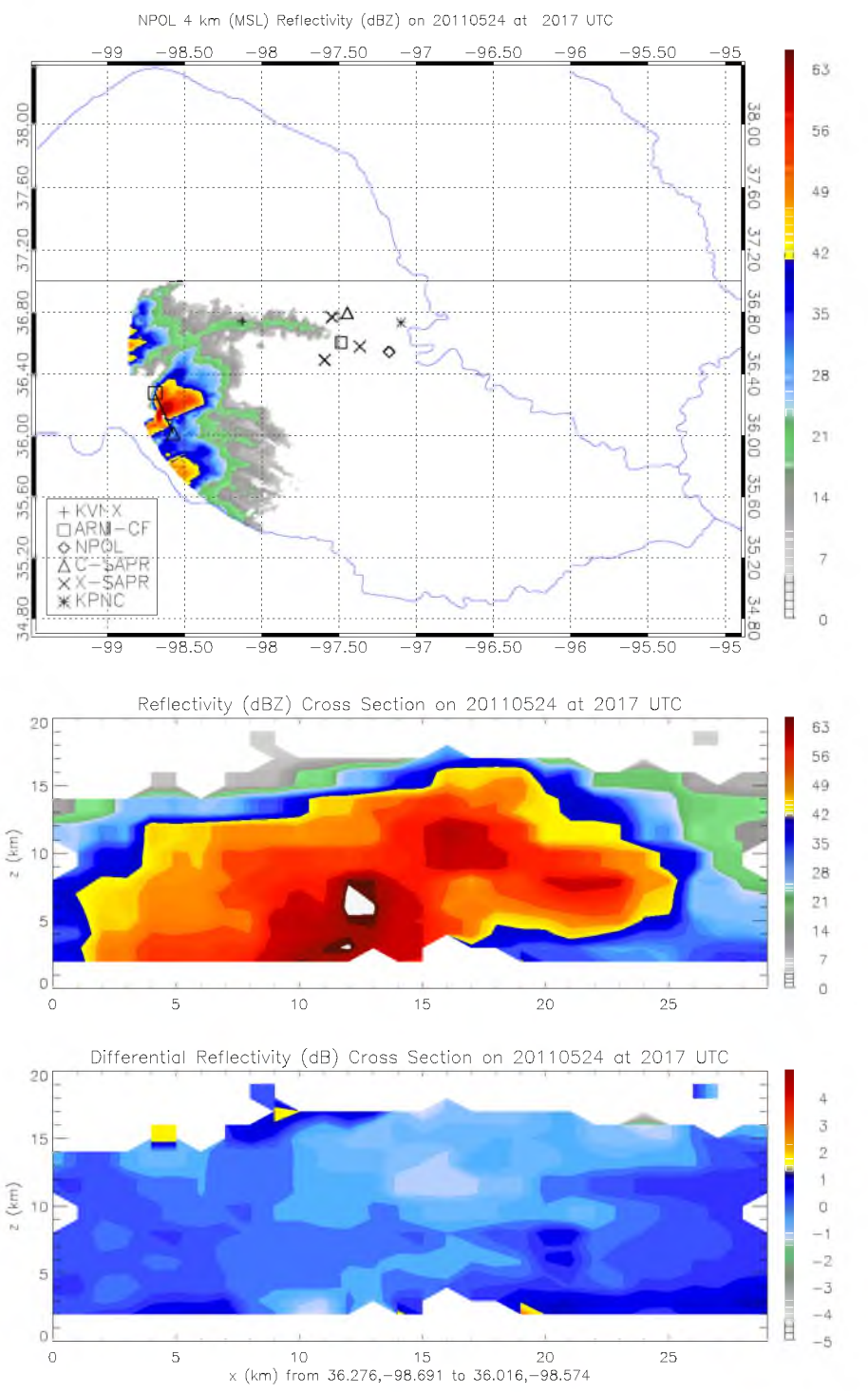

Figure 5.14. NPOL 4 km CAPPI at 2017 UTC 24 May (top). The cross-section transect is shown in black and goes from square to triangle. NPOL reflectivity (dBZ) cross-section (middle) NPOL differential reflectivity (dB) cross-section (bottom).

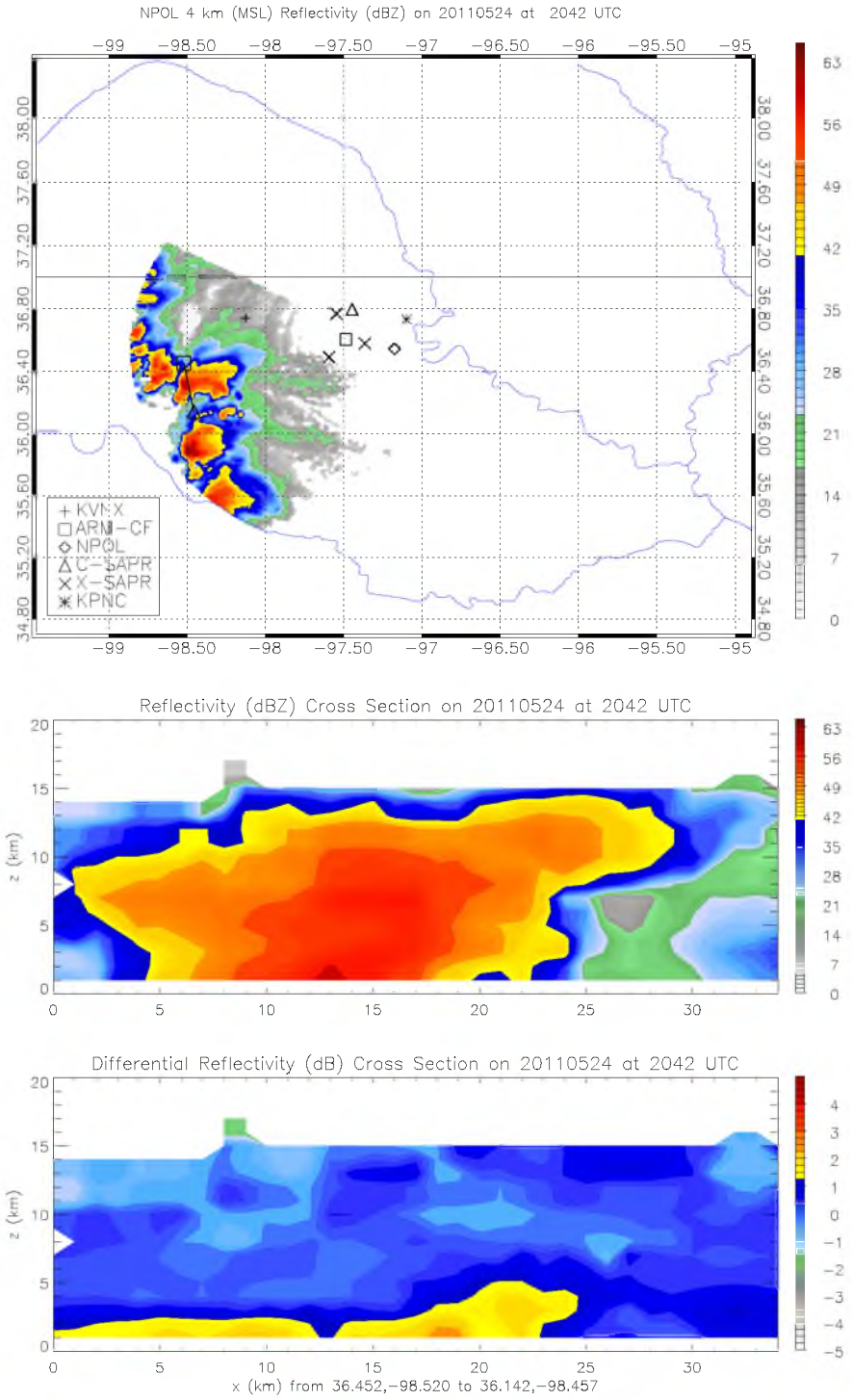

Figure 5.15. NPOL 4 km CAPPI at 2042 UTC 24 May (top). The cross-section transect is shown in black and goes from square to triangle. NPOL reflectivity (dBZ) cross-section (middle) NPOL differential reflectivity (dB) cross-section (bottom).

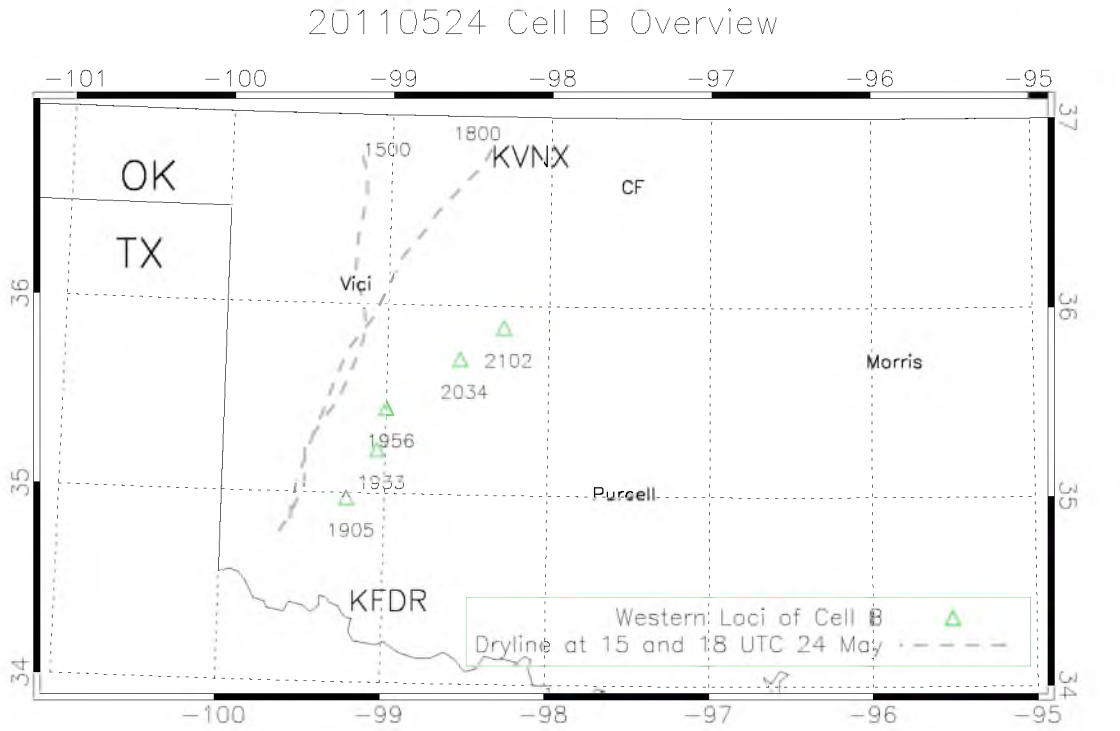

Figure 5.16. Overview of the subjectively determined dryline location and the loci of the westernmost extent of the convective cell B that fired along the dryline (convection fired at 1902 UTC 24 May 2011, positions here shown at several times to show the extent of the cell's lifecycle).

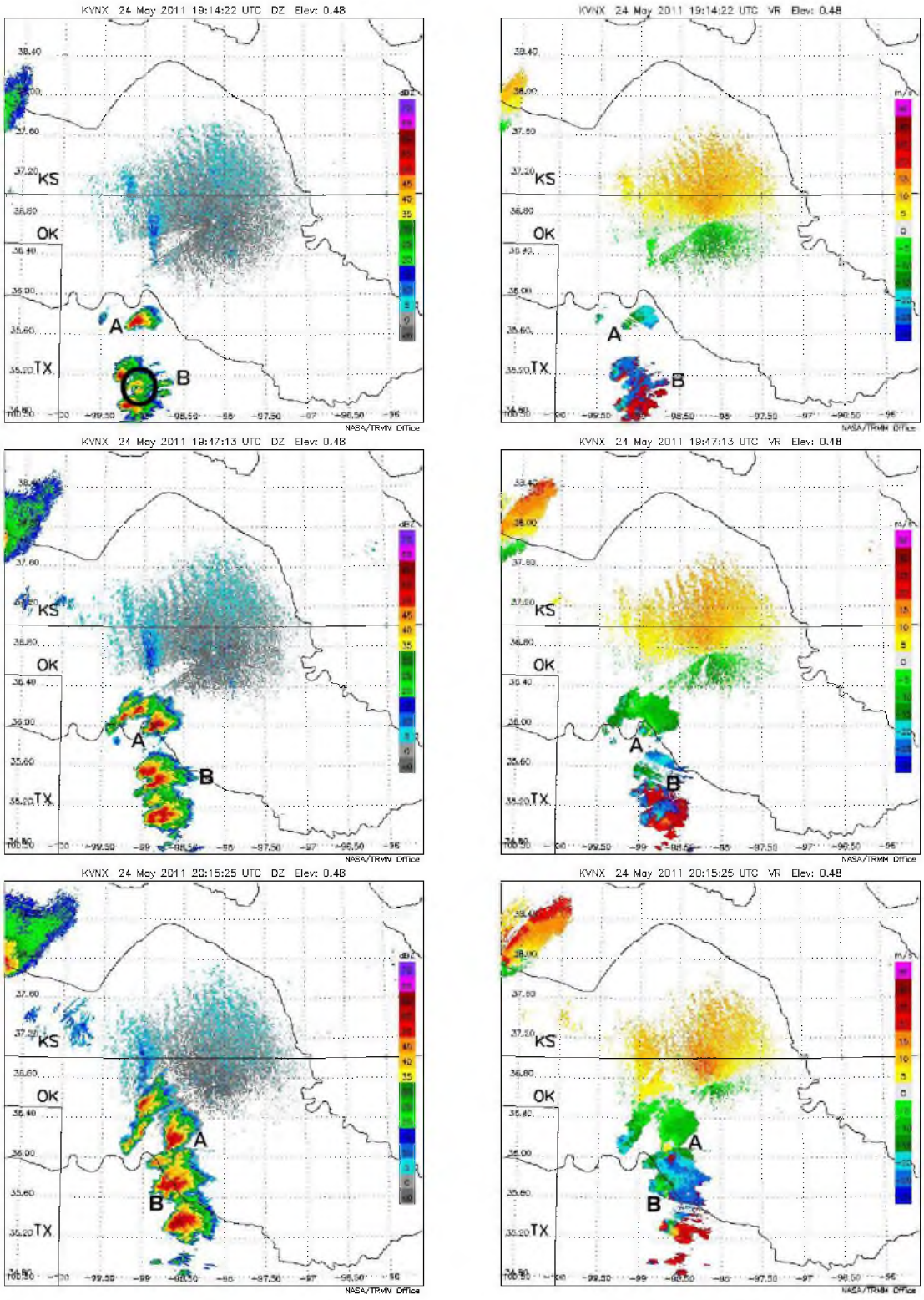

Figure 5.17. Radar timeline of Cell B from the Vance, OK (KVNX) WSR-88D radar. The timeline illustrates the early cell cluster (1914 UTC); merging and strengthening (1947 UTC); and a hook echo (2015 UTC). (Timeline continued on the next page).

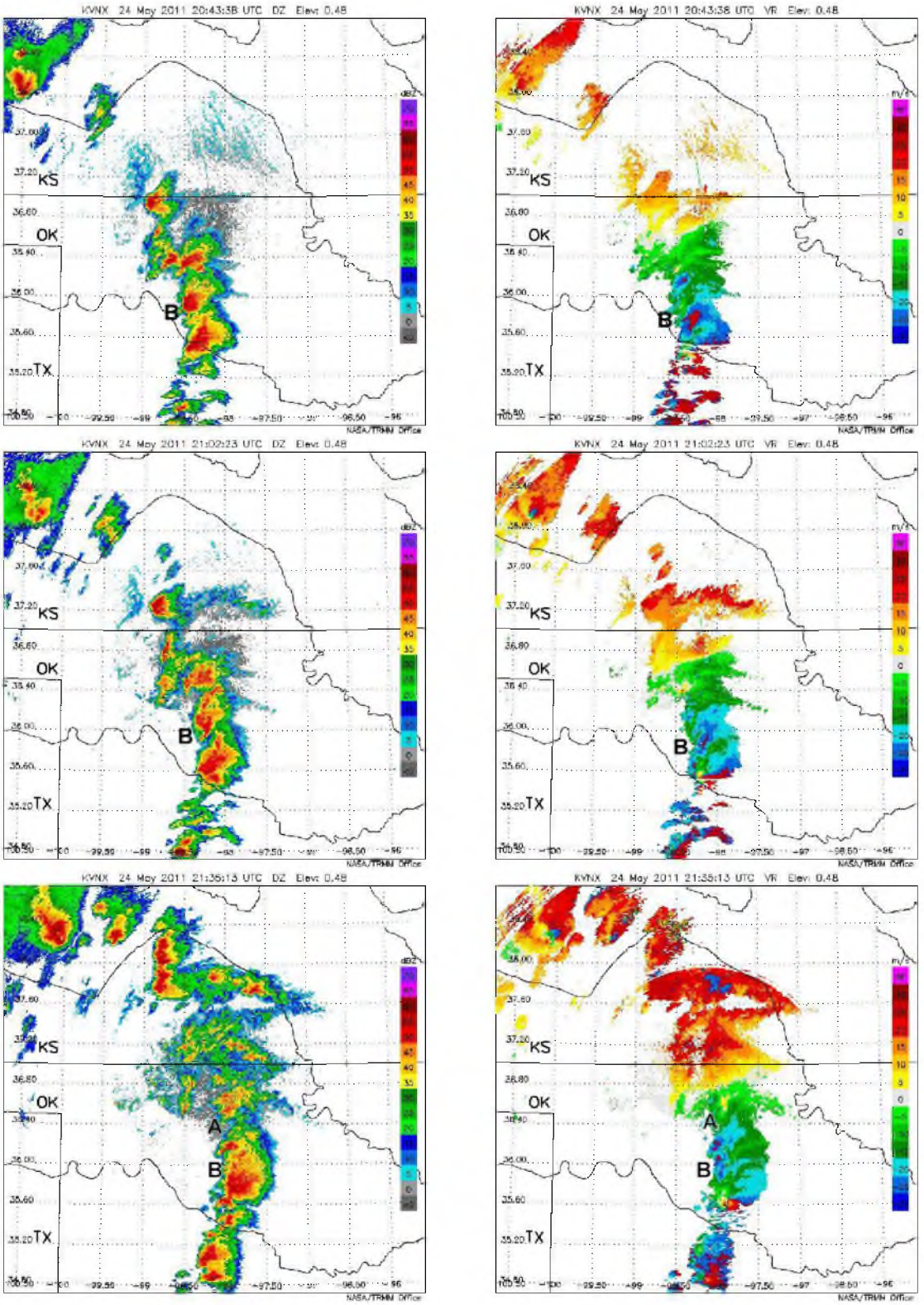

Figure 5.18. Radar timeline of Cell B continued, illustrating the continued supercell-like structure (2043 UTC); linearization of Cell B (2102 UTC); and dissolution (2135 UTC).

5.2.3 Cell C

Cell "C" fires on the dryline at 1924 UTC at (34.8°N/99.1°W). The cell's trajectory is shown in Figure 5.19. Reflectivities over 50 dBZ occur at 1910 UTC, and a rotation signature appears in the radar velocity observations at 1945 UTC (Figure 5.20) and the rotation remains prevalent and visible in cell C until 2318 UTC. The first tornado was reported with extensive damage at 2110 UTC at (35.65°N/98.15°W), just southeast of the detected velocity signature in Figure 5.21, and tornado reports continued for this cell until 2339 UTC. Cell C becomes indistinguishable from the rest of the line by 2208 UTC (Figure 5.21).

The line of severe cells is constituted not only of the A, B, and C cells, but also of cells that fired on the dryline to the south and propagated northwards and remnant left-movers and smaller convective cells that grow on the periphery of the larger supercells. The line is roughly oriented north-south (Figure 5.8). There is significant forward anvil ahead of the

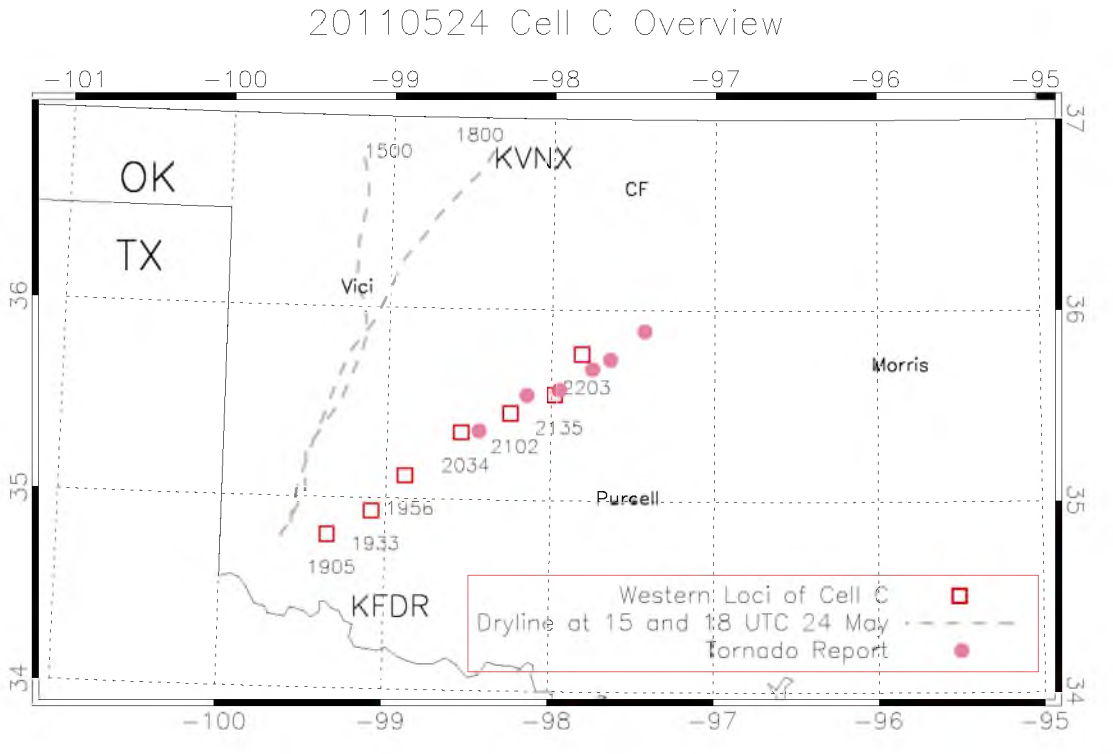

Figure 5.19. Overview of the subjectively determined dryline location and the loci of the westernmost extent of the convective cell C that fired along the dryline at 1924 UTC 24 May 2011, positions here shown at several times to show the extent of the cell's lifecycle. Positions of reported tornadoes along this storm's track are marked in pink.

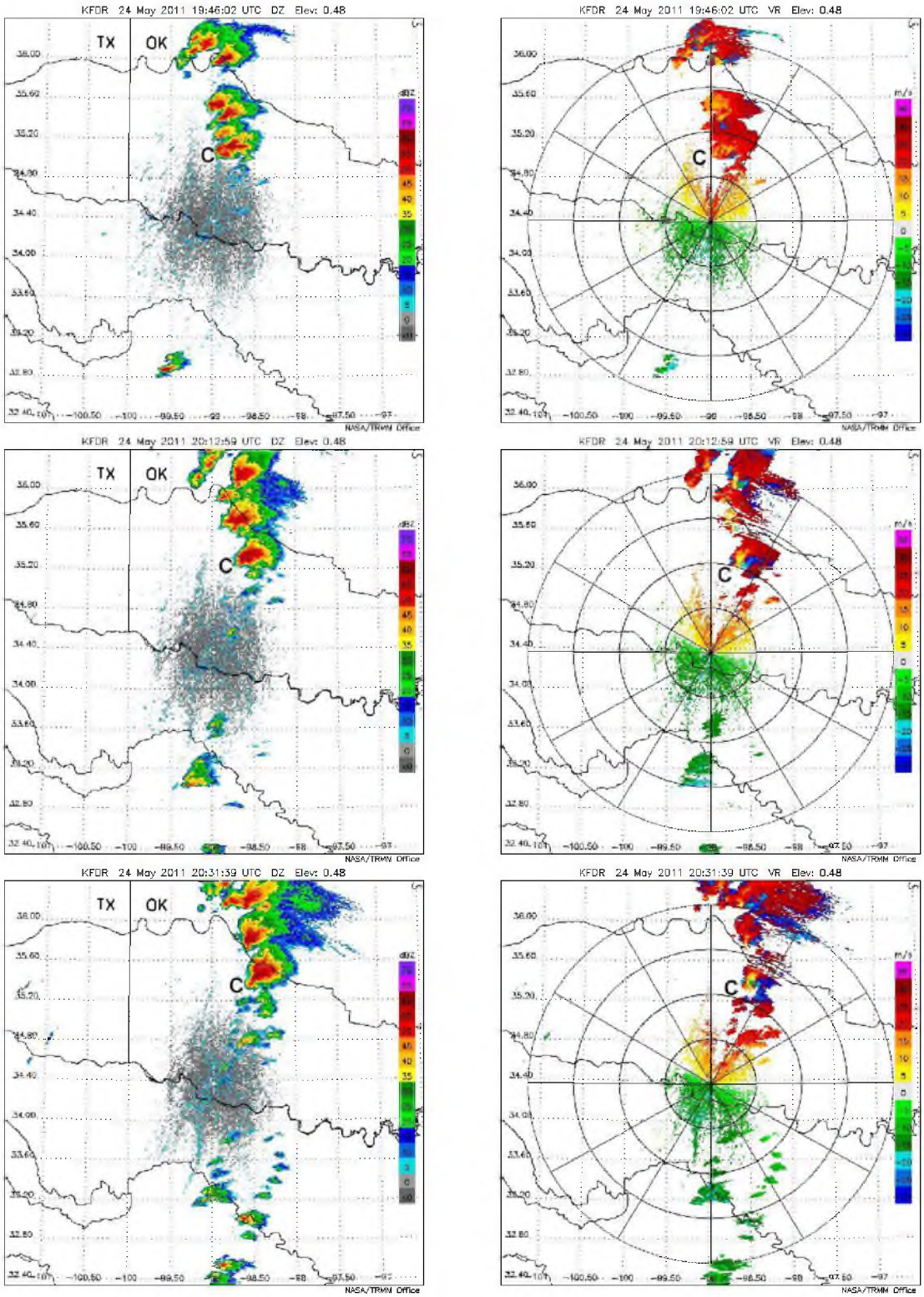

Figure 5.20. Radar timeline of Cell C from the Frederick, OK (KFDR) WSR-88D radar. The timeline illustrates the early cell (1946 UTC); supercell structure (2012 UTC); and hook echo structure (2031 UTC). (Timeline continued on the next page).

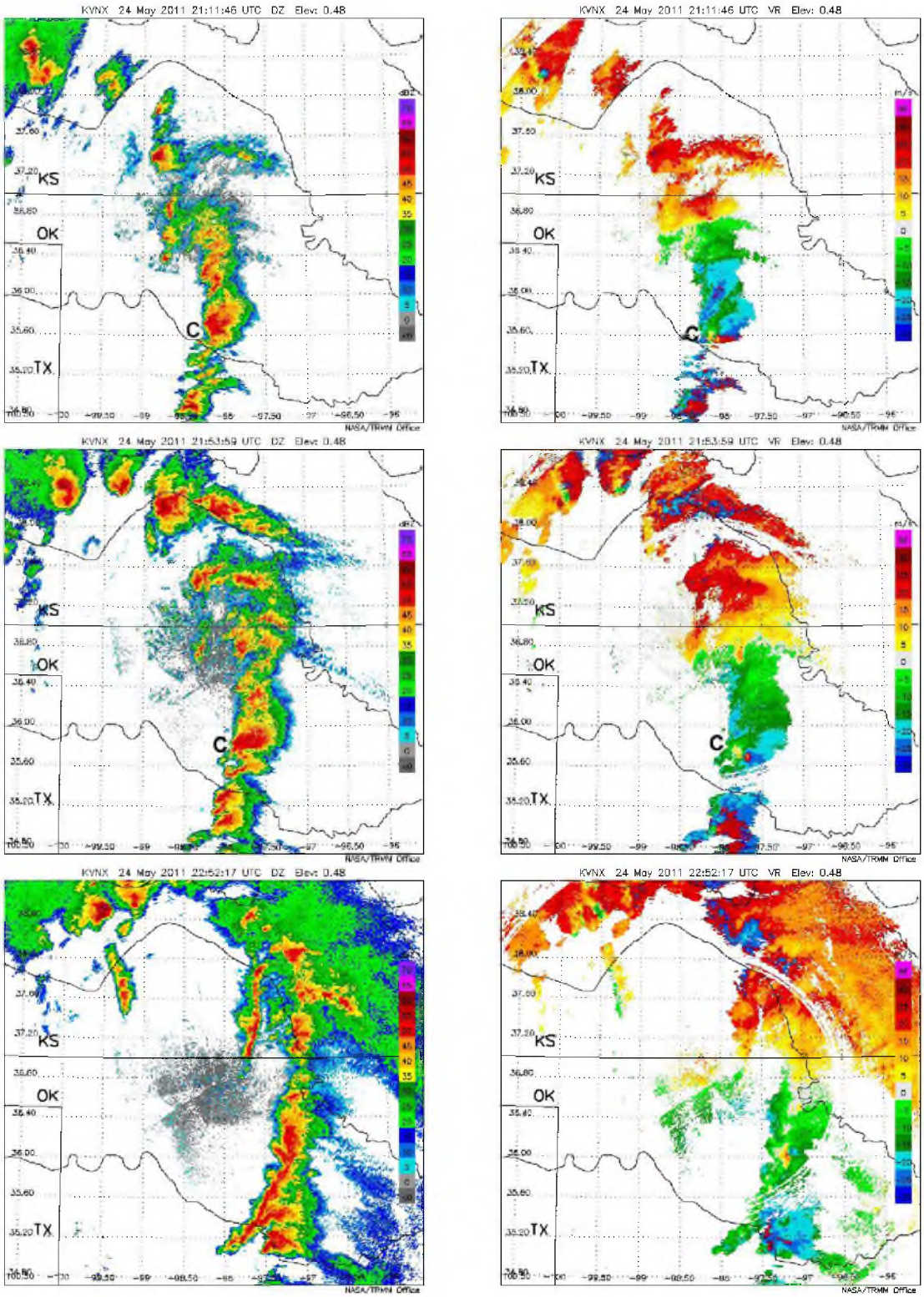

Figure 5.21. Radar timeline of Cell C, continued, illustrating a strong, developed mesocyclone (2111 UTC); hook echo and mesocyclone (2153 UTC); and linearity (2252 UTC).

convective line, as seen in the ultra high-frequency (UHF) vertical S-band radar profiler imagery (Figure 5.22), indicating that the forward anvil cloud reached the Central Facility at 2010 UTC, and the region of convective precipitation reached the CF by 2130 UTC.

The NASA ER-2 aircraft's mission on 24 May was twofold: first, observations were made over convection in Colorado before the ER-2 flew east and observed convection in Oklahoma. As a result, the best overpass of Oklahoma convection is made at 2212 UTC, when the majority of the supercells have weakened and evolved into a line. The ER-2 flew over the remnants of cell C, which was still severe, with echo tops exceeding 13 km and CoSMIR 89 GHz (vertical) brightness temperatures near 80 K (Figure 5.23)

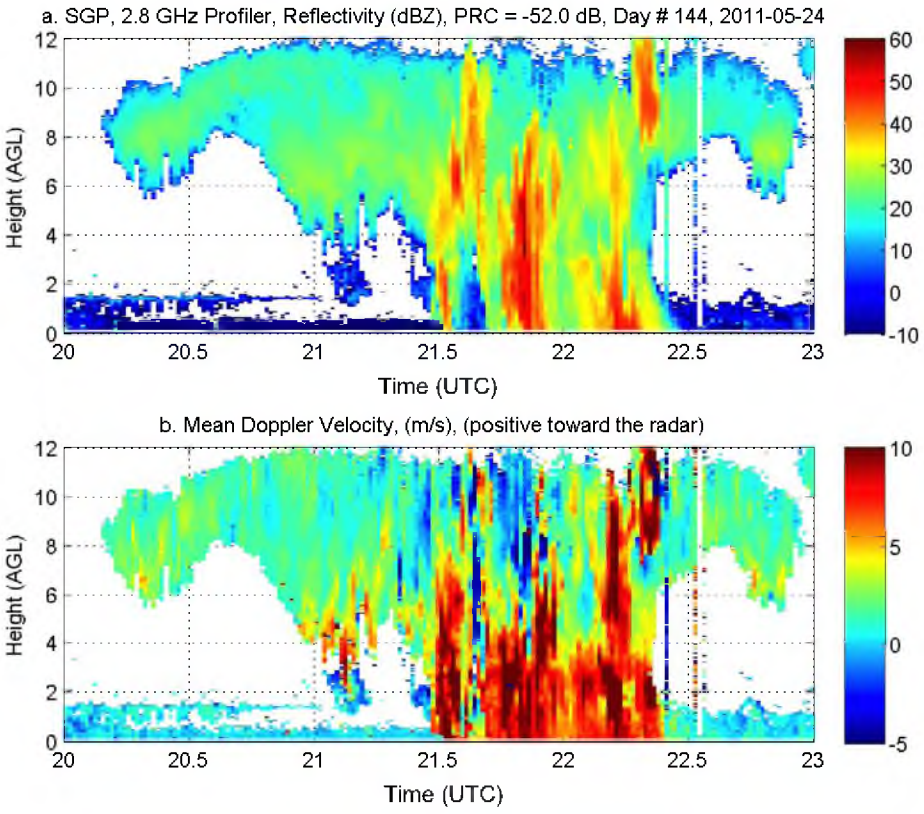

Figure 5.22. Vertically pointing S-band profiler observations (top) Reflectivity (dBZ), (bottom) Vertical Velocity (m s^{-1}) for the duration of the precipitation over the Central Facility.

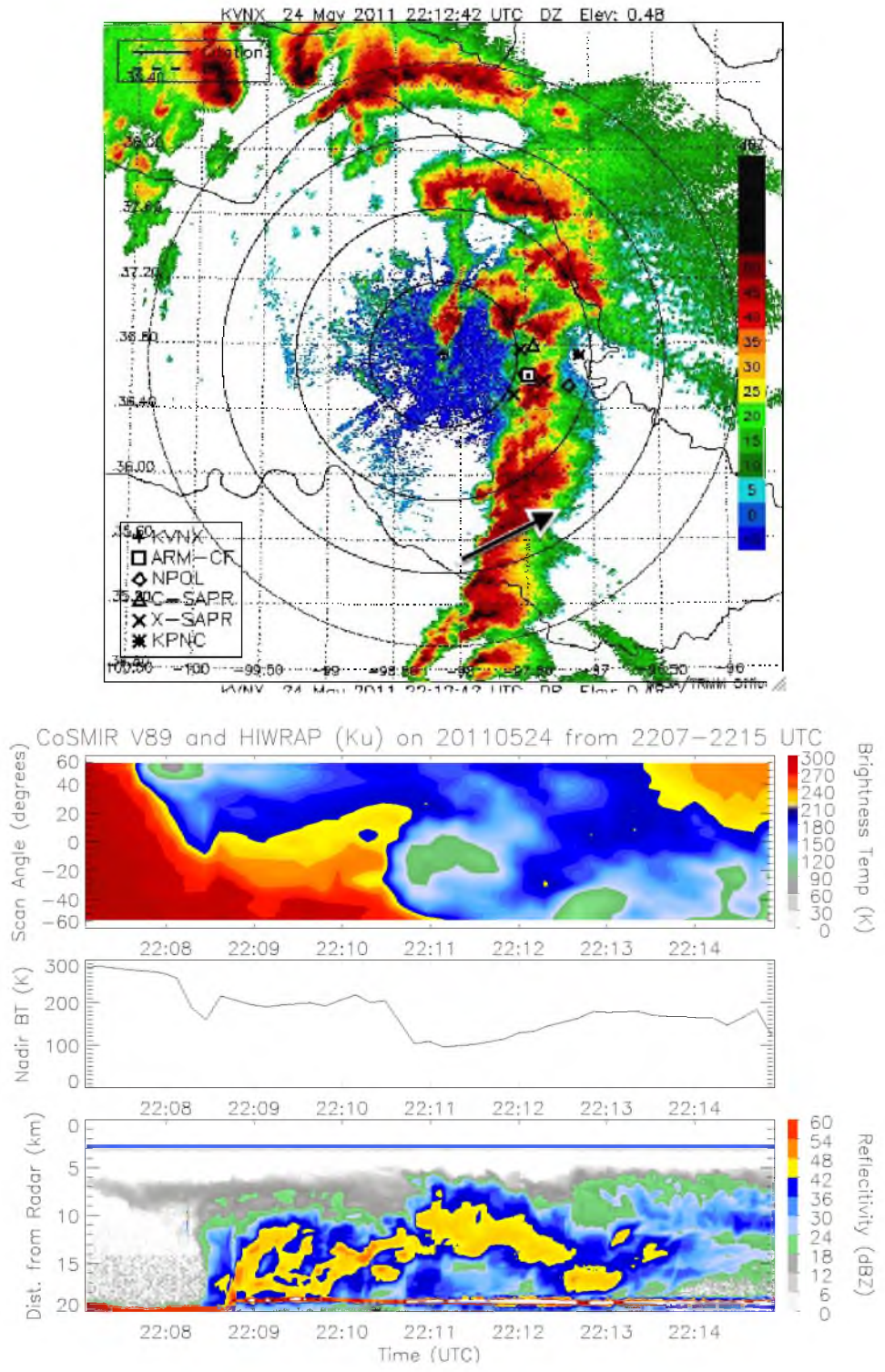

Figure 5.23. Vance, OK (KVNX) WSR-88D PPI and ER-2 HIWRAP and CoSMIR cross sections. Top: KVNX radar imagery overlaid with the flight path of the ER-2 (dashed) from 2207-2212 UTC 24 May 2011. Bottom: CoSMIR 89 GHz brightness temperature contour, 89 GHz nadir brightness temperature, HIWRAP Ku-band nadir vertical reflectivity profile.

5.2.4 Propagation

Vertical shear profiles and interaction among supercells both play major roles in the convective development on 24 May. Bluestein and Weisman (2000) found in their simulations that an obtuse angle of shear relative (from 1.7 to 5 km AGL) to the line of forcing actually supports anticyclonically rotating supercells (left-movers) and a cyclonically rotating right-mover downshear. If the 1.7 - 5 km obtuse shear angle discussed above is matched with veering at the lowest levels, the other cells in their simulations become diagnosed as multicellular. These phenomena are present in the lifecycle of the storms on 24 May and the hodographs embody this obtuse angle and veering low-level shear. Also in play on 24 May is strong linear vertical wind shear, which Rotunno et al. (1988) found is supportive of multicellular development as well.

The soundings taken at Purcell, OK over the course of 24 May tell an interesting story of this nature. At 1430 UTC, the Purcell hodograph shows veering from the surface to 2 km, and the 1.7 - 5 km line of shear extends 138° from the line of forcing (found to be 6° west of north, or 354°W) (Figure 5.24). Later, at 1730 UTC, there is still veering from the surface to 1.7 km; however, the 1.7 - 5 km line of shear has rotated to 10° from the line of forcing (Figure 5.24b). Further still, at 2029 UTC, the line of forcing is 72° from the line of forcing, and the shear profile is much more linear, with only a hint of veering up to 1 km (Figure 5.24c). At this time, (2022 UTC at CF and 2029 at Purcell), the Central Facility and Purcell, OK hodographs are similarly linear (Figure 5.25).

The lifecycles of A, B, and C are affected differently by interactions with other cells. A goes through a reintensification period after it collides with a left-mover to its south, and the convergence at A's southern flank may have incited the mesocyclone, which persisted long past the disintegration of the left-mover. Cell B, however, resulted from the amalgamation of many cells, and while the final merged cell persisted for several hours and became part of the multicell line, it never formed a mesocyclone. Cell C, at the southerly end of the first line of convection, bloomed into a right-mover and created a strong mesocyclone that resulted in a fatal EF-5 tornado before joining its northern colleagues in the line.

The line, unlike the convection that formed on 20 May, did not morph into a leading line/trailing stratiform MCS. Instead, weak forward anvil echoes are seen downshear of the convective line. The shear on this day, even in the later stages, differed from the shear on 20 May because while linearity appears in the hodographs later in the evening, the angle relative to the line of forcing in the later hours was nearer to 60° from the line of forcing,

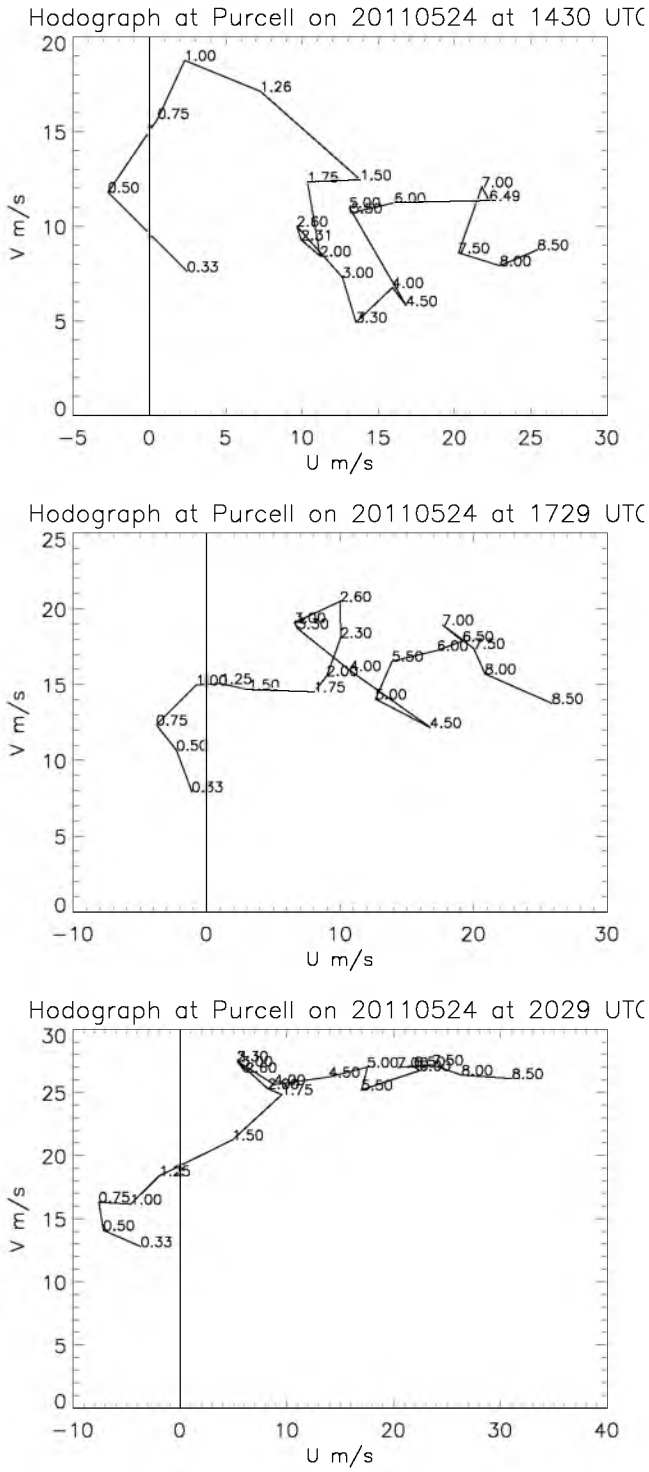

Figure 5.24. Hodographs created from the radiosondes launched at Purcell, OK (35.02°N/97.37°W) at 1430, 1729, and 2029 UTC. Radiosonde locations can be found in Chapter 2.

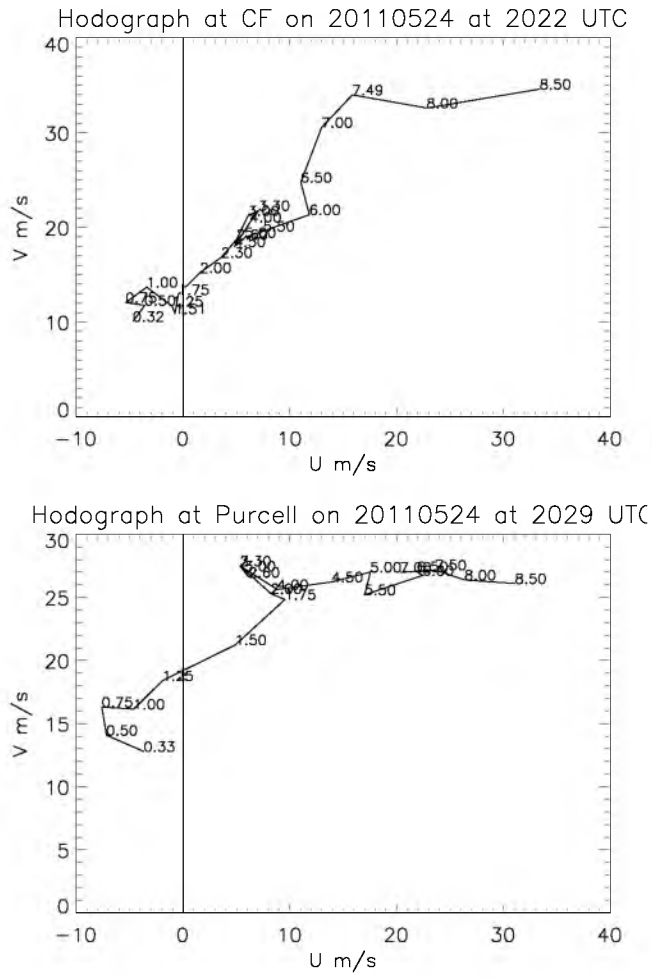

Figure 5.25. Hodographs created from the radiosondes launched at the Central Facility, OK (36.6°N/97.49°W) and Purcell, OK (35.02°N/97.37°W) at 2022 and 2033 UTC, respectively. Radiosonde locations can be found in Chapter 2.

unlike the normal shear that would support squall line maintenance (Figure 5.25).

The convective cells of 24 May did, in fact, produce cold pools. Between the hours of 2030 UTC and 2330 UTC, cold pools are created at various times, but they dissipate and new pools form elsewhere (Figure 5.26). After 2330 UTC, in the northern half of Oklahoma, the cold pool presence is more pronounced and steadier. This coincides with the beginning of the linear structure of the cells; long-lasting cold pools are not associated with the early supercells of 24 May. The long-lived cold pool in northern Oklahoma persists past 0200 UTC 25 May, whereupon it cannot be distinguished from the cool nighttime air surrounding it.

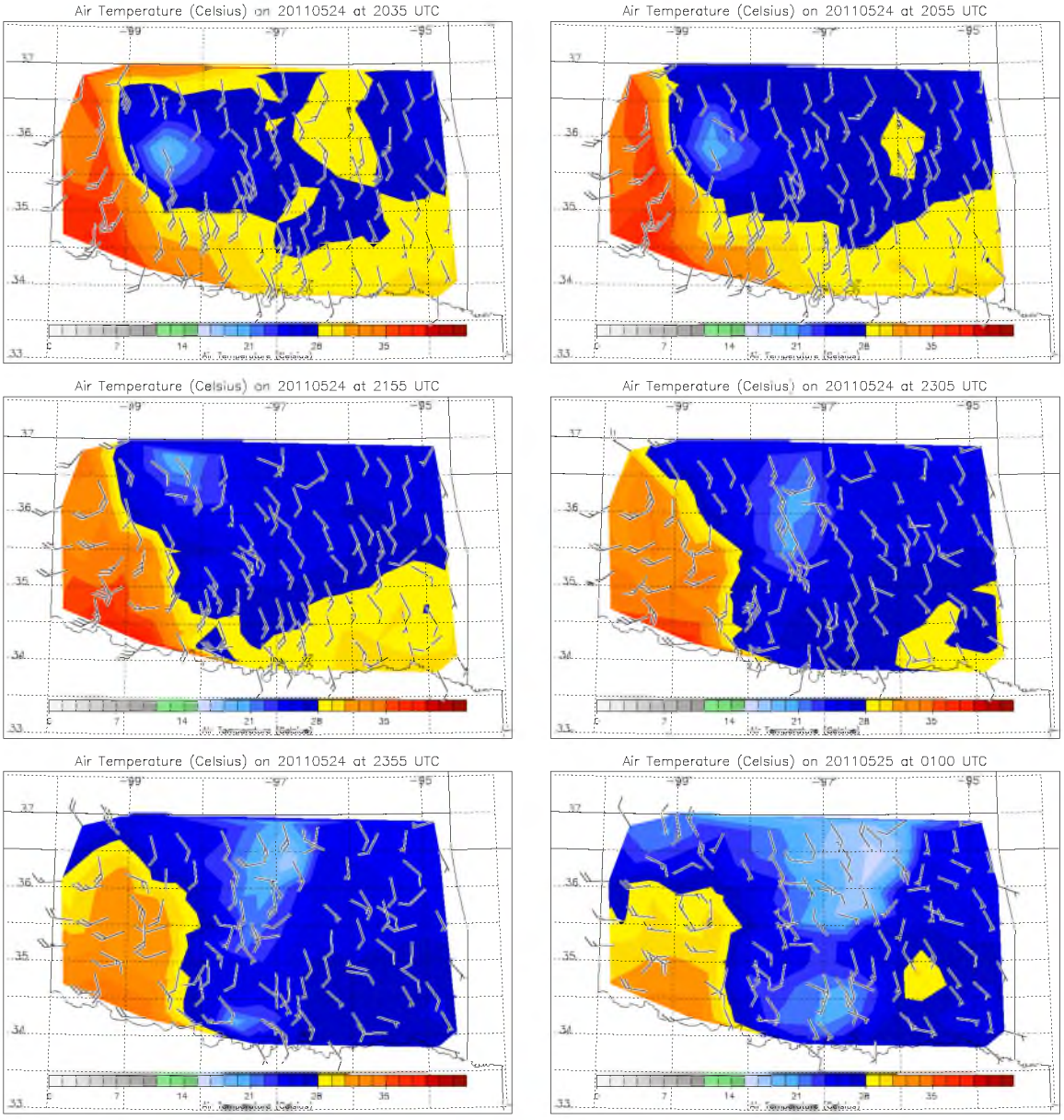

Figure 5.26. Timeline of altitude adjusted surface air temperature (contours) and wind observations (barbs). The timeline illustrates the temporary nature of the earlier cold pools (2035, 2055, 2155, 2305 UTC) and the second phase of a longer-lived cold pool in northern Oklahoma (2355 and 0100 UTC) from 24 and 25 May 2011 Oklahoma Mesonet observations.

CHAPTER 6

DISCUSSION

The convection on 20, 23, and 24 May all presented examples of well-documented severe midlatitude convection whose behavior, however, was far from conventional. Each day experienced multiple forcing mechanisms on the synoptic, mesoscale, and convective scales, all of which were vying for dominance over the convective development. Throughout the three events discussed above, however, there are two effects that rose to prominence: the vertical shear profile and the convective downdraft. Once the conditions for convection were satisfied, and once initiation had occurred, these two mechanisms were the dominant controlling factors of the subsequent convective lifecycle.

6.1 Environmental Consistencies

The preconditioning mechanisms discussed in Chapter 1 were present in the prestorm environments for all three cases. The approach of upper-level troughs in all 3 days of study (the passage of such a trough occurred on 20 and 24 May) provided the necessary destabilization of the atmosphere such that convection could be sustained once it was initiated. Running throughout this paper is the held assumption that secondary propagation requires the maintenance of a steady source of fuel and an unstable atmosphere. Indeed, even after the passage of the aforementioned troughs, southerly winds continued to advect heat and moisture from the Gulf of Mexico into Central Oklahoma (Figure 6.1).

6.2 Shear as a Determining Factor of Morphology

The vertical shear profiles aloft determined the overarching convective morphologies in two ways. The strength of the vertical wind shear provided the necessary displacement and pressure perturbation aloft; however, the direction and alignment of the shear played a massive role in the actual lifecycle of the storms. Veering curvature of the shear in lower levels supported right-moving supercells, which occurred at one point on all 3 days of study. Above 1 km, however, the orientation of the shear was of paramount importance. Once the

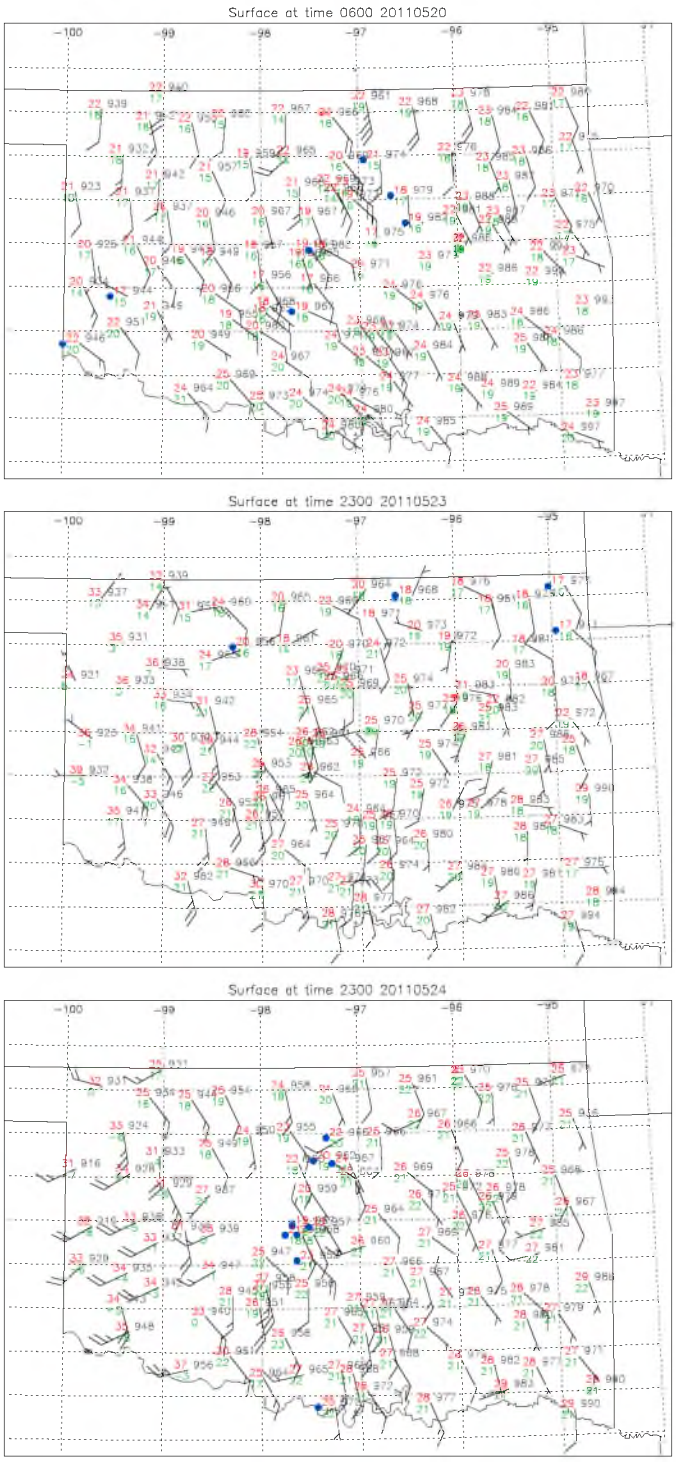

Figure 6.1. Surface maps created from the Oklahoma Mesonet. Wind speed and direction (barbs), temperature in Celsius (red, upper left), dew point temperature (green, lower left), pressure in hPa (black, right), and occurrence of rain within the previous 5-min period (blue dots) are shown. These maps illustrate the surface conditions at 0600 UTC 20 May, 2300 UTC 23 May, and 2300 UTC 24 May, times during which convection had reached maturity.

supercells were developing, as the shear and instability demanded, their alignment and positioning determined if they would compete with each other. The angle of the 1.67 - 5 km shear relative to the line of forcing at the surface (in all 3 days this was the dryline, which was roughly south-north oriented each day) (as discussed by Bluestein and Weisman (2000)), determined the positioning of the newly developing cells, and thus their propensity to compete for the available warm, moist air at the surface. An acute angle of 1.7-5 km shear relative to the line of forcing is supportive of isolated supercells, 45° being opportune. 23 May 2011 supercells were subject to an angle of 24°, and while this was not the ideal angle, most of the cells, with the exception of the back-builder, matured in isolation until they dissipated. While their simulation incorporated idealized and perfectly straight hodographs above 1.7 km, there were remarkable similarities in behavior for the convective storms analyzed in this study when the bulk shear angle between 1.7 and 6 km was considered.

The shear-line of forcing angle for 24 May, on the other hand, was obtuse (Figure 6.2), and in this case, left-moving supercell development was not suppressed, and thus left-movers were able to propagate northward and collide with neighboring right-movers along the line of forcing. This competition and intersection of downdrafts may have resulted in the disintegration of right-moving supercell "A."

May 20, the shear began as a veering lower level hodograph; however, by 2030 UTC, the hodographs in southern Oklahoma were undeniably linear (Figure 6.3). Supercell development was no longer supported, and "system 3" propagated as an MCS across the state.

6.3 The Role of Cold Pools

The vertical wind shear profile, again, in the presence of moisture and instability, was the controlling factor of the storms' morphologies, and their alignment was what determined the potential for cells to interact; however, it was the nature of the convective downdraft that determined the extent to which cells competed, the characteristics of a cold pool, should one be produced, and ultimately the longevity of the storm cells themselves.

Supercell downdrafts that were unimpeded, such as in the case of cell "C" on 24 May at the southern end of the line, were able to maintain the propagation and rotation for an extended period of time. When the downdrafts interacted, however, such as in the case of cell "A," the mesocyclone was destroyed.

The storms of 20 May, particularly the MCS generated by "system 3," produced strong

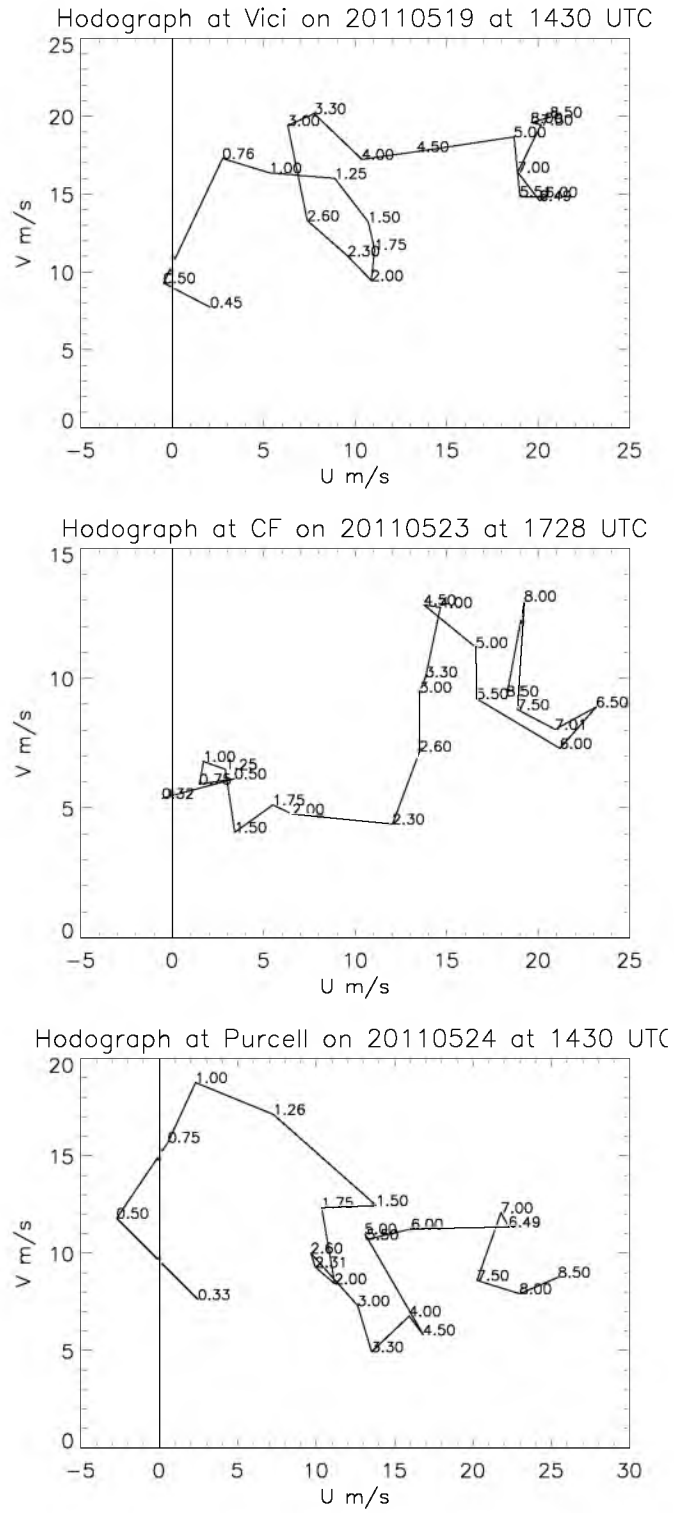

Figure 6.2. Hodographs created for 20, 23, and 24 May at the Central Facility, Vici, and Purcell, OK, respectively. 1.7 - 5 km angle of shear relative to the lines of forcing were 57°, 24°, and 138 °, respectively. Radiosonde launch locations are shown in Chapter 2.

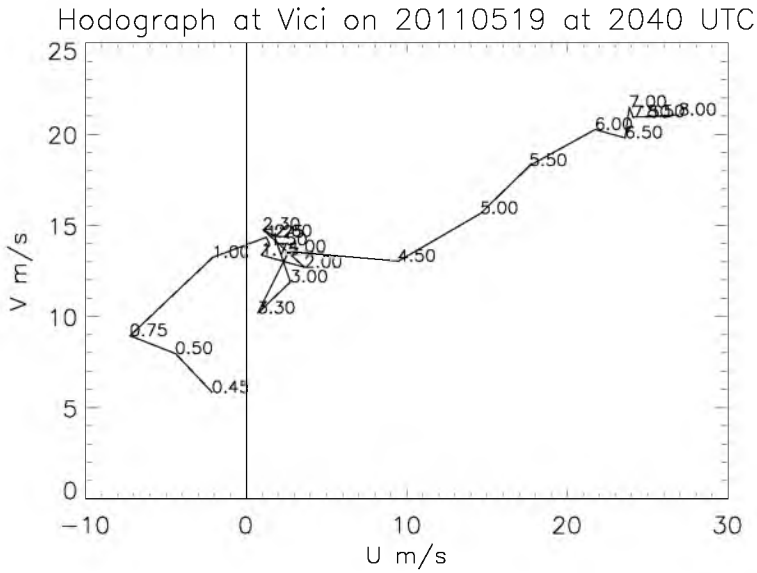

Figure 6.3. Hodograph created from the 2040 UTC19 May 2011 Vici, OK (36.15°N/99.3°W) radiosonde data.

cold pools. The early supercells produced cold pools, albeit short-lived ones. Looking at the 2330 soundings, there remains high lapse rate drier air above 800 hPa at Vici, Morris, and the Central Facility. As mentioned by Wakimoto (2001), the midlevel troposphere air is an important determining factor of the strength of the convective downdraft, and the midlevel lapse rates determine the amount of cooling that the sinking air undergoes.

23 May supercells for the most part were able to propagate in isolation and diminished after 5 hours. The cell that ultimately back-built, however, was made possible not only by outflow from the neighboring cell's downdraft, but also by the initial presence of the dryline to its west. In this situation, then, a surface boundary played an extremely important role, as the environmental conditions supported its development yes, but no other supercells that formed that day back-built; therefore, the storm that interacted with the bend in the dryline at (36.4°N/98.5°W) was able to back-build.

The dryline, however, is not the entire reason for the back-building process, nor was it responsible for maintaining the back-building after 2 hours into the back-builder's development. As discussed by Schumacher and Johnson (2005), this back-building event began on a surface boundary (dryline) but was maintained by convergence along its own gust front, and in this case, as demonstrated by the extreme drop in temperature at the surrounding Mesonet stations, its convectively generated cold pool.

6.4 Contrasting Structures on 20 and 24 May

With respect to changing morphology and the role of large-scale environmental shear, why were 20 and 24 May so drastically different when the arrival of a trough was ultimately the reason for the destabilization and triggering that occurred at the dryline, and the evolution of the shear profiles were similar? 20 May exhibited a widespread, long-lived stratiform region throughout its maturity whereas 24 May only showed leading anvil development.

Both cases exhibited veering hodographs early on, and while the angles of the midlevel shear relative to the lines of forcing were very different (57°, 20 May and 138°, May 24), that likely explains the prevalence (or lack thereof) of left-movers in the earliest convection. Both systems had linear elements in the mature phases of their lifecycle, but 20 May's lines evolved into leading-line/trailing stratiform whereas on 24 May, there was no trace of trailing stratiform precipitation. A cross-section through the storms of 24 May once they have developed into a line (Figures 6.4 and 6.5) from both HIWRAP and NPOL show very little development west of the convective line and a very sharp reflectivity gradient at the convective line's western edge.

Both cases exhibited cold pool structures at the surface. The convectively generated cold pool is the lifeline of the MCS, and on 20 May, a very strong cold pool was created by system 3 throughout its lifecycle (Figure 6.6), whereas on 24 May, cold pools were generated, but only after the storms were long into maturity, and even then they are spotty and shorter lived (Figure 6.6). The 0231 UTC sounding from the Central Facility shows the cold pool at the surface (Figure 6.7). This cold pool is 636 meters deep and shows approximately an 8°C temperature depression from the surroundings. This cold pool, while not significantly, is weaker than the cold pool that formed on 20 May.

Houze et al. (1990) suggest that mesoscale convective lines that do not exhibit trailing stratiform structure have shear and instability values closer to those of supercells but linear shear that is predominantly westerly, unlike its more characteristic MCS LL/TS colleagues that have higher Bulk-Richardson numbers and more southwesterly shear. In an MCS, front-to-rear flow is a predominant mechanism for trailing stratiform development (Smull and Houze 1985). For front-to-rear circulation to be sustained, the vertical shear profile needs to be sufficiently strong to create an upshear-tilting updraft (Newton 1966; Misumi et al. 1994), but must still balance the downdraft circulation (cold pool strength) (Rotunno et al. 1988).

Perhaps, then, the critical difference between the 20 May and 24 May cases and the

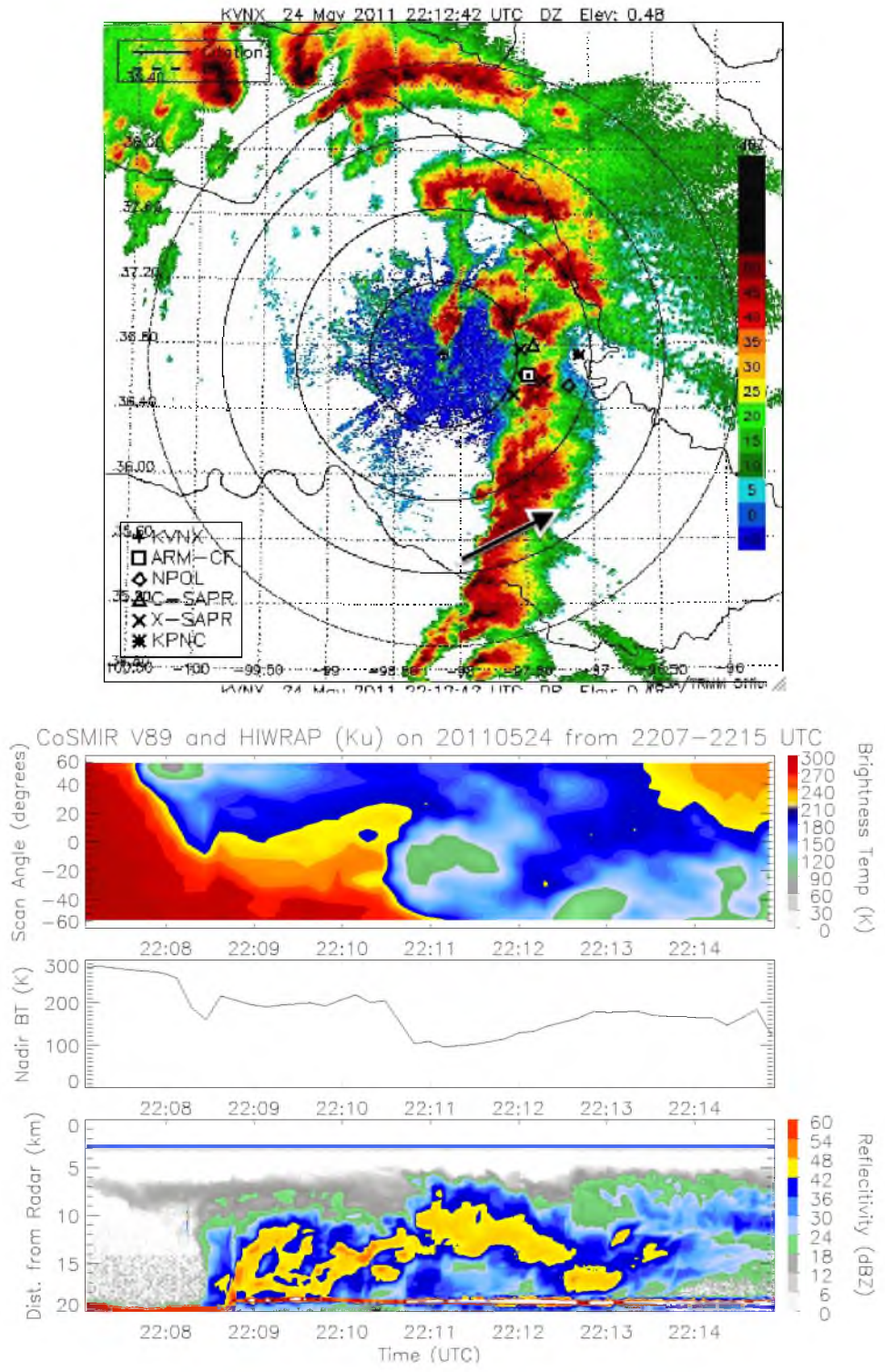

Figure 6.4. Vance, OK (KVNX) WSR-88D PPI scan and ER-2 HIWRAP and CoSMIR cross sections. Top: KVNX radar imagery overlaid with the flight paths of the ER-2 (dashed) and the UND Citation (solid) from 2208-2212 UTC 24 May 2011. Bottom: CoSMIR 89 GHz brightness temperature contour, 89 GHz nadir brightness temperature, HIWRAP Ku-band nadir vertical reflectivity profile.

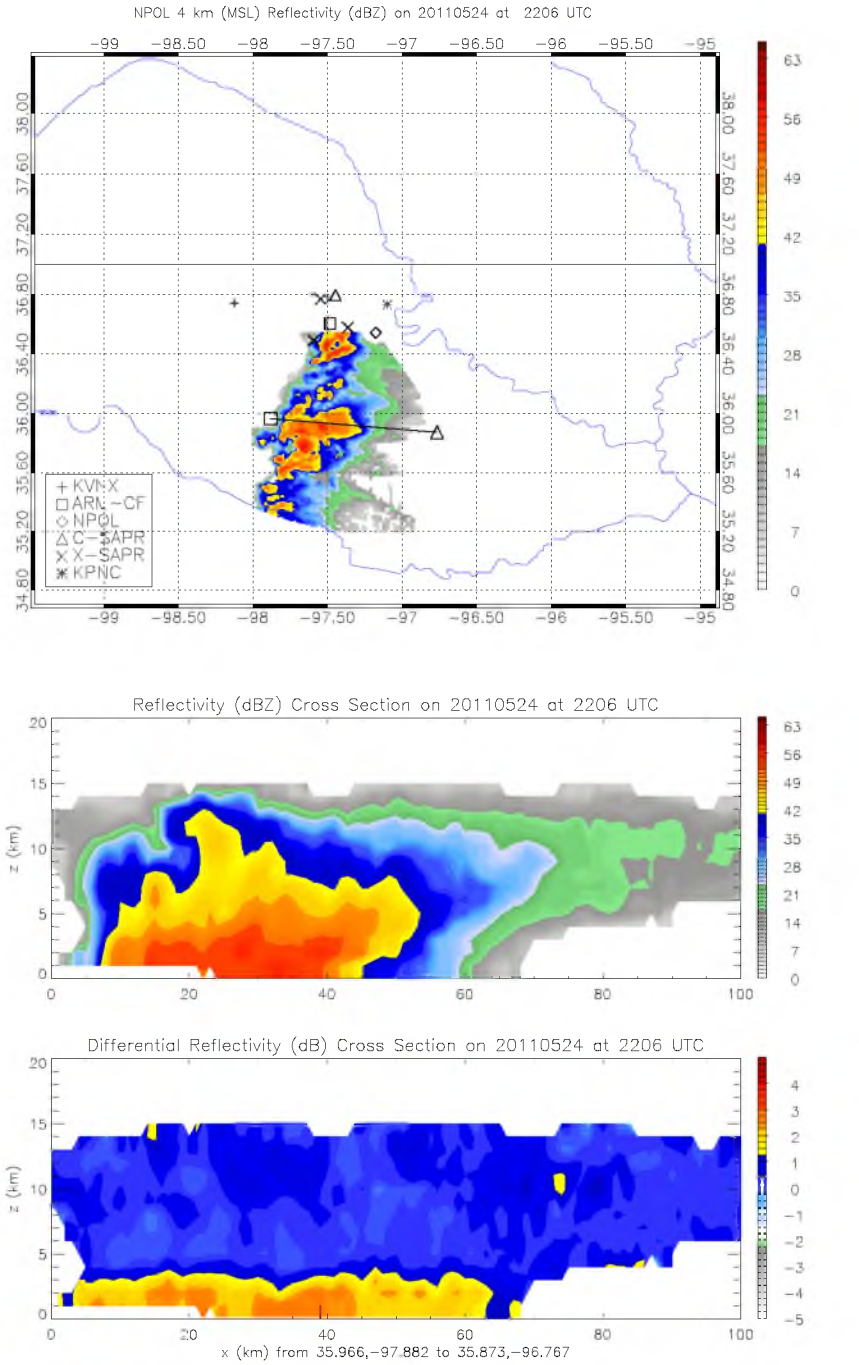

Figure 6.5. NPOL 4 km CAPPI overlaid with the path of the cross-section shown in b. NPOL reflectivity (top) and differential reflectivity (bottom) cross-sections at 2206 UTC 24 May 2011.

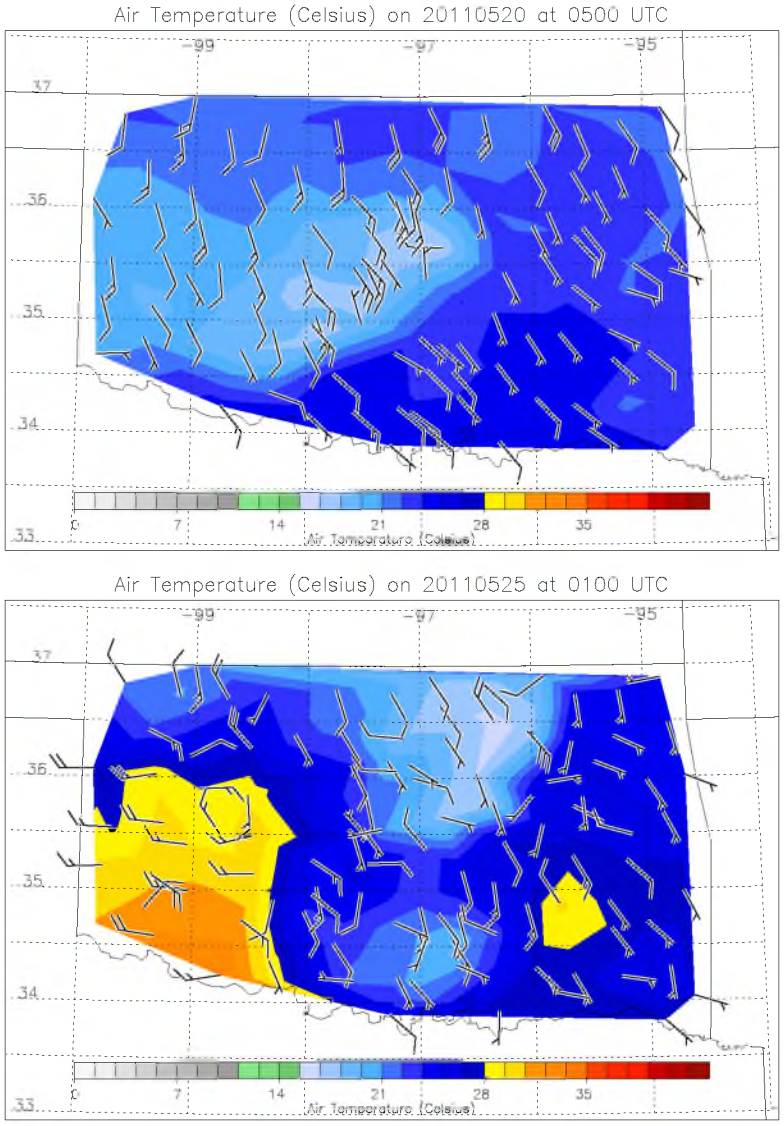

Figure 6.6. Oklahoma Mesonet altitude adjusted surface air temperature (contours) overlaid with wind observations (barbs) at 0500 UTC 20 May (left) and 0100 UTC 25 May (right). Note the difference in the extent of the cold pools on each day. Note also that the cold pool on 20 May occurred during the night.

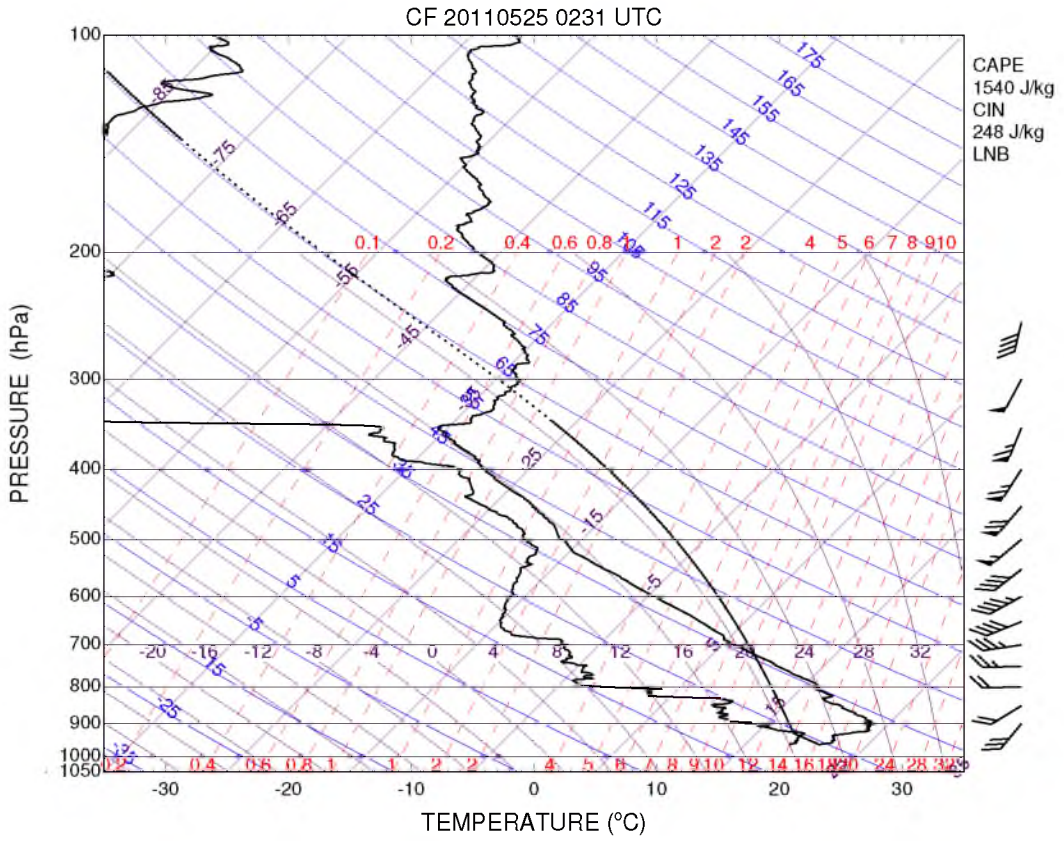

Figure 6.7. 0231 UTC 25 May 2011 skew-T/log-P representation of the sounding taken at the Central Facility, OK (36.6°N/97.49°W). Radiosonde launch locations are shown in Chapter 2.

reason why the 20 May case formed a trailing stratiform region and exhibited the classic MCS structure, is the interaction between the midlevel wind shear and the developing storms. The 24 May case, though phenotypically resembled a "classic supercell" case, presented not only left-moving supercells, but also a linear structure that could not be categorized according the MCS conventions put forth by Houze et al. (1990).

The importance of vertical wind shear has been well documented by observational studies and simulations alike. Both the strength and magnitude of the vertical wind shear determine, to an extent, the morphologies of a convective system. The cases presented here do not refute this. In each case, the shear profile had a profound effect on the initial and mature morphologies of the convection and how they evolved. While finding the ideal 45° shear profile may be elusive in observational datasets, the shear profiles examined on these 3 days behaved very similarly to the simulated supercells as described by Bluestein and Weisman (2000). Note for the entirety of this analysis, the hodographs analyzed for the forcing-shear angle are not idealized in the way of Bluestein and Weisman (2000). The angles calculated here are bulk, and are shown in comparison to those of Bluestein and Weisman to note the similarity. The 19 May 2040 UTC sounding taken at Vici, OK shows 20 - 30 knot winds in the midlevels, whereas the 24 May 2030 UTC sounding taken at Purcell, OK shows 50 knot winds from 900 to 600 hPa (Figure 6.8); thus, while both days presented the necessary stronger vertical wind shear for supercellular development, the vertical shear in the midlevels was much strong on 24 May, and may have prevented the maturing convection from developing a trailing stratiform region.

6.5 The Role of Convective Downdrafts

The second most important determining factor of convective evolution, the downdraft, has also long been recognized as a major player in the convective lifecycle. These cases support this theory, as in some cases, the downdraft was the hero of the developing convection, as was the case for the MCS line on 20 May, the back-builder's gust front in phase 2 of its back-building, and the southernmost supercell's (cell C) longevity as a supercell and mesocyclone. Other times, such as cell A's destruction by colliding with a left-mover or the early supercells of 20 May that dropped a cold pool and quickly dissipated, the downdraft was the downfall of the convection.

The modeling community laments the lack of knowledge of convective propagation (Moncrieff and Liu 2006), and while the environmental shear is more widespread and is often

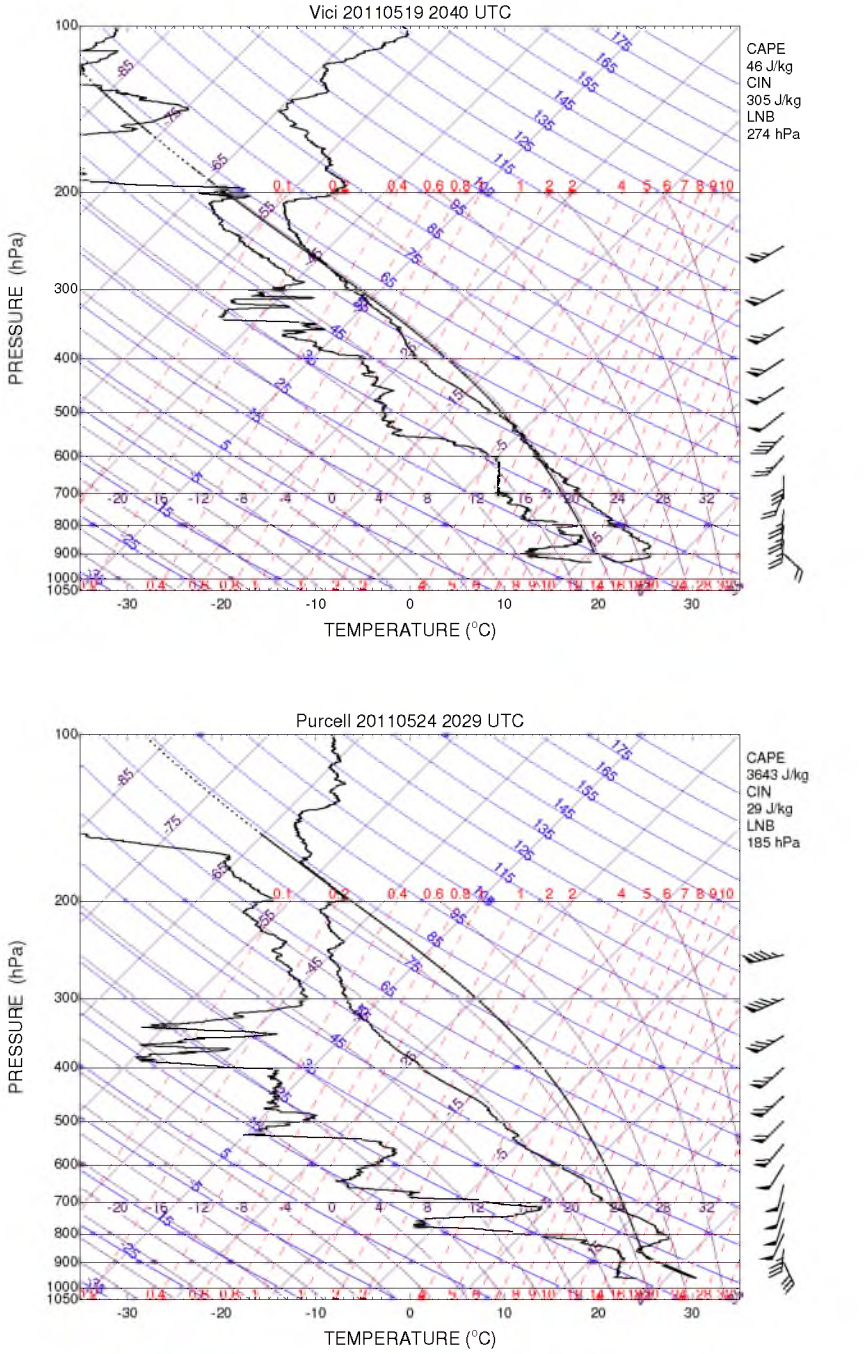

Figure 6.8. 2040 UTC 19 May 2011 skew-T/log-P representation of the sounding taken at the Vici, OK (36.15°N/99.3°W) (top). 2029 UTC 24 May 2011 skew-T/log-P for Purcell, OK (36.15°N/97.37°W) (bottom). Radiosonde launch locations are shown in Chapter 2.

associated with synoptic forcing (Hane 1986), resolving the downdraft processes becomes more difficult and is a pressing problem. Wakimoto (2001) states that the air into which hydrometeors falls is of paramount importance for determining the characteristics and strength of the downdraft. Also important, however, are the characteristics of the hydrometeors that precipitate in the first place, as the melting and sublimation of these particles are the cooling mechanisms that drive the downdraft (Wakimoto 2001). Simulations of convective downdrafts are strongly sensitive to changes in the microphysics that govern hydrometeor states, and in order to resolve the downdrafts correctly, hydrometeor parameterization is a major ongoing concern of the modeling community (Bryan and Morrison 2012; Morrison and Milbrandt 2011). This work further supports that effort and the need to characterize downdrafts correctly in order to resolve convective organization and longevity accurately.

The evolution of the convective events described in this study does not depend heavily on the existence of diverse forcing boundaries. Initiation along a boundary, such as the dryline and the cold pool edge (23 May), was prevalent; however, with the exception of the initial back-building phase along the dryline, the storms were maintained the propagation of their own gust fronts in the sustained presence of warm, moist, southerly air. Perhaps, then, less emphasis need be placed on replicating exact boundaries, as the downdraft behavior outweighed other effects on the developing convection in this study, particularly in the case of the back-builder that, in phase 2, regardless the advance of the cold pool from the east and the stationary front from the north, propagated due to its own outflow.

6.6 Future Work

As discussed above, this work suggests that the convective downdraft plays a major role in the lifecycle and longevity of an organized convective system. Further analysis of the convective downdrafts of these events is needed to validate this conclusion. A multi-Doppler wind profile of the area surrounding the Central Facility is made possible by the presence of the C-band, X-band, and multiple S-band radars at the site, and provides insight into the vertical velocities that occurred during the campaign, and analysis of such a dataset is extremely valuable. The data analyzed here is insufficient to characterize a convective downdraft, and the multi-Doppler retrieval is the most viable, albeit imperfect,

Another logical direction this work may take is to simulate the convective events studied here, especially with the ability to compare the results with the detailed observations made during the MC3E campaign. As discussed in the first chapter, the primary goal

of this field campaign was to make detailed microphysical observations of convection. The University of North Dakota Citation aircraft data, not analyzed here, contains detailed *in situ* microphysics observations that are immensely valuable for analyzing the hydrometeor characteristics that are so important to the downdraft behavior discussed above. Regards for human safety, however, prevented the UND Citation from sampling hydrometeors within the convective updraft and downdrafts. The Central Facility also contained a myriad of disdrometers and precipitation gauges for microphysical observations at the surface.

What determines the nature of convection has long been the subject of analysis, and with so many competing multiscale factors, full characterization may not yet be in reach. The MC3E campaign provides a rich dataset with observations along all of these scales, however, and as the aforementioned cases suggest, parameterizing the consistently dominant factors is paramount.

REFERENCES

Barnes, G. M. and M. Garstang, 1982: Subcloud layer energetics of precipitating convection. *Monthly Weather Review*, **110**.

Bluestein, H. B. and M. H. Jain, 1985: Formation of mesoscale lines of precipitation: Severe squall lines in Oklahoma during the spring. *Journal of the Atmospheric Sciences*, **42**, 1711–1732.

Bluestein, H. B. and S. S. Parker, 1993: Modes of isolated, severe convective storm formation along the dryline. *Monthly Weather Review*, **121 (5)**, 1354–1372.

Bluestein, H. B. and C. R. Parks, 1983: A synoptic and photographic climatology of low-precipitation severe thunderstorms in the southern plains. *Monthly Weather Review*, **111**, 2034–2046.

Bluestein, H. B. and M. L. Weisman, 2000: The interaction of numerically simulated supercells. *Monthly Weather Review*, **128**, 3128–3149.

Browning, K. A., 1964: Airflow and precipitation trajectories within severe local storms which travel to the right of the winds. *Journal of the Atmospheric Sciences*, **21**, 634–639.

Browning, K. A. and F. H. Ludlam, 1961: Airflow in convective storms. *Quarterly Journal of the Royal Meteorological Society*, **88 (376)**, 117–135.

Bryan, G. H. and H. Morrison, 2012: Sensitivity of a simulated squall line to horizontal resultion and parameterization of microphysics. *Monthly Weather Review*, **140**, 202–225.

Bunkers, M. J., 2002: Vertical wind shear associated with left-moving supercells. *Weather and Forecasting*, **17**.

Carlson, T. N. and F. H. Ludlam, 1968: Conditions for the occurrence of severe local storms. *Tellus*, **2**.

Chappell, C. F., 1986: Quasi-stationary convective events. American Meteorological Society, 289–310.

Coniglio, M. C., H. E. Brooks, S. J. Weiss, and S. F. Corfidi, 2007: Forecasting the maintenance of quasi-linear mesoscale convective systems. *Weather and Forecasting*, **22**, 556–570.

Corfidi, S., 2003: Cold pools and MCS propagation: Forecasting the motion of downwind-developing MCSs. *Weather and Forecasting*, **18**, 997–1017.

Crook, N. A. and M. W. Moncrieff, 1988: The effect of large-scale convergence on the generation and maintenance of deep moist convection. *Journal of the Atmospheric Sciences*, **45 (2)**, 3606–3624.

Davies-Jones, R., 2002: Linear and nonlinear propagation of supercell storms. *Journal of the Atmospheric Sciences*, **59**, 31783 205.

Doswell, C. A., 2001: Severe convective storms: An overview. American Meteorological Society, Severe Convective Storms, 1–26.

Doswell, C. A. and D. W. Burgess, 1993: Tornadoes and tornadic storms: a review of conceptual models. *The Tornado: Its Structure, Dynamics, Prediction, and Hazards*, C. D. C. Church, D. Burgess and E. R. Davies-Jones, Eds., American Geophysical Union, Geophysical Monographs, Vol. 79, 161–172.

Emanuel, K. A., 1994: *Atmospheric convection*. Oxford University Press, 172-173 pp.

Fovell, R. G. and P. S. Dailey, 1995: the temporal behavior of numerically simulated multicell-type storms. part I: Modes of behavior. *Journal of the Atmospheric Sciences*, **52**, 2073–2095.

Fovell, R. G. and Y. Ogura, 1988: Numerical simulation of a midlatitude squall line in two dimensions. *Journal of the Atmospheric Sciences*, **45**, 3846–3879.

Gallus, W. A., N. A. Snook, and J. E. V., 2008: Spring and summer severe weather reports over the midwest as a function of convective mode: A preliminary study. *Weather and Forecasting*, **23**, 101–113.

Gilmore, M. S. and L. J. Wicker, 1998: the influence of midtropospheric dryness on supercell morphology and evolution. *Monthly Weather Review*, **126**, 943–958.

Hane, C. E., 1986: Extratropical squall lines and rainbands. American Meteorological Society, 359–389.

Heymsfield, G. M., L. Tian, L. Lihua, M. Mclinden, and J. Cervantes, 2013: Airborne radar observations of severe hail storms: Implications for future spaceborne radar. *Journal of Applied Meteorology and Climatology*.

Hoch, J. and P. Markowski, 2005: A climatology of springtime dryline position in the u.s. great plains region. *Journal of Climate*, **18**, 2132–2137.

Hocker, J. E. and J. B. Basara, 2008: A 10-year spatial climatology of squall line storms across Oklahoma. *International Journal of Climatology*, **28**, 765–775.

Houston, A. L. and R. B. Wilhelmson, 2007: Observational analysis of the 27 May 1997 central Texas tornadic event. Part I: Prestorm environment and storm maintenance/propagation. *Monthly Weather Review*, **135**, 701–726.

Houze, R. A., 1989: Observed structure of mesoscale convective systems and implications for large-scale heating. *Quarterly Journal of the Royal Meteorological Society*, **115 (487)**, 425–461.

Houze, R. A., 2004: Mesoscale convective systems. *Reviews of Geophysics*, **42 (RG4003)**, 1–43.

Houze, R. A., B. F. Smull, and P. Dodge, 1990: mesoscale organization of springtime rainstorms in Oklahoma. *Monthy Weather Review*, **118**, 613–654.

Johnson, R. H. and B. E. Mapes, 2001: Mesoscale processes and severe convective weather. American Meteorological Society, Severe Convective Storms, 71–122.

Klemp, J. B., 1987: Dynamics of tornadic thunderstorms. *Annual Review of Fluid Mechanics*, **19**, 369–402.

Klemp, J. B. and R. B. Wilhelmson, 1978: The simulation of three-dimensional convective storm dynamics. *Journal of the Atmospheric Sciences.*, **35**, 1070–1096.

Knupp, K. R. and W. R. Cotton, 1985: Convective cloud downdraft structure: an interpretive survey. *Reviews of geophysics*, **23 (2)**.

Lemon, L. R. and C. A. Doswell, 1979: Severe thunderstorm evolution and mesocyclone structure as related to tornadogenesis. *Monthly Weather Review*, **107**, 1184–1197.

LeMone, M. A., G. M. Barnes, and E. J. Zipser, 1984: Momentum flux by lines of cumulonimbus over the tropical oceans. *Journal of the Atmospheric Sciences*, **41 (12)**.

Lilly, D. K., 1979: The dynamical structure and evolution of thunderstorms and squall lines. *Annual Review of Earth and Planetary Sciences*, **7**, 117–161.

Maddox, R. A., 1980: Mesoscale convective complexes. *Bulletin of the American Meteorological Society*, **61 (11)**, 1374–1387.

Mapes, B. E., 1993: Gregarious tropical convection. *Journal of the Atmospheric Sciences*, **50 (13)**, 2026–2037.

Markowski, P. M., 2002: Hook echoes and rear-flank downdrafts: a review. *Monthly Weather Review*, **130**, 852–876.

Mesonet, 2012: Oklahoma Mesonet: Oklahoma Climatological Survey. [Online; accessed Apr 2012], `www.mesonet.org`.

Misumi, R., M. Divjak, S. Tanahashi, and T. Takeda, 1994: A numerical study on the formation of organized convective storms: Part I. formation patterns of lang-lasting cells. *Journal of the Meteorological Society of Japan*, **72 (2)**, 235–253.

Moncrieff, M. W. and C. Liu, 2006: Representing convective organization in prediction models by a hybrid strategy. *Journal of the Atmospheric Sciences*, **63**, 3404–3420.

Morrison, H. and J. Milbrandt, 2011: Comparison of two-moment microphysics schemes in idealized supercell thunderstorm simulations. *Monthly Weather Review*, **139**, 1103–1130.

Naylor, J., M. A. Askelson, and M. S. Gilmore, 2012: Influence of low-level thermodynamic structure on the downdraft properties of simulated supercells. *Monthly Weather Review*, **140**, 2575–2589.

Newton, C. W., 1966: Circulations in large sheared cumulonimbus. *Tellus*, **4**.

Parker, M. D. and R. H. Johnson, 2000: Organizational modes of midlatitude convective systems. *Monthly Weather Review*, **128**, 3413–3436.

Petersen, W. and M. Jensen, 2012: The NASA-GPM and DOE-ARM Midlatitude Continental Convective Clouds Experiment (MC3E). *The Earth Observer*, **24**, 12–18.

Purdom, J. F. W., 1976: Some uses of high-resolution GOES imagery in the mesoscale forecasting of convection and its behavior. *Monthly Weather Review*, **104**, 1474–1483.

Purdom, J. F. W., 1982: Subejctive interpretation of geostationary satellite data for nowcasting. Academic Press, Nowcasting, 149–166.

Rigo, T. and M. C. Llasat, 2005: Radar analysis of the life cycle of mesoscale convective systems during the 10 June 2000 event. *Natural Hazards and Earth System Sciences*, **5**, 959–970.

Rotunno, R. and J. Klemp, 1985: On the rotation and propagation of simulated supercell thunderstorms. *Journal of the Atmospheric Sciences*, **42 (3)**, 271–292.

Rotunno, R. and J. B. Klemp, 1981: The influence of shear-induced pressure gradient on thunderstorm motion. *Monthly Weather Review*, **110**, 136–151.

Rotunno, R., J. B. Klemp, and M. L. Weisman, 1988: a theory for strong, long-lived squall lines. *Journal of the Atmospheric Sciences*, **45**, 463–485.

Saxion, D. and R. Ice, 2012: New science for the WSR-88D: Status of the dual polarization upgrade. *28th Conference on Interactive Information and Processing Systems.*

Schaefer, J. T., 1986: The dryline. American Meteorological Society, Mesoscale Meteorology and Forecasting, 549–572.

Schmidt, J. M. and W. R. Cotton, 1990: Interactions between upper and lower tropospheric gravity waves on squall line structure and maintenance. *Journal of the Atmospheric Sciences*, **47 (10)**, 1205–1222.

Schumacher, R. S. and R. H. Johnson, 2005: Ogranization and environmental properties of extreme-rain-producing mesoscale convective systems. *Monthly Weather Review*, **133**, 961–976.

Schumacher, R. S. and R. H. Johnson, 2008: Mesoscale processes contributing to extreme rainfall in a midlatitude warm-season flash flood. *Monthey Weather Review*, **136**, 3964–3986.

Scofield, R. A. and J. Robinson, 1990: Satellite estimates and forecasts of heavy rainfall from mesoscale convective systems (mcss). *Conference of operational precipitation estimation and prediction*, Boston, Mass., American Meteorological Society.

Smull, B. F. and R. A. Houze, 1985: A midlatitude squall line with a trailing region of stratiform rain: radar and satellite observations. *Monthly Weather Review*, **113**.

UCAR Archive, 2012: University Corporation for Atmospheric Research UCAR image archive. [Online; accessed Apr 2012], `http://locust.mmm.ucar.edu`.

Wakimoto, R. M., 2001: Convectively driven high wind events. American Meteorological Society, Severe Convective Storms, 255–298.

Weaver, J. F., 1979: Storm motion as related to boundary-layer convergence. *Monthly Weather Review*, **107**, 612–619.

Weaver, J. F. and S. P. Nelson, 1982: Multiscale aspects of thunderstorm gust fronts and their effects on subsequent storm development. *Monthly Weather Review*, **110**, 707–718.

Weisman, M. L., 1992: The role of convectively generated rear-inflow jets in the evolution of long-lived mesoconvective systems. *Journal of the Atmospheric Sciences*, **49 (19)**, 1826–1847.

Weisman, M. L. and J. B. Klemp, 1982: The dependence of numerically simulated convective storms on vertical wind shear and buoyancy. *Monthly Weather Review*, **110**, 504–520.

Weisman, M. L. and J. B. Klemp, 1986: Characteristics of isolated convective storms. American Meteorological Society, 331–358.

Westcott, N. and P. Kennedy, 1989: Cell development and merger in an Illinois thunderstorm observed by doppler radar. *Journal of the Atmospheric Sciences*, **46**, 117–131.

Wilson, J. W. and W. E. Schreiber, 1986: Initiation of convective storms at radar-observed boundary-layer convergence lines. *Monthly Weather Review*, **114**, 2516–2536.

Zipser, E. J., 1977: Mesoscale and convective-scale downdrafts as distinct components of squall-line structure. *Monthly Weather Review*, **105**, 1568–1589.

Zipser, E. J., 1982: Use of a conceptual model of the lifecycle of mesoscale convective systems to improve very-short-range forecasts. Academic Press, Nowcasting, 191–204.

Zrnic, D. S. and A. V. Ryzhkov, 1999: Polarimetry for weather surveillance radars. *Bulletin of the American Meteorological Society*, **80 (3)**.